A Mechanism of Mechanotransduction Mediated by the Primary Cilium

Kristen L. Lee

Submitted in partial fulfillment of the

requirements for the degree of

Doctor of Philosophy

in the Graduate School of Arts and Sciences

COLUMBIA UNIVERSITY

2014

ABSTRACT

A Mechanism of Mechanotransduction Mediated by the Primary Cilium

Kristen L. Lee

Mechanotransduction is a process by which cells sense and convert mechanical loads into biochemical signals and transcriptional changes. This process is particularly critical in bone, a metabolically active tissue that continously remodels and adapts to mechanical loads in its local environment. Osteocytes are the most prevalent bone cell type and are responsible for coordinating skeletal adaptation. Recently, the loss of primary cilia, nonmotile antenna-like cellular structures, has been attributed to causing defects in skeletal development and loading-induced bone formation. While primary cilia have been implicated in osteocyte mechanotransduction, the molecular mechanism associated with this process is not understood. In this thesis, we demonstrate that the osteocyte primary cilium forms a microdomain that mediates osteogenic responses to mechanical loads. In the first study, we build a genetically encoded primary cilium-localized calcium biosensor and characterize ciliary calcium mobilization in response to mechanical loading with unprecedented sensitivity. Next, we apply similar techniques to monitor levels of another second messenger, cyclic AMP (cAMP), and are the first to demonstrate that the primary cilium segregates ciliary cAMP from the cytosol. In the third study, we link loading-induced bone formation *in vivo* to adenylyl cyclase 6 enzyme function, a component of the primary cilium-mediated mechanotransduction mechanism. Collec-

tively, this thesis elucidates how osteocyte primary cilia convert mechanical stimuli into osteogenic responses at the molecular and tissue levels and characterizes the primary cilium as a microdomain that serves as a biochemical and mechanical signaling nexus. Improvements in our understanding of primary cilia-regulated mechanotransduction will advance research efforts in the bone, tissue engineering, and mechanobiology communities.

Contents

List of Figures

List of Tables

Acknowledgments

The work to complete this thesis involved countless contributions from many others, and I hope that they share a part of this achievement in some way.

I thank my parents, Peter and Gin, and sister, Kelsey, for their love, support, and generosity, throughout the past five years of my Ph.D. and my life in general. Thank you for teaching me to be a hard worker, step out of my shell, have an appreciation for science and healthcare, and enjoy cooking and good food on any occasion.

I thank my advisor, Dr. Chris Jacobs, for helping shape me professionally and personally. His guidance- from improving the way I communicate and work with others to career advice- has been valuable in many ways. I have appreciated Chris's scientific direction, fun stories, and conversations over the years. Once I graduate, I am allowed to be his Facebook friend!

My day-to-day experience at Columbia would never have been the same without the members of the Cell and Molecular Biomechanics Lab. I thank Drs. David Hoey and Julia Chen for being endless sources of knowledge, experience, laughter, and friendship. I appreciate An Nguyen for her expert thoughts covering a wide range of topics including medicine, biomechanics, and business, and for her shared obsession with dogs.

I would probably not graduate for another few years without the technical assistance and dedication of Marie Guevarra, Mardonn Chua, and Divya Pathack. I would like to acknowledge the most recent graduate students joining the team, Milos Spasic and Emily Moore, for their contributions to my work and the lab. I also thank Drs. Ron Kwon, Sara Temiyasathit, and Jennifer Blundo for providing the intriguing scientific groundwork that influenced my own research projects and for their help getting me up and running on those experiments.

Completing my research and doctoral thesis involved many people. First, I appreciate the time and feedback of my proposal and defense committee members. Their advice, questions, and expertise have helped mold my research projects into a complete thesis and interesting scientific story. Additionally, I would like to thank our experienced and resourceful lab manager, Keith Yeager; our administrative team: Shila Maghji, Kidest Shenkoru, Jarmaine Lomax, Michelle Cintron, and Paulette Louissant; and the husbandry and veterinarian staff at the animal facility: Vivian Carbonell, Haydee Velez, Ed Torres, Vaughn Francis, Dr. Kelly Yamada, and Dr. Kevin Prestia.

I have been lucky to meet and become great friends with several people at Columbia: Sonal Sampat, who has been my longest friend in the program and can relate to me on almost anything; Ofer Idan, who never fails to impress me and is one of the most helpful people I know; and Kevin Dooley, who has been incredibly supportive and understanding over the past few years. I thank many students in the Columbia Univeristy Department of Biomedical Engineering for their help and discussions in lab and their friendship, especially the fellow bone people: Dr. Andrew Baik, Dr. Isabel Leong, Genevieve Brown, Bin Zhou, Ji Wang, and Eric Yu, and other members of the depart-

ment including Sarah De Leo, Venk Hariharan, Maggie Boushell, Dr. Jarett Michaelson, Dr. Keenan Bashour, Gwen Effgen, Dr. Corina Curschellas, and Dr. Rodney Agayan.

In the past five years, I was lucky to travel extensively for conferences, summer school, and volunteering opportunities (to list some highlights: Puerto Rico, Hawaii, Turkey, Germany, and California). I am very grateful to the National Science Foundation's Graduate Research Fellowship Program, Columbia Engineering's Egleston Doctoral Fellows Program, Dr. Metin Akay at the Unversity of Houston, Dr. Davide Calebiro at the University of Würzburg in Germany, and Dr. Tiffany Simon at Columbia University for providing me with funding and the opportunity to travel, connect with other scientists and engineers, and ultimately broaden my view of the world.

Chapter 1

Introduction

1.1 Opportunities

Ciliopathies are a collection of diseases caused by mutations affecting a cellular organelle called the primary cilium. Syndromes classified as ciliopathies often consist of multiple kidney, brain, retina, liver, and bone disorders, and the severity of these conditions vary broadly. Skeletal dysplasia occurs in many ciliopathies including Alström syndrome, Jeune syndrome, Verma-Naumoff syndrome, Majewski syndrome, Ellis-van Creveld syndrome, Senior-Loken syndrome, and Sensenbrenner syndrome [Huber and Cormier-Daire, 2012, Haycraft et al., 2007, Nguyen and Jacobs, 2013]. Although there is a clincal focus on the clear developmental importance of primary cilia, primary cilia serve diverse functional roles and are also critical for mechanosensing. Recent studies in bone show that primary cilia defects impair mechanotransduction and repair [Temiyasathit et al., 2012, Leucht et al., 2013]. Interestingly, primary cilia were

considered vestigial organelles up until only a decade ago, and now, primary cilia characterization is a growing research subject in various scientific communities.

Advances in the development of genetically encoded biosensors, also in the last decade, has enabled researchers to monitor intracellular signaling events with unprecedented sensitivity. Scientists and engineers have honed these tools to track and measure specific ion, molecule, and enzyme activity levels in live cells, in real-time, and at targeted subcellular locations [Palmer et al., 2011]. One particular biosensor system harnesses Fluorescence Resonance Energy Transfer (FRET), where the relative emission intensities of donor and acceptor fluorophores change due to a conformational modification that occurs when the target is added. Ratiometric measurements like this overcome the disadvantage of uneven loading of traditional diffusive single fluorescent indicator dyes [Rudolf et al., 2003]. Our ability to add targeting sequences combined with improved dynamic ranges of FRET-based biosensors make it possible to monitor the local signaling environment within the primary cilium, which is approximately 1/30,000 the cell volume [Praetorius and Spring, 2003].

1.2 Bone

Bone is a metabolically active tissue that continously remodels and adapts to mechanical loads in its local environment. While bone formation occurs with mechanical loading above normal levels, resorption occurs with insufficient loading [Chow et al., 1993, Turner et al., 1994]. Individuals are unable to experience regular dynamic or ambulatory activity in space or when immobilized during bed rest, and this lack of movement

clearly leads to bone loss [Lang et al., 2004, Tsuzuku et al., 1999]. In bone, remodeling occurs with the coordinated balance of bone matrix secretion by osteoblasts and bone resorption by osteoclasts. Our ability to create treatments for disuse-induced bone loss and engineer bone constructs depends on our understanding of how bone cells sense mechanical cues and maintain homeostasis in a mechanical environment.

The osteocyte is a terminally-differentiated, osteoblast-derived cell that makes up approximately 95% of all bone cells [Bruder and Caplan, 1990, Franz-Odendaal et al., 2006]. Osteocytes are embedded in interconnected cave-like structures and channels in the mineralized bone matrix called the lacunar-canalicular (LC) network. Under normal loading conditions, osteocytes are theoretically exposed to surface shear stress ranging 8-30 $dynes/cm^2$ as interstitial fluid moves within the LC network [Han et al., 2004, Weinbaum et al., 1994, You et al., 2001b]. Under these levels of fluid flow-induced shear stress, osteocytes exhibit intracellular calcium (Ca^{2+}) oscillations *in vitro* and *in situ* [Hung et al., 1995, Lu et al., 2012, Yellowley et al., 1997, Jing et al., 2013]. Given its sensitivity to mechanical stimuli, ability to regulate osteoblast, osteoclast, and mesenchymal stem cell function, and demonstrated role in mediating unloading-induced bone loss *in vivo*, the osteocyte is viewed as a mechanosensing cell required for mechanotransduction in bone [Cardoso et al., 2009, Heino et al., 2004, Hoey et al., 2011, Tatsumi et al., 2007, Taylor et al., 2007]. The osteocyte's ability to sense mechanical loads depends on cellular mechanosensors which include stretch-activated ion channels, integrins and focal adhesions, the cytoskeleton, and the primary cilium [Duncan and Hruska, 1994, Huo et al., 2008, Castillo et al., 2012, Litzenberger et al., 2009, Myers et al., 2007, Malone et al., 2007].

1.3 Mechanotransduction

Mechanotransduction is a process by which cells sense and convert mechanical signals into biochemical and transcriptional changes. Mechanical forces influence almost every stage of life including embryogenesis, tissue development, physiology, and apoptosis and is studied in different tissue contexts, in various biological contexts, and at multiple scales [Ingber, 2006]. Responses to mechanical loads at the cellular level include adapting to high strain environments by shortening the primary cilium, exerting contractile force at a magnitude that scales with substrate stiffness, and migrating preferentially towards more rigid substrates [Solon et al., 2007, McGlashan et al., 2010, Lo et al., 2000]. The cell's ability to interpret and react to mechanical forces is critical to cell function and health, as disruption in mechanotransduction or abnormal tissue mechanical properties cause disease, including cancer and osteoporosis [PaszeK et al., 2005, Provenzano et al., 2008, Nelson and Bissell, 2006, Tatsumi et al., 2007]. Our understanding of the intricacies of mechanotransduction has broad relevance in multiple cell types, stages of development and adult function, and pathologies.

Stretch-activated ion channels

The application of fluid flow causing surface shear stress or movement of transmembrane lipid bilayer components can open stretch-activated ion channels. As expected, opening these ion channels affects ion transport and distribution. Mechanically-activated channels have been implicated in a wide range of functions such as touch, hearing, and detecting osmotic gradients, volume, and pressure [Hamill and Martinac, 2001]. Many families

of stretch-activated ion channels exist, including weakly inward-rectifying K^+ channels named TREK and TRAAK, the amiloride-sensitive epithelial Na^+ channel called ENaC, and the TRP family of cation channels, many of which are Ca^{2+}-permeable [Martinac, 2004]. Polycystin 2 (PC2) and Transient Receptor Potential Vanilloid 4 (TRPV4) are both channels in the TRP family that mediate fluid flow-induced Ca^{2+} oscillations in kidney epithelial cells [Nauli et al., 2003, Köttgen et al., 2008].

Integrins and focal adhesions

Integrins are transmembrane adhesion receptors that anchor cells to the extracellular matrix, and thus, serve as direct physical connections to the local environment. An integrin associates with an assembly of several proteins called a focal adhesion within the cell which links directly to the cytoskeleton. Several groups have demonstrated that the integrin-focal adhesion complex mediates mechanotransduction [Katsumi et al., 2004]. This extensive collection of evidence includes the stretch-induced phosphorylation of multiple focal adhesion constituents in smooth muscle cells and fibroblasts and focal adhesion kinase-mediated mechanotransduction in osteoblasts *in vitro* [Hamasaki et al., 1995, Sai et al., 1999, Castillo et al., 2012]. Other groups have manipulated cell shape and stiffness by modifying substrate spatial and mechanical properties [Yeung et al., 2005, Tee et al., 2011, Han et al., 2012]. In particular, a pivotal study performed by *Chen et al* demonstrated that the amount of focal adhesions increases as a function of cell spreading and cytoskeletal tension which suggests that cell shape, cytoskeletal tension, and local focal adhesion dynamics are part of a feedback system controlled by the external mechanical environment [Chen et al., 2003].

Cytoskeleton

The cytoskeleton is composed of three distinct classes: actin, intermediate filaments, and microtubules. While each of these three elements have different roles in mediating cell motility, maintaining cell shape, and providing structure, there is evidence that they all play a role in mechanotransduction. Actin stress fibers are tethered to and mediate dynamics of focal adhesions, potentially because changes in actin filament tension and curvature affect interactions with actin-binding proteins [Geiger et al., 2009, Wehrle-Haller, 2012, Hayakawa et al., 2011, Risca et al., 2012, Romet-Lemonne and Jégou, 2013]. While intermediate filaments were once considered only structural cytoskeletal elements, they have been shown to control essential mechanical signal transduction events. For example, a major intermediate filament, desmin, is involved in the structural and mechanical integration of muscle [Shah et al., 2004]. In alveolar epithelial cells, shear stress-induced disassembly of keratin, another intermediate filament, is mediated by protein kinase C phosphorylation [Ridge et al., 2005]. Microtubules are the largest type of cytoskeletal class and have also been shown to mediate mechanotransduction. Microtubule polymerization increases as a function of tensional force magnitude applied through integrins in neurons and vascular smooth muscle cells [Dennerll et al., 1988, Putnam et al., 2001]. Additionally, pharmacologic disruption of the microtubule network before strain application abolishes the force-induced redistribution of GTPases RhoA and Rac [Putnam et al., 2003].

1.4 The Primary Cilium

The primary cilium is a solitary, non-motile organelle that extends from the surface of nearly all vertebrate cells [Huang et al., 2006, Wheatley et al., 1996]. Primary cilia are approximately 250 nm in diameter and typically 1-4 μm in length [Kiprilov et al., 2008]. The ciliary axoneme is a hollow cylindrical structure composed of nine microtubule doublets (in 9+0 configuration) that extends out from the cell (Figure 1.1) [Wilsman and Fletcher, 1978]. It anchors into the basal body which also serves as a microtubule organizing center (MTOC) and is one of two centrioles. Primary cilia are formed by intraflagellar transport, requiring the anterograde motor-forming protein KIF3A and another motor complex protein IFT88 [Lee et al., 2010].

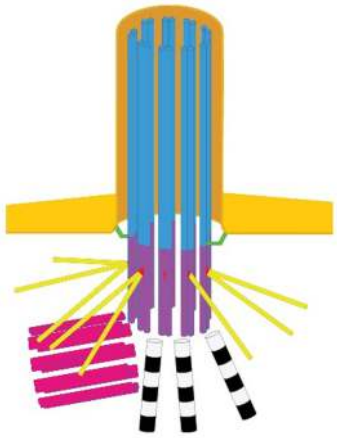

Figure 1.1: The primary cilium consists of a 9+0 microtubule doublet axoneme (blue), a microtubule organizing center (MTOC)/mother centriole (purple), and a daughter centriole (pink). Basal feet (red) connect the MTOC to the microtubule cytoskeleton (yellow). Distal appendages (green) attach the basal body to the plasma membrane, which is contiguous with the plasma membrane covering the axoneme. Striated rootlets (black and white) are associated with the basal body.

Defects in KIF3A, IFT88, and other ciliary components are associated with numerous human diseases called ciliopathies. Primary cilia serve as important cellular sensors and mediate Hedgehog and Wnt signaling, which are involved in developmental processes [Wong and Reiter, 2008, Lancaster et al., 2011]. The primary cilium's role in mediating skeletal development has been exhibited in a conditional knockout of *Kif3a* linked to the late stage osteoblast and osteocyte *Osteocalcin* promotor in mice, which resulted in osteopenia, impaired osteoblast function as measured by decreased tibial *Runx2*, *Osterix*, *Osteocalcin*, and *Dmp1* mRNA expression, and attenuated Hedgehog and Wnt signaling [Qiu et al., 2012].

The primary cilium's role in numerous cellular processes is underlined by its function as a mechanosensor. The primary cilium possesses general features of mechanosensory transduction: an extracellular component, transduction channels, and an intracellular link [Gillespie and Walker, 2001]. It has been described as a "mechanosensory toggle switch" because it extends from the apical cell membrane and deflects with fluid movement postulated to occur within the LC system and bends during cartilage compression [Malone et al., 2007, Whitfield, 2008, Jensen et al., 2004]. Our understanding of primary cilium bending mechanics and bending-induced forces on the plasma membrane covering the primary cilium is essential to elucidating the molecular mechanism of mechanotransduction mediated by the primary cilium. Recently, *Young et al* studied the tension force distribution along a primary cilium under flow and suggest that stretch-activated ion channels are likely to be activated and open near the base of the primary cilium where tension force is the highest [Young et al., 2012]. Another characteristic of

the primary cilium that highlights its mechanosensory role is its intracellular interaction with the cytoskeleton. Actin filaments and microtubules are sensitive to mechanical loading, and their dynamics have been shown to affect cilia length which suggests that the primary cilium plays a role in mechanotransduction [Kim et al., 2010, Sharma et al., 2011].

Many groups have demonstrated that primary cilia serve as mechanosensors in multiple tissue contexts including kidney, liver, and skeletal tissues. Interestingly, mechanical stimulation shortens primary cilia in kidney epitheia and chondrocytes, suggesting that modulating primary cilium length is a way to minimize overstimulation [Miyoshi et al., 2011, McGlashan et al., 2010, Besschetnova et al., 2010]. Primary cilia clearly mediate mechanotransduction as they are neccessary for fluid flow-induced Ca^{2+} transients in kidney epithelial cells and bile duct epithelial cells [Nauli et al., 2003, Praetorius and Spring, 2003, Masyuk et al., 2006]. A pivotal study by *Praetorius and Spring* suggested that local stimulation of the primary cilium is critical for mechanotransduction because the same local stimulus applied to the apical membrane did not elicit a Ca^{2+} influx within renal epithelial cells [Praetorius and Spring, 2001]. Recently, the development of a murine osteoblast and osteocyte conditional knockout of *Kif3a* which resulted in a loading-induced bone formation defect *in vivo* implicates the primary cilium in mechanotransduction in tissues other than kidney and liver [Temiyasathit et al., 2012]. At the level of transcription and translation, loss of primary cilia impaired flow-induced increases in *Cox-2*, *Opn*, and *Opg/Rankl* mRNA levels and inhibited PGE_2 release in osteoblasts and osteocytes *in vitro* [Malone et al., 2007, Delaine-Smith et al., 2014]. Taken together, these data suggest that the primary cilium is necessary for transducing

mechanically-stimulated osteogenic and antiresorptive signals. However, the primary cilium-mediated molecular mechanism of osteocyte mechanotransduction is unknown.

1.5 Second Messengers

Calcium

Ca^{2+} is a ubiquitous second messenger serving as a biochemical signal that regulates a variety of cellular processes including proliferation, development, and transcription factor activation [Berridge et al., 2003]. In bone cells specifically, mechanically-induced Ca^{2+} oscillations have been shown to mediate increased expression of the bone matrix protein osteopontin [You et al., 2001a]. The transient elevation of intracellular Ca^{2+} is one of the earliest cellular responses to mechanical stimuli in osteoblasts and osteocytes. In osteoblasts and osteocytes, fluid flow-induced Ca^{2+}mobilization is dependent on extracellular Ca^{2+} influx and intracellular Ca^{2+} release from the endoplasmic reticulum [Hung et al., 1996,Lu et al., 2012,Huo et al., 2008]. As mentioned in the previous section, flow-stimulated Ca^{2+} increases occur in renal and bile duct epithelial cells and are dependent on primary cilia. Interestingly, primary cilia removal does not inhibit flow-induced cytosolic Ca^{2+}increases in osteoblasts, but a different primary cilium-restricted Ca^{2+}-dependent mechanism has been suggested by *Kwon et al* and will be explained in Chapters 2 and 3, illustrating the diversity of Ca^{2+} signaling in different tissue contexts [Malone et al., 2007, Kwon et al., 2010].

Cyclic AMP

Another second messenger is cyclic adensosine monophosphate (cAMP) which is catalyzed from adenosine triphosphate (ATP) by members of the adenylyl cyclase (AC) enzyme family. cAMP is involved in a wide range of cellular processes by activating the phosphorylating enzyme protein kinase A (PKA) and exchange proteins activated by cAMP (Epac) [Wadhwa et al., 2002, Seino and Shibasaki, 2005]. Ca^{2+} oscillations play an important physiologic role in cAMP production via inhibition or activation of different AC isoforms, such as the Ca^{2+}-inhibitable enzymes AC5 and AC6 and the Ca^{2+}-stimulated enzymes AC1, AC3, and AC8 [Willoughby and Cooper, 2007]. AC3 and AC6 have been observed on the primary cilium membrane [Bishop et al., 2007, Ou et al., 2009, Kwon et al., 2010, Masyuk et al., 2006]. Thus, the primary cilium may mediate mechanotransduction by orchestrating intricate molecular interactions involving Ca^{2+} and cAMP signaling.

1.6 Central Hypothesis and Organization

The central hypothesis of this thesis is that the osteocyte primary cilium forms a microdomain that serves as a biochemical and mechanical signaling nexus.

Hypothesis 1: The mechanically-stimulated ciliary Ca^{2+} microdomain is distinct from the cytosol.

In Chapter 2 of this thesis, we create a novel primary-cilium localized Ca^{2+} biosensor and monitor loading-induced ciliary Ca^{2+} increases. Several candidate mechanosensi-

tive Ca^{2+}-permeable channels are knocked down to identify the source of this Ca^{2+} mobilization, and we compare flow-induced Ca^{2+}increases in cells with *Pkd2*, *Trpv4*, or *Piezo1* deficiency.

Hypothesis 2: The mechanically-stimulated ciliary cAMP microdomain is distinct from the cytosol.

In Chapter 3 of this thesis, we measure flow-induced cAMP levels in real-time. By extending the plasmid design techniques used in Chapter 2, we create a novel primary cilium-localized cAMP biosensor and monitor mechanically-stimulated ciliary cAMP responses.

Hypothesis 3: Deletion of AC6 inhibits loading-induced bone formation *in vivo*.

In Chapter 4 of this thesis, we examine the link between primary cilia, AC6, and bone adaptation to mechanical loads. A previous study in our lab showed that loading-induced cAMP changes and *Cox-2* expression increases are dependent on both AC6 and primary cilia *in vitro*. Here, we demonstrate that AC6 mediates loading-induced bone formation *in vivo* using mice with a global deletion of AC6.

Chapter 2

Calcium in the Osteocyte Primary Cilium

Project Collaborators: Kristen L. Lee, Marie D. Guevarra, Mardonn C. Chua, Mingxing ouyang, yingxiao wang, Christopher R. Jacobs

2.1 Abstract

The primary cilium is an antennae-like, nonmotile structure that extends from the surface of most mammalian cell types and is critical for chemosensing and mechanosensing in a variety of tissues including cartilage, bone, and kidney. Flow-induced intracellular calcium ion (Ca^{2+}) increases in kidney epithelia depend on primary cilia and primary cilium-localized Ca^{2+}-permeable channels Polycystin 2 (PC2) and Transient Receptor Potential Vanilloid 4 (TRPV4). While primary cilia have been implicated in osteo-

cyte mechanotransduction, the molecular mechanism that mediates this process is not fully understood. Here, we show that fluid flow induces Ca^{2+} increases in osteocyte primary cilia which depend on intracellular Ca^{2+} release and extracellular Ca^{2+} entry. We directed a Fluorescence Resonance Energy Transfer (FRET)-based Ca^{2+} biosensor with the primary cilium-specific sequence of *Arl13b*. Using this tool, we investigated the role of several Ca^{2+}-permeable channels that may mediate flow-induced Ca^{2+} entry into the primary cilium: PC2, TRPV4, and PIEZO1. Our data demonstrate that TRPV4, but not PC2 or PIEZO1, mediates flow-induced ciliary Ca^{2+} increases and loading-induced *Cox-2* mRNA increases, an osteogenic response. These results demonstrate that the mechanism of mechanotransduction mediated by primary cilia varies in different tissue contexts. Furthermore, our data suggest that the primary cilium forms a calcium microdomain that is distinct from the cytosol. In this study, we report the first measurements of Ca^{2+} signaling within osteocyte primary cilia, and we anticipate that this work is a starting point for more studies investigating the role of TRPV4 in mechanotransduction.

2.2 Introduction

Mechanotransduction is a process by which cells sense and convert mechanical signals into biochemical and transcriptional changes. The calcium ion (Ca^{2+}) is a ubiquitous second messenger that regulates numerous signaling pathways. Despite how universal Ca^{2+} is, discrete intracellular signaling mechanisms occur because Ca^{2+} gradients are spatiotemporal and do not comprise one general pool that changes uniformly. For example, there are discrete microdomain Ca^{2+} signals including "Ca^{2+} sparks," "Ca^{2+} sparklets," and "scraps," that modulate constriction and relaxation in vascular smooth muscle cells [Wang et al., 2004, Nelson et al., 1995]. Mechanical loading generates rapid and temporal intracellular Ca^{2+} increases in many cell types including osteocytes, osteoblasts, neurons, and kidney cells. Ca^{2+} mobilization is required for flow-induced PGE_2 release and flow-induced osteopontin gene regulation in osteocytes, demonstrating that Ca^{2+} is upstream of mechanotransduction activies and paracrine signaling [Ajubi et al., 1999, You et al., 2001b].

Studies characterizing flow-induced intracellular Ca^{2+} increases in osteoblasts and osteocytes have spanned almost two decades, starting with identifying that osteoblasts are more responsive to fluid shear stress than mechanical strain and that oscillatory fluid flow is a less potent stimulus than steady flow [Owan et al., 1997, Jacobs et al., 1998, Lu et al., 2012]. Both extracellular Ca^{2+} and intracellular Ca^{2+} stores are critical for generating the flow-induced Ca^{2+} response [Hung et al., 1996, Lu et al., 2012]. Ryanodine and inositol trisphosphate (IP_3) receptors have been shown to mediate loading-induced intracellular Ca^{2+} storage release and are part of extracellular Ca^{2+}-induced Ca^{2+} release (CICR) from the endoplasmic reticulum [Lu et al., 2012, You et al., 2001a]. Further-

more, ATP-gated purinergic receptors have been implicated in regulating flow-induced Ca^{2+} responses [Lu et al., 2012, Jing et al., 2013]. While these studies were seminal in understanding fluid flow-induced intracellular Ca^{2+}mobilization, they did not resolve Ca^{2+} microdomain transients from cytosolic Ca^{2+} events.

Recent advances in monitoring ciliary Ca^{2+} mobilization have improved our understanding of the primary cilia-mediated mechanism of mechanotransduction in kidney epithelia. In the past, traditional diffusive BAPTA-based fluorescent indicator dyes were used to measure intracellular Ca^{2+} levels but did not target specific subcellular domains. In some pivotal studies, *Praetorious and Spring* and *Nauli et al* demonstrated that primary cilia are required for mechanically-induced Ca^{2+} increases in kidney epithelial cells [Praetorius and Spring, 2001, Praetorius and Spring, 2003, Nauli et al., 2003]. The dependence of flow-induced Ca^{2+} increases on kidney epithelia primary cilia and the presence of mechanosensitive Ca^{2+}-permeable channels on the ciliary membrane suggest that mechanical loading opens stretch-activated ion channels on the primary cilium that mediate Ca^{2+} entry. In the last year, *Delling et al*, *Su et al*, and *Jin et al* directed genetically encoded single fluorescence Ca^{2+} biosensors to the primary cilium using a variety of ciliary targeting sequences in human retina pigmented epithelia and kidney epithelial cells [Delling et al., 2013, Su et al., 2013, Jin et al., 2013]. *Su et al* and *Jin et al* exposed kidney epithelial cells to fluid flow, which bent primary cilia and increased ciliary and cytosolic Ca^{2+} levels [Jin et al., 2013, Su et al., 2013]. The Ca^{2+}-permeable channel polycystin-2 (PC2) associates with the mechanosensitive protein polycytin 1 and localizes to the primary cilium. *Jin et al* reported that flow-induced Ca^{2+} elevations occur first in the primary cilium and are followed by cyotosolic Ca^{2+} mo-

bilization. Both ciliary and cytosolic Ca^{2+} increases were dependent on PC2 [Jin et al., 2013]. Furthermore, blocking ryanodine receptors inhibited cytosolic Ca^{2+} increases without affecting the flow-induced ciliary Ca^{2+} response [Fill and Copello, 2002, Jin et al., 2013]. Collectively, these recent flow studies on kidney epithelia primary cilia demonstrate that fluid flow activates PC2 through which extracellular Ca^{2+} enters and triggers ryanodine receptors in CICR.

Current knowledge of the osteocyte primary cilia-mediated mechanism of mechanotransduction is relatively poor compared with recent progress in kidney epithelia primary cilia mechanotransduction research. Our group previously used the fluorescent dye Fura 2-AM to demonstrate that flow-induced Ca^{2+} increases in MLO-Y4 osteocyte-like cells are independent of primary cilia and stretch-activated channels, which is different from kidney cells [Malone et al., 2007]. While these results suggest that the osteocyte primary cilia-regulated mechanism of mechanotransduction is not linked to intracellular Ca^{2+} levels, it is unknown if the local primary cilium Ca^{2+} environment is distinct from the cytosol. We hypothesized that the osteocyte primary cilium mediates mechanotransduction by forming a distinct Ca^{2+} microdomain. Therefore, the objective of this study was to monitor flow-induced ciliary Ca^{2+} levels and elucidate the intricate role of the osteocyte primary cilium as a biochemical and mechanical signaling nexus.

In this study, we directed a Fluorescence Resonance Energy Transfer (FRET)-based Ca^{2+} biosensor to the primary cilium by fusing a biosensor sequence to the primary cilium-specific sequence of *Arl13b*. The modified YC3.6 Ca^{2+}-sensitive FRET-based biosensor contains a calmodulin (CaM) region with four Ca^{2+} binding domains [Ouyang et al., 2008]. Binding of Ca^{2+} results in a conformational change that increases FRET

signal, which is characterized by decreased ECFP and increased YPet fluorescence [Whitaker, 2010]. YPet as an acceptor produces the largest FRET dynamic range in live cells compared to Citrine, Venus, or cpVenus [Ouyang et al., 2008]. Using a targeted version of YC3.6 and the diffusive Ca^{2+} indicator dye Fura Red, we detected ciliary and cytosolic Ca^{2+} increases within individual MLO-Y4 cells exposed to fluid flow stimulation. Additionally, we examined the role of several Ca^{2+}-permeable channels on the primary cilium: Polycystin-2 (PC2), Transient Receptor Potential Vanilloid 4 (TRPV4), and PIEZO1. Our data demonstrate that TRPV4, but not PC2 or PIEZO1, mediates flow-induced ciliary Ca^{2+} increases and a loading-induced osteogenic response at the transcriptional level. Collectively, our study demonstrates that the osteocyte primary cilium microdomain is distinct from the cytosol and that sources of loading-induced ciliary Ca^{2+} mobilization are different in kidney epithelia and osteocytes. These are the first measurements of Ca^{2+} signaling within the osteocyte primary cilium, and we anticipate this work is a starting point for more studies investigating the role of TRPV4 in osteocyte mechanotransduction [Prasad et al., 2014].

2.3 Materials and Methods

2.3.1 Summary

A FRET-based Ca^{2+} biosensor was directed to the primary cilium using *Arl13b*. Fura Red-AM indicator was used to detect flow-induced Ca^{2+} changes within the cytosol. Defects in flow-induced Ca^{2+} signaling caused by *Pkd2*, *Trpv4*, and *Piezo1* siRNA-mediated knockdowns were measured. siRNA-mediated knockdowns were verified using real-time qRT-PCR and Western blotting. MLO-Y4 cells deficient in *Tprv4* and *Piezo1* were flowed, and *Cox-2* mRNA expression levels were quantified.

2.3.2 Plasmid construction

Drs. Yingxiao Peter Wang and Mingxing Ouyang previously modified the YC3.6 Ca^{2+}-sensitive FRET-based biosensor composed of an ECFP donor, calmodulin region, M13 calmodulin-binding region, and YPet acceptor (CaB). Drs. Kenji Kontani and Kristen Verhey generously shared with us the *Arl13b* gene. We fused *Arl13b* to the N terminus of CaB using a 15 amino acid-long flexible linker to form *Arl13b-L-CaB* (ALC) [Wang et al., 2005]. Deletions of $Trp^{3}$and Phe^{17} in the M13 region were performed to block Ca^{2+}-induced changes in FRET, serving as negative controls of CaB and ALC (mutCaB and mutALC) [Ikura et al., 1992].

2.3.3 Cell culture and transfection

MLO-Y4 osteocyte-like cells were cultured in MEM alpha (Life Technologies) with 5% FBS, 5% CS, and 1% PS at 37°C in 5% CO_2. 1.25 million cells were transfected with

10 μg plasmid by electroporation using the BTX 360 with a single 300 V, 100 Ω, 1000 μF pulse. Cells were co-transfected with the ALC plasmid and 0.5 nmol siRNA. siRNA sequences were: *Pkd2* (5'-CCUCUUGGCAGUUUCAGCCUGUAAA- 3'), *Trpv4* (5'-GAUGGACUGCUCUCCUUCUUGUUGA -3'), and *Piezo1* (5'-CACCGGCAUCUACG UCAAAUA-3') [Coste et al., 2010]. Transfected MLO-Y4 cells were seeded onto collagen I-coated glass slides (#1.5 glass, Warner Instruments) at a density of 4k cells/cm^2 and cultured for 3 days in reduced serum containing 2.5% FBS and 2.5% CS. IMCD cells were cultured in DMEM (Life Technologies) with 10% FBS and 1% PS. Transfected IMCD cells were seeded onto fibronectin-coated glass slides at a density of 8k cells/cm^2 and cultured for 3 days in 1% FBS. Prior to imaging, cells were incubated in 20 μM Fura Red-AM (Life Technologies, F-3021) with 0.1% Pluronic® F-127 (20% Solution in DMSO) (Life Technologies) for 1 hour at room temperature to label cytosolic Ca^{2+}.

2.3.4 Imaging flow chamber

Slides were placed in the RC-30 Confocal Imaging Chamber (Warner Instruments) and attached to a syringe containing phenol red-free MEM alpha with 1% FBS and 1% CS for MLO-Y4 cells or phenol red-free DMEM with 1% FBS for IMCD cells. MLO-Y4 cells were exposed to oscillatory fluid flow resulting in 10 dyne/cm^2 shear stress, and IMCD cells were exposed to steady fluid flow resulting in 1 dyne/cm^2 shear stress, both within physiologic range for each cell type. Thapsigargin was added to the imaging media at a final concentration of 10 μM for appropriate samples. A separate syringe with 10 μM ionomycin was connected to the chamber to verify cell viability and show biosensor activation after the initial flow stimulus.

2.3.5 Ca^{2+} imaging in cilia and cytosol

Fluorescent samples were imaged on an Olympus IX71 inverted epifluorescence microscope with a 1.30 N.A. 40X oil-immersion objective. Donor excitation was achieved using a xenon lamp with a 430/24 nm filter. ECFP, YPet, and Fura Red images were collected simultaneously using a Quad-View system (QV2, Photometrics) containing 470/28 nm, 530/30 nm, and 641/75 nm emission filters. Cells were left to rest for 20 minutes prior to imaging. For calibration studies, we added ionomycin at a final concentration of 5 μM and $CaCl_2$ at a final concentration of 0.1, 0.25, or 0.5 mM. During fluid flow studies, baseline signal was recorded for 30 seconds followed by 5 minutes of flow. Images were taken at 4 Hz with 150 msec exposure.

2.3.6 Antibodies

We used the following primary antibodies: Rabbit anti-Polycystin 2 (Santa Cruz, sc-25749), rabbit anti-sera to TRPV4 (generously provided by Dr. Stephan Heller), rabbit anti-Piezo1 (Novus NBP1-78537 for immunostaining and NBP2-10504 for Western blotting), mouse anti-acetylated alpha tubulin (Abcam, ab24610), and mouse anti-actin (Abcam, ab11003). We used the following secondary antibodies: Alexa Fluor 488 goat anti-rabbit IgG (Life Technologies, A11008), Alexa Fluor 568 goat anti-mouse IgG (Life Technologies, A11031), goat anti-rabbit IgG-HRP (Santa Cruz, sc-2004) and HRP goat anti-mouse Ig (BD Biosciences, 554002).

2.3.7 Immunocytochemistry and confocal microscopy

MLO-Y4 and IMCD cells were seeded on 35 mm glass bottom dishes at approximately 1 k cells/cm^2 and 2 k cells/cm^2 respectively. Upon reaching 80-90% confluence after 2 days of culture, cells were fixed with 10% Formalin, permeabilized with 0.1% Triton X-100, and blocked with 10% goat serum and 1% BSA in PBS. Cells were labeled with primary antibodies for acetylated alpha tubulin and PC2, TRPV4, or PIEZO1, followed by incubation in appropriate Alexa Fluor-labeled secondary antibodies. Nucleic stain was achieved using DAPI (0.5 mg/mL). Confocal images were obtained on a Leica SP5 using a 1.46 N.A. 100X oil-immersion objective.

2.3.8 Western blot

Cells transfected with *Pkd2*, *Trpv4*, *Piezo1*, and MedGC scrambled siRNA (Life Technologies) were lysed in RIPA buffer (Santa Cruz, sc-24948) supplemented with sodium orthovanadate, PMSF, and protease inhibitor cocktail 3 days post electroporation. 5 μg of each protein sample was run through NuPAGE® Novex® 4-12% Bis-Tris gels (Life Technologies). After electrophoresis, proteins were transferred to Invitrolon™ PVDF membranes (Life Technologies). The membranes were cut in half to separately label actin bands. Membranes for PC2, PIEZO, and actin were blocked with 5% BSA (Sigma-Aldrich) and membranes for TRPV4 were blocked with 5% non-fat milk. HRP-conjugated antibodies were detected with chemiluminescence (Clarity Western ECL substrate, BioRad) on a Fujifilm LAS-4000 biomolecular imager.

2.3.9 Flow chamber

Transfected MLO-Y4 cells were seeded onto collagen I-coated glass slides at approximately 5k cells/cm^2 and cultured for 3 days. Slides were placed in parallel plate flow chambers (56 × 24 × 0.28 mm), incubated for 30 minutes, and then exposed to 5 minutes of oscillatory fluid flow (OFF) at 1 Hz with a peak shear stress of 10 dynes/cm^2. Slides were removed from chambers after 55 minutes, and RNA was isolated immediately.

2.3.10 Quantitative real-time RT-PCR

RNA was extracted from cells using TriReagent (Sigma-Aldrich) and isolated, followed by cDNA synthesis using TaqMan reverse transcriptase (Applied Biosystems). cDNA samples were amplified with *Trpv4* (Mm00499025_m1), *Pkd2* (Mm00435829_m1), *Piezo1* (Mm01241570_g1), *Piezo2* (Mm01262433_m1), *Cox-2* (Mm00478374_m1) and *Gapdh* (4352339E) primers and probes (Applied Biosystems) by quantitative real-time RT-PCR using the ABI PRISM 7900 detection system (Applied Biosystems). Samples and standards were run in triplicate and were normalized to the endogenous *Gapdh* expression. Relative gene levels between samples were determined using the relative standard curve method (ABI Prism 7700 User Bulletin 2; Applied Biosystems).

2.3.11 Data analysis

Images were corrected for background and bleedthrough. Average intensity data of a region of interest over time was smoothened using a 1D Savitsky-Golay filter. Peaks

were identified by finding local maxima using Matlab. Unless otherwise specified, a cell was considered responsive if a flow-induced Ca^{2+} peak height was equal or greater to 1.5 times the maximum baseline oscillation. Results are shown as mean ± SEM. Unpaired t-tests (two-tailed) were used to analyze differences between treated and untreated groups. Comparisons of multiple groups were performed using 1-way ANOVA followed by Dunnett's multiple comparison post hoc test or Bonferroni's multiple comparison post hoc test for *Cox-2* mRNA level comparisons. For all tests, $p < 0.05$ was considered significant.

2.4 Results

2.4.1 Arl13b-linker-Ca^{2+} biosensor detects ciliary Ca^{2+}

For this study, we developed a novel primary cilium-localized, fully ratiometric biosensor using the modified YC3.6 Ca^{2+}-sensitive FRET-based biosensor (CaB) fused to ARL13B. First, we established that ARL13B localizes to primary cilia in MLO-Y4 osteocyte-like cells and verified ARL13B localization to IMCD primary cilia (A.1a-b) [Sharma et al., 2011]. Interestingly, we found that another reported primary cilium-localized protein, Somatostatin receptor 3 (SSTR3), which localizes to the IMCD primary cilium, did not localize to the MLO-Y4 primary cilium, excluding it as a ciliary targeting sequence (Figure A.1c-d). Our biosensor design consisted of *Arl13b* at the N terminus followed by a 15 amino acid-long flexible linker, ECFP, calmodulin, M13 calmodulin-binding region, and YPet at the C terminus (Figure 2.1a) [Wang et al., 2005, Ouyang et al., 2008]. Addition of Ca^{2+} leads to increased FRET signal, and transfecting Arl13b-linker-CaB (ALC) enabled us to detect Ca^{2+} levels within the primary cilium separate from the cytosol. The addition of 5 μM ionomycin, a Ca^{2+} ionophore, in media containing 1.8 mM Ca^{2+} led to detectable increases in FRET (represented by the emission ratio of YPet:ECFP fluorescence intensity) (Figure 2.1b). Furthermore, the FRET signal increased at a slower rate and with delay to smaller concentrations of calcium chloride ($CaCl_2$) added with ionomycin in Ca^{2+}-free media compared with higher concentrations of $CaCl_2$ (Figure 2.1c). Thus, we determined that ALC was sensitive to different levels of ciliary Ca^{2+}.

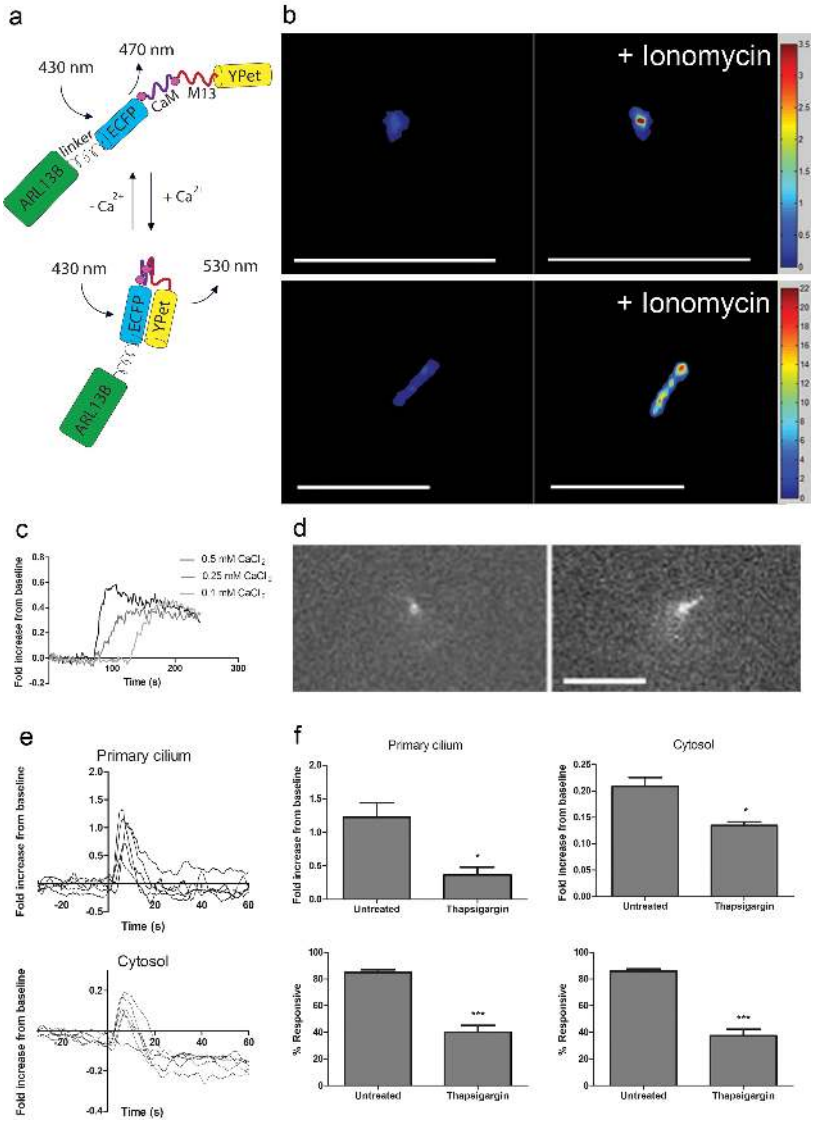

Figure 2.1: ALC localizes to the primary cilium and detects Ca^{2+} level changes. (a) Schematic of the primary cilium-localized biosensor, ALC. (b) ALC FRET signal increases when ionomycin is added to media. Scale bars, 5 μm. (c) Traces of baseline-normalized FRET signal over time with different [$CaCl_2$]. (d) YPet fluorescence images of a vertical primary cilium which bent to the right during flow. Scale bars, 10 μm. (e) Individual ciliary and cytosolic Ca^{2+} measurements during oscillatory fluid flow starting at t = 0 s. (f) Ca^{2+} increases with untreated or thapsigargin-treated media (untreated (n=17 or 18), thapsigargin (n=6)) and percent of MLO-Y4 primary cilia and cytosolic domains exhibiting flow-induced Ca^{2+} increases (n=15-21). (***, $p<0.0001$; *, $p<0.05$). Error bars show mean ± SEM.

2.4.2 Mechanical stimulation of MLO-Y4 cells transfected with ALC led to ciliary and cytosolic Ca^{2+} mobilization

Primary cilia with a vertical component prior to flow typically bent in the direction of flow (Figure 2.1d). We loaded the Ca^{2+} indicator dye Fura Red into cells transfected with ALC to monitor cytosolic Ca^{2+} levels. Use of a Quad-View beam splitter allowed us to collect images through several emission filters, and we monitored ECFP, YPet, and Fura Red signals simultaneously [Baik et al., 2013]. Application of 1 Hz oscillatory fluid flow resulting in 10 dynes/cm^2 surface shear stress led to ciliary and cytosolic Ca^{2+} peaks within approximately 8.2 $\pm$ 0.8 s and 8.2 $\pm$ 0.6 s, respectively (Figure 2.1e). On an individual cell basis, 57% of Ca^{2+} peaks occurred in the primary cilium prior to the cytosol of the same cell, suggesting that Ca^{2+} increases in the primary cilium do not trigger intracellular Ca^{2+} release as it does in kidney epithelial cells. We also transfected and stimulated cells transfected with inactive biosensors, mutCaB and mutALC, to verify that the observed peaks were indeed due to increased Ca^{2+} levels (Figure A.2). Next, cells were treated with thapsigargin, which depletes intracellular Ca^{2+} stores. We continued to observe flow-induced ciliary Ca^{2+} peaks, although there were significant decreases in responsiveness and peak magnitude (Figure 2.1f). These results imply that Ca^{2+}-permeable channels on the primary cilium also mediate flow-induced Ca^{2+} entry.

2.4.3 PC2, TRPV4, and PIEZO1 are Ca^{2+}-permeable channels on the primary cilium

We examined three Ca^{2+}-permeable channels localized to the osteocyte primary cilium: Polycystin- 2 (PC2), Transient Receptor Potential Vanilloid 4 (TRPV4), and PIEZO1. PC2 and TRPV4, among other channels, localize to kidney epithelia primary cilia and mediate flow-induced Ca^{2+} increases [Nauli et al., 2003, Köttgen et al., 2008].

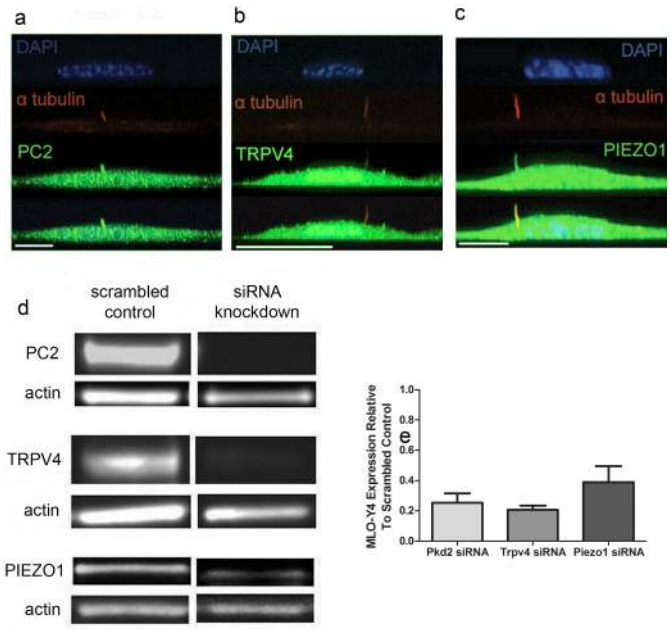

Figure 2.2: PC2, TRPV4, and PIEZO1 localize to MLO-Y4 primary cilia and plasma membrane. (a-c) Co-immunostaining of acetylated α-tubulin and PC2, TRPV4, and PIEZO1 on MLO-Y4 cells. Scale bars, 10 μm. (d) Western blot of PC2, TRPV4, PIEZO1, and actin protein in MLO-Y4s treated with scrambled control siRNA and *Pkd2*, *Trpv4*, or *Piezo1* siRNA. (e) Quantified knockdown of *Pkd2* (n=4), *Trpv4* (n=10), and *Piezo1* (n=4) mRNA levels in MLO-Y4 cells treated with siRNA relative to controls (n=10). Error bars show mean ± SEM.

Coste et al reported that mechanically-activated ion channels PIEZO1 and PIEZO2 are expressed in several murine tissues including kidney and have relatively lower expression in brain and heart tissue [Coste et al., 2010]. We observed *Piezo1* mRNA expression in MLO-Y4 and IMCD cells and *Piezo2* mRNA expression only in IMCDs (Figure A.3). We immunostained MLO-Y4 cells for PC2, TPRV4, and PIEZO1 and found that all three channels are present in both the primary cilium and plasma membrane (Figure 2.2a-c). siRNA transfection reduced protein and mRNA levels compared with scrambled siRNA controls (all groups vs. control mRNA levels, $p<0.005$)(Figure 2.2d-e).

2.4.4 TRPV4 mediates osteocyte flow-induced ciliary Ca^{2+} increases

PC2 mediates mechanically-induced ciliary and cytosolic Ca^{2+} signaling in kidney epithelia, and here, our data suggest that osteocyte mechanotransduction is independent of PC2. Following co-transfection of ALC and either *Pkd2*, *Trpv4*, or *Piezo1* siRNA, MLO-Y4 cells were loaded with Fura Red and exposed to oscillatory flow stimulation. To illustrate the role of candidate mechanically-activated channels in regulating Ca^{2+} entry, we plotted the percent of responsive cells exhibiting flow-induced Ca^{2+} peaks as a function of minimum peak height (a multiple of the sample's baseline oscillation) for all treatment groups. Out of all the Ca^{2+}-permeable channels, only the loss of *Trpv4* clearly impaired the percent of responding cells (Figure 2.3a).

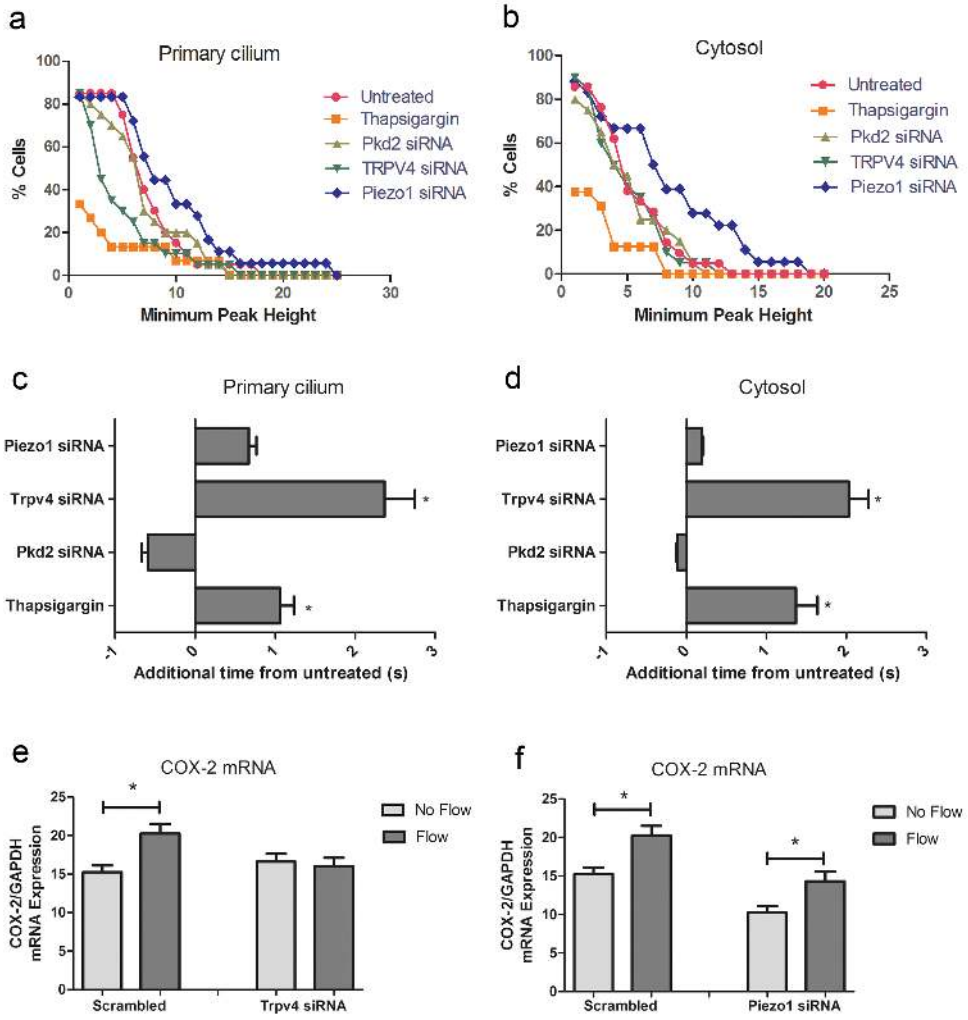

Figure 2.3: TRPV4 plays a role in osteocyte mechanotransduction. (a-b) Percent of responsive cells exhibiting flow-induced Ca^{2+} peaks as a function of minimum peak amplitude (a multiple of the sample's baseline oscillation)(n=15-21). (c-d) Timing of ciliary and cytosolic Ca^{2+} peaks of treated cells relative to untreated controls ((untreated (n=15), thapsigargin (n=5 or 6), *Pkd2*, *Trpv4*, and *Piezo1* (n=14-16)). (e-f) Levels of normalized *Cox-2* mRNA expression in scrambled, *Trpv4*, or *Piezo1* siRNA-treated cells with and without 5 minutes of oscillatory flow exposure (n=9-11). (*, $p<0.05$) Error bars show mean $\pm$ SEM.

Using a threshold cutoff of 5 times the baseline oscillation, 75% of untreated cells demonstrated ciliary Ca^{2+} peaks compared with 30% of *Trpv4* siRNA-treated cells. *Trpv4* deficiency did not lower the percent of cells exhibiting cytosolic Ca^{2+} peaks (Figure 2.3b). In fact, only thapsigargin treatment affected the percent of cells exhibiting flow-induced cytosolic Ca^{2+} increases (Figure 2.3b). *Pkd2* and *Piezo1* deficiencies did not inhibit the percent of ciliary or cytosolic Ca^{2+} peaks. Interestingly, *Piezo1* knockdown sensitized the cytosolic Ca^{2+} response to flow perhaps because a different Ca^{2+}-permeable channel. As mentioned earlier, there is a delay in peak FRET signal with lower Ca^{2+} concentrations relative to higher Ca^{2+} concentrations. Compared with untreated samples, ciliary and cystolic Ca^{2+} peaks were delayed in MLO-Y4 cells treated with thapsigargin or deficient in *Trpv4* and *Piezo1* (Figure 2.3c-d). These differences were not statistically significant in cells lacking *Piezo1*. Collectively, these results suggest that fluid flow mechanically activates TRPV4 channels on the primary cilium and independent intracellular Ca^{2+} release, allowing extracellular Ca^{2+} and Ca^{2+} from internal stores to enter the primary cilium microdomain.

2.4.5 Primary cilia-regulated mechanisms of mechanotransduction are different in kidney epithelia and osteocytes

With the suggestion that the osteocyte primary cilia-mediated mechanism of mechanotransduction depends on TRPV4 and not PC2, we conducted similar flow studies with kidney epithelial cells to verify that this difference was due to cell type and not experimental approach. We immunostained IMCD cells for PC2 and found similar localization relative to MLO-Y4 cells (Figure 2.4a). As expected and previously reported, *Pkd2*

knockdown (11.85 ± 0.03% relative to IMCD control mRNA levels, $p<0.005$) blocked steady flow-induced ciliary and cytosolic Ca^{2+} increases in IMCDs, and these differences were statistically significant (Figure 2.4b-g) [Jin et al., 2013]. Consistent with the study by *Jin et al*, IMCD ciliary Ca^{2+} peaks preceded cyotosolic Ca^{2+} increases in all samples ($p<0.005$) [Jin et al., 2013].

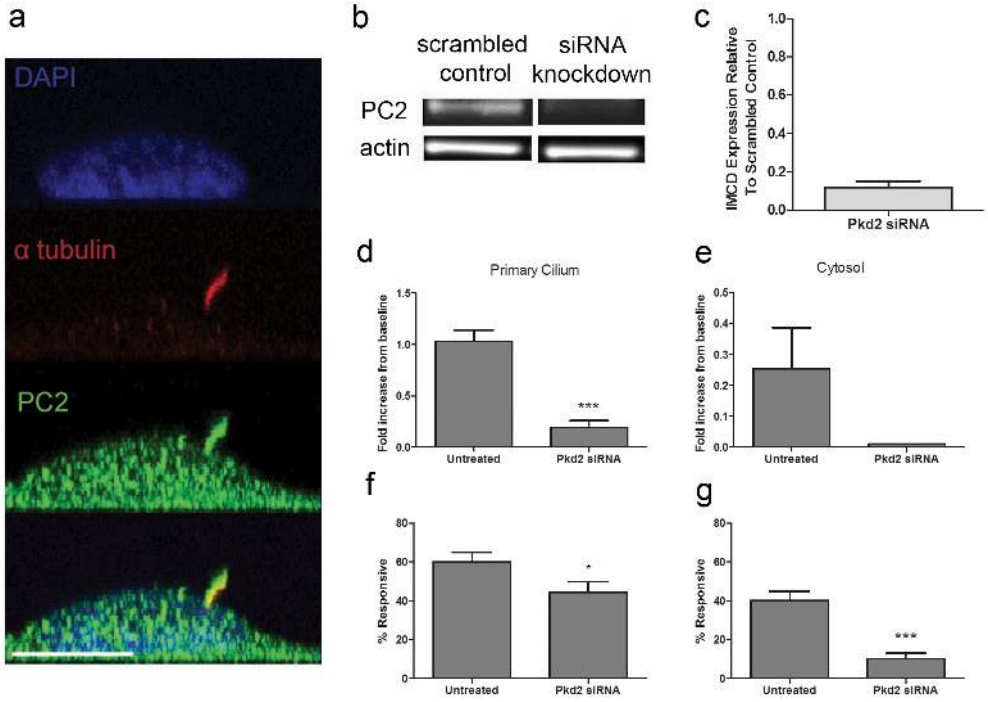

Figure 2.4: PC2 mediates kidney epithelial mechanotransduction. (a) PC2 localizes to IMCD primary cilia and plasma membrane. Scale bar, 10 μm. (b) Western blot of PC2 and actin protein in IMCDs treated with scrambled control or *Pkd2* siRNA. (c) Quantified knockdown of *Pkd2* mRNA expression in IMCD cells treated with siRNA relative to controls (n=4). (d-e) Flow-induced Ca^{2+} increases in responsive cells deficient in *Pkd2* (primary cilium: untreated (n=6), *Pkd2* (n=4), cytosol: untreated (n=4), *Pkd2* (n=1)). (f-g) Percent of IMCD exhibiting flow-induced Ca^{2+} increases (n=9-10). (***, $p<0.0005$; *, $p<0.05$) Error bars show mean ± SEM.

2.4.6 TRPV4 is required for osteocyte mechanotransduction

Next, we were interested in determining if TRPV4 also mediates osteocye mechanotransduction at the transcriptional level in addition to regulating early ciliary Ca^{2+} mobilization. The *Cox-2* gene encodes an enzyme which catalyzes formation of prostaglandin-E_2 (PGE2), an osteogenic cytokine released by osteoblasts and osteocytes in response to mechanical stimulation, and *Cox-2* expression increases correspond to more PGE_2 release [Malone et al., 2007]. After 5 minutes of oscillatory fluid flow stimulation (identical to the imaging experiments) and a rest period of 55 minutes, we isolated and quantified *Cox-2* mRNA expression relative to the endogenous control *Gapdh*. Scrambled siRNA-transfected cells exhibited a flow-induced increase in *Cox-2* mRNA expression levels, and this flow-induced response was blocked in cells lacking *Trpv4* (1.3 ± 0.3 (control) vs. 1.0 ± 0.1 (*Trpv4*) fold increase) (Figure 2.3e). MLO-Y4 cells transfected with scrambled control siRNA and *Trpv4* siRNA expressed similar levels of *Cox-2* mRNA expression at baseline. Interestingly, Piezo1 deficiency did not affect downstream flow-induced changes in Cox-2 mRNA. MLO-Y4 cells transfected with *Piezo1* siRNA demonstrated a 1.4 ± 0.2 fold flow-induced increase in *Cox-2* mRNA expression which was not significantly different from controls although they exhibited lower baseline Cox-2 mRNA expression levels (Figure 2.3f). Taken together, these data suggest that loss of TRPV4, and not PIEZO1, alters osteocyte mechanotransduction at molecular and transcriptional levels.

2.5 Discussion

In this study, we directed a FRET-based Ca^{2+} biosensor to the primary cilium and loaded cells with a nontargeted fluorescent Ca^{2+} indicator dye to resolve the local Ca^{2+} enviornment in the osteocyte primary cilium from the cytosol. We monitored ciliary and cytosolic Ca^{2+} levels using an epifluorescence microscopy system and observed flow-induced Ca^{2+} peaks in both domains. *Trpv4* deficiency reduced flow-induced ciliary Ca^{2+} peaks but did not impair flow-induced cytosolic Ca^{2+} peaks, illustrating that the primary cilium microdomain is distinct from the cytosol. Thapsigargin treatment impaired flow-induced ciliary and cytosolic Ca^{2+} peaks, demonstrating that intracellular Ca^{2+} release and Ca^{2+} entry through TRPV4 are both components of ciliary Ca^{2+} mobilization. In contrast, knockdown of *Pkd2* and *Piezo1* did not affect ciliary or cytosolic Ca^{2+} peaks. Last, we linked the role of TRPV4 in regulating flow-induced ciliary Ca^{2+} mobilization with a downstream osteogenic response at the transcriptional level by determining that flow-induced changes in *Cox-2* expression depend on TRPV4. Collectively, our study demonstrates that the loading-induced ciliary Ca^{2+} mechanism is different between kidney epithelia and osteocytes.

After observing flow-induced Ca^{2+} peaks in both the osteocyte primary cilium and cytosol, we were motivated to identify the source of the ciliary Ca^{2+} peak. To deplete intracellular Ca^{2+} stores, we treated cells with thapsigargin and continued to observe ciliary Ca^{2+} peaks, suggesting that Ca^{2+}-permeable channels on the primary cilium have a role in mediating flow-induced Ca^{2+} entry. However, thapsigargin treatment did lower flow-induced ciliary and cytosolic Ca^{2+} peak magnitudes and responsiveness compared with untreated cells, indicating that intracellular Ca^{2+} release is a component of flow-

induced ciliary Ca^{2+} mobilization in osteocytes. Furthermore, a statistically significant delay in ciliary and cytosolic Ca^{2+} peaks occurred in thapsigargin-treated cells compared with controls. Thus, our data demonstrate that intracellular Ca^{2+} release contributes, in part, to the local primary cilia Ca^{2+} environment and suggests that the primary cilium serves as an important signal integrator.

In this study, we present evidence that fluid flow activates TRPV4 on the primary cilium and mediates Ca^{2+} entry into the primary cilium microdomain but does not trigger CICR. Using immunocytochemistry techniques, we determined that the stretch-activated Ca^{2+}-permeable channel TRPV4 localizes to the primary cilium and plasma membrane. Our flow experiments revealed that *Trpv4* knockdown lowered flow-induced ciliary Ca^{2+} peaks but did not impair cytosolic Ca^{2+} peaks. Unlike kidney epithelia, where Ca^{2+} reportedly enters the primary cilium through PC2 and induces CICR via ryanodine receptor activation, *Trpv4* deficiency in osteocytes did not affect cytosolic Ca^{2+} mobilization [Jin et al., 2013]. This result suggests that the TRPV4-mediated ciliary Ca^{2+} microdomain does not regulate CICR in osteocytes. This is different from astrocytes, where TRPV4-mediated CICR regulates neurovascular coupling in an IP_3R regulated system [Dunn et al., 2013]. It is also possible that other mechanically-activated Ca^{2+} permeable channels compensate for the loss of TRPV4 function in the cytosol, which is consistent with data from this study showing that the loss of *Piezo1* may sensitize cells to flow. Knockdown of each channel did not impair the flow induced cytosolic cytosolic Ca^{2+} response, which suggests that a different mechanism is in play that maintains normal cytosolic Ca^{2+} levels. Taken together, TRPV4's location in an area of high membrane strain on the primary cilium and dependence of

the flow-induced ciliary Ca^{2+} peak on TRPV4 suggest that the primary cilium acts as a Ca^{2+} and mechanical signaling nexus dependent on TRPV4.

Our understanding of primary cilium bending mechanics and mechanical forces on the plasma membrane covering the primary cilium is essential to elucidating the molecular mechanism of mechanotransduction mediated by the primary cilium. Recently, *Young et al* studied the tension force distribution along a primary cilium under flow and suggested that stretch-activated ion channels are likely to be activated and open near the base of the primary cilium where tension force is the highest [Young et al., 2012]. While primary cilia bending is one potential physical event, it is possible that primary cilium deflection is not physiologic and that mechanical loading of the primary cilium occurs in other ways. For example, β-1 integrins are localized to MDCK primary cilia, and β-1 integrins have been implicated in mediating osteocyte mechanotransduction and loading-induced bone formation [Praetorius et al., 2004, Litzenberger et al., 2010, Litzenberger et al., 2009]. Thus, increased membrane tension is not limited to primary cilia bending and may involve primary cilia integrin-extracellular matrix interactions.

We anticipate that TRPV4 will be an attractive pharmacologic target for treating disuse-induced bone loss due to its role mediating osteocyte mechanotransduction and its sensitivity to existing biochemical agents (agonists: 4α-PDD, GSK1016790A, RN1747 and antagonist: RN1734) [Watanabe et al., 2003, Thorneloe et al., 2008, Vincent et al., 2009]. Treatment with TRPV4 agonists and therapies that elongate osteocye primary cilia (lithium chloride, hydrogen sulfide, interleukin-1) to enhance mechanical strain levels may amplify osteogenic responses and prevent disuse-induced bone loss

in patients restricted to bed rest [Wann et al., 2012, Miyoshi et al., 2011, Han et al., 2014]. Interestingly, *Trpv4* is also expressed by osteoclastic lineages, and osteoclast differentiation and function have been shown to dependend on *Trpv4 in vivo* [Mizoguchi et al., 2008, Masuyama et al., 2012, van der Eerden et al., 2013]. Thus, the development of an osteoblastic lineage-specific therapeutic targeting TRPV4 rather than systemic drug therapy would likely be necessary to promote bone formation. Furthermore, *O'Conor et al* have shown that TRPV4 plays a role as a physical transducer in chondrocytes, which may provide insight into functional cartilage tissue engineering approaches [OConor et al., 2014].

While *Jin et al* reported that flow-induced Ca^{2+} mobilization occurs in primary cilia before cytosolic Ca^{2+} increases in the kidney epithelial cells, our flow studies do not demonstrate a clear difference in the timing between ciliary and cytosolic Ca^{2+} peaks in osteocytes [Jin et al., 2013]. This timing similarity could suggest that extracellular Ca^{2+} enters the primary cilium at the same time as distinct cytosolic Ca^{2+} increases. However, the ciliary Ca^{2+} peaks occurred roughly equally before and after cytosolic Ca^{2+} peaks, suggesting that ciliary Ca^{2+} does not trigger cytosolic Ca^{2+} increases. Thus, we are unable to characterize a relationship between ciliary and cytosolic Ca^{2+} peak timing unlike in kidney epithelial cells.

Several other groups have demonstrated that flow-induced ciliary Ca^{2+} mobilization is dependent on PC2 in kidney epithelia [Nauli et al., 2003, Köttgen et al., 2008, Jin et al., 2013]. Our data suggest that flow-induced ciliary Ca^{2+} mobilization is dependent on TRPV4, and not PC2, in osteocytes. We conducted similar flow studies with kidney epithelial cells to verify that this difference was due cell type and not experimental ap-

proach. Our studies with IMCD cells also showed that flow-induced ciliary and cytosolic Ca^{2+} increases depend on PC2. The consistency in our results suggest that the mechanism of mechanotransduction mediated by primary cilia varies across different tissue contexts. Another difference between the MLO-Y4 and IMCD flow studies was the type of flow regime, consisting of oscillatory fluid flow resulting in 10 dynes/cm^2 shear stress for MLO-Y4 cells and steady flow resulting in 5 dynes/cm^2 shear stress for IMCD cells. Previously, *Malone et al* determined that flow-induced Ca^{2+} flux differences in MC3T3-E1 osteoblasts and MDCK kidney cells did not depend on these specific flow regimes which suggests that primary cilium-mediated mechanosensation in osteoblasts and kidney cells are indeed different [Malone et al., 2007]. Thus, the application of different but physiologically relevant mechanical loads was appropriate for elucidating intricacies in the mechanotransduction mechanism in IMCD and MLO-Y4 cells.

In conclusion, this study highlights the specialization of primary cilia mechanisms across different tissue contexts. Here, we demonstrate that mechanically-stimulated ciliary Ca^{2+} mobilization is different between kidney epithelia and osteocytes. Strikingly, the osteocyte primary cilium forms a distinct microdomain from the cytosol during mechanical loading. The primary cilium microdomain may help maintain spatiotemporal organization within the cell which allows numerous molecular mechanisms to occur with just a limited number of signaling molecules. We expect that the Ca^{2+}-permeable channel TRPV4 will be an attractive therapeutic target for bone loss disease because of its location in an area of high membrane strain on the primary cilium, demonstrated role as a physical transducer in osteocytes in this study and chondrocytes in a recent study by *O'Conor et al*, and sensitivity to existing biochemical agents [OConor et al., 2014].

Furthermore, we anticipate that other flow studies on second messenger-mediated pathways in the primary cilium microdomain and loading-induced bone formation studies using mice with an osteocyte-targeted deletion of TRPV4 will elucidate how TRPV4-mediated Ca^{2+} entry in the primary cilium microdomain regulates osteogenic responses to mechanical loads.

Chapter 3

Cyclic AMP in the Osteocyte Primary Cilium

Project Collaborators: Kristen L. Lee, Davide Calebiro, Martin J. Lohse, Christopher R. Jacobs

3.1 Abstract

Cyclic adenosine monophosphate (cAMP) is a ubiquitous second messenger that regulates a broad range of intracellular signaling pathways. In a previous study by our lab, we demonstrated that mechanical loading lowered osteocyte cAMP levels, which was dependent on primary cilia. The osteocyte primary cilium deflects with mechanical stimulation and forms a Ca^{2+} microdomain, however, the local cAMP signaling environment is unknown. In this study, we present the first real-time measurements of flow-induced ciliary and cytosolic cAMP levels in osteocytes. We directed a FRET-based

cAMP biosensor and red single fluorescence Ca^{2+} biosensor to the primary cilium by fusing the biosensor sequences to the primary cilium-specific sequence of *Arl13b* which allowed us to compare cAMP and Ca^{2+} changes within the same cell. Here, we show that fluid flow induces sustained ciliary cAMP increases and cytosolic cAMP decreases. Interestingly, flow-induced ciliary Ca^{2+} levels peak and return to baseline before the maximal cAMP response occurs. Our data suggest that the primary cilium forms a distinct cAMP microdomain protected from the cytosol and serves as a biochemical and mechanical signaling nexus. Ultimately, our study points to the involvement of cAMP-producing adenylyl cyclases (ACs) in primary cilium-mediated mechanosensation, and we believe this work is a launching point for more studies identifying the signals governing AC activity in osteocyte mechanotransduction.

3.2 Introduction

Cyclic adenosine monophosphate (cAMP) is a ubiquitous second messenger that regulates a broad range of processes such as metabolism, differentiation, and proliferation, and actin cytoskeletal dynamics [Sutherland et al., 1972,Perez et al., 2005,Banales et al., 2009,Siddappa et al., 2009,Masyuk et al., 2008]. Adenylyl cyclases (ACs) are a family of enzymes that convert adenosine monophosphate (ATP) into cAMP. cAMP has two effectors, protein kinase A (PKA) and exchange proteins activated by cAMP (Epac), both of which mediate diverse cellular functions [Seino and Shibasaki, 2005]. In a previous study by our lab, we demonstrated that osteocyte cAMP levels decreased with two minutes of fluid flow stimulation and that loss of primary cilia impaired this flow-induced cAMP response [Kwon et al., 2010]. Furthermore, treatment with gadolinium chloride, which blocks stretch-activated Ca^{2+} channels, impaired the flow-induced cAMP response, suggesting that Ca^{2+} entry through mechanically-sensitive Ca^{2+}-permeable channels mediates cAMP changes [Kwon et al., 2010]. The osteocyte primary cilium deflects with mechanical stimulation and forms a Ca^{2+} microdomain, however, the local cAMP signaling environment is unknown.

The primary cilium microdomain is approximately 1/30,000 the size of the cell body and serves as a mechanical signal transducer [Praetorius and Spring, 2003, Praetorius and Spring, 2001]. Interestingly, *Besschetnova et al* showed that increased cAMP levels elongated primary cilia in kidney epithelial and mesenchymal cells [Besschetnova et al., 2010]. In their study, fluid flow decreased intracellular cAMP levels and reduced primary cilium length [Besschetnova et al., 2010]. While it has been suggested that cAMP mediates primary cilia length to minimize overexposure to high mechanical loads, it is

unknown how the primary cilium cAMP microdomain changes with fluid flow stimulation. Understanding the flow-induced cAMP changes within the primary cilium and cytosol may elucidate the role of cAMP in mechanotransduction. Therefore, the objective of this study was to characterize how ciliary cAMP levels change with mechanical stimulation.

Epac1, one of the two Epac isoforms, has a single cAMP binding domain with EC_{50}=2.4 μM [Bos, 2003]. The Epac1-based cAMP sensor, Epac1-camps, is composed of amino acids E157–E316 from the human Epac1 protein flanked by fluorescent proteins YFP and CFP [Börner et al., 2011]. Binding of cAMP to Epac1-camps causes a conformational change that separates CFP from YFP and decreases the resulting FRET signal which is composed of increased CFP and decreased YFP fluorescence. Epac1-camps has several advantages over other biosensors such as faster kinetics and larger dynamic range compared with PKA-based biosensors. Additionally, it is more sensitive to lower concentrations of cAMP relative to the full length Epac-based Indicator for cAMP Using Epac (ICUE, EC_{50}=12.5 μM) which may also have unwanted signaling capabilities [Ponsioen et al., 2004, Violin et al., 2008]. Thus, we used the FRET-based Epac1-camps biosensor to monitor flow-induced ciliary and cytosolic cAMP levels in real-time.

In this study, we directed the Epac1-camps FRET-based biosensor to the primary cilium and detected flow-induced ciliary cAMP increases in contrast to flow-induced cytosolic cAMP decreases within MLO-Y4 cells. Additionally, co-transfection of the genetically encoded single fluorescence Ca^{2+} biosensor (R-CaMP1.07), which contains the circularly permuted red fluorescent protein mApple linked to calmodulin and M13,

allowed us to compare flow-induced changes in ciliary cAMP and Ca^{2+} within the same cells. Our data demonstrate that loading-induced ciliary Ca^{2+} increases preceded ciliary cAMP increases, suggesting that Ca^{2+} regulates cAMP levels within the primary cilium microdomain. Here, we present the first real-time measurements of flow-induced ciliary and cytosolic cAMP changes in osteocytes. Our data suggest that the primary cilium forms a cAMP microdomain that mediates mechanotransduction and points to the involvement of adenylyl cyclases in primary cilium-dependent mechanosensing.

3.3 Materials and Methods

3.3.1 Summary

FRET-based Epac1-camps and single fluorescence Ca^{2+} biosensor, R-CaMP1.07, were directed to the primary cilium using *Arl13b* to detect flow-induced ciliary cAMP and Ca^{2+} changes. Diffusive Epac1-camps was used to monitor flow-induced cytosolic cAMP levels.

3.3.2 Plasmid construction

Drs. Martin Lohse and Davide Calebiro generously provided the *Epac1-camps* plasmid composed of a YFP acceptor, Epac1 cAMP binding region, and CFP donor. Drs. Junichi Nakai and Masamichi Ohkura generously provided the *R-CaMP1.07* plasmid. Drs. Kenji Kontani and Kristen Verhey shared with us the *Arl13b* gene. We fused *Arl13b* to the N terminus of *Epac1-camps* and *R-CaMP1.07* using a 15 amino acid-long flexible linker to form *Arl13b-L-Epac1* (ALE) and *Arl13b-L- R-CaMP1.07* (ALR) [Wang et al., 2005].

3.3.3 Cell culture and transfection

MLO-Y4 osteocyte-like cells were cultured in MEM alpha (Life Technologies) with 5% FBS, 5% CS, and 1% PS at 37°C in 5% CO_2. 1.25 million cells were transfected with 10 μg plasmid by electroporation using the BTX 360 with a single 300 V, 100 Ω, 1000 μF pulse. Transfected MLO-Y4 cells were seeded onto collagen I-coated glass slides (#1.5 glass, Warner Instruments) at a density of 4k cells/cm^2 and cultured for 3 days

in reduced serum containing 2.5% FBS and 2.5% CS.

3.3.4 Imaging flow chamber

Slides were placed in the RC-30 Confocal Imaging Chamber (Warner Instruments) and attached to a syringe containing phenol red-free MEM alpha with 1% FBS and 1% CS. Oscillatory fluid flow was applied to MLO-Y4 cells resulting in 10 dyne/cm^2 shear stress. A separate syringe with 10 μM ionomycin and 10 μM forksolin was connected to the chamber to verify cell viability and show biosensor activation after the initial flow stimulus.

3.3.5 cAMP and Ca^{2+} imaging

Fluorescent samples were imaged on an Olympus IX71 inverted epifluorescence microscope with a 1.30 N.A. 40X oil-immersion objective. Donor excitation was achieved using a xenon lamp with a 430/24 nm filter for Epac1-camps and 577/25 nm filter for R-CaMP1.07. Images were collected using a Quad-View system (QV2, Photometrics) containing 470/28 nm, 530/30 nm, and 641/75 nm emission filters. Cells were left to rest for 20 minutes prior to imaging. During fluid flow studies, baseline signal was recorded for 30 seconds followed by 5 minutes of flow. ALE and ALR images were taken at 2 Hz with 150 msec exposure. Untargeted Epac1-camps signal was taken at 0.5 Hz with 150 msec exposure.

3.3.6 Data analysis

Images were corrected for background and bleedthrough. Average intensity data of a region of interest over time was smoothened using a 1D Savitsky-Golay filter. Peaks were identified by finding local maxima using Matlab. Results are shown as mean ± SEM. Unpaired t-tests (two-tailed) were used to analyze differences between two groups. For all tests, $p < 0.05$ was considered significant.

3.4 Results

3.4.1 Arl13b-linker-Epac1-camps biosensor detects ciliary cAMP

For this study, we developed a novel primary cilium-localized FRET-based Epac1-camps biosensor which was fused to ARL13B at the N terminus followed by a 15 amino acid-long flexible linker (ALE) (Figure 3.1a) [Wang et al., 2005].

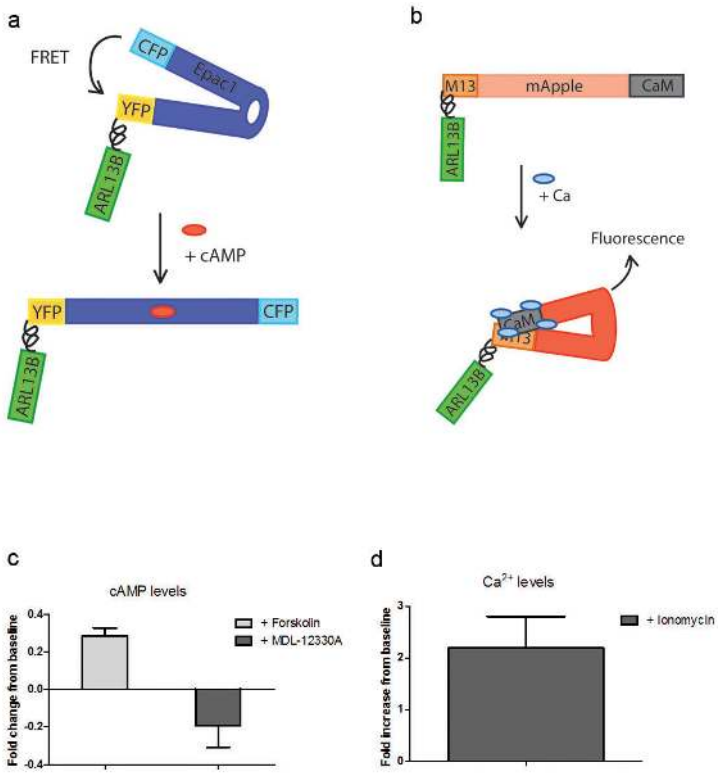

Figure 3.1: ALE localizes to the primary cilium and detects changes in ciliary cAMP levels. (a-b) Schematic of primary cilium-localized cAMP biosensor, ALE, and primary cilium-localized Ca^{2+} biosensor, ALR. (c) cAMP levels change with the addition of AC activator and inhibitor (n=5 (forskolin) or n=3 (MDL-12,330A)). (d) Ca^{2+} levels increase with the addition in ionomycin in media containing 1.8 mM Ca^{2+} (n=4). Error bars show mean ± SEM.

Use of ALE allowed us to detect cAMP levels within the primary cilium distinct from the cytosol. Addition of the AC activator forskolin led to a 28% drop in FRET signal corresponding to increased cAMP, and addition of the AC inhibitor MDL-12,330A led to a 19% increase in FRET signal corresponding to decreased cAMP (Figure 3.1c). We designed Arl13b-linker-R-CaMP1.07 (ALR) with the same primary cilium localization sequence and linker (Figure 3.1b). Addition of 10 μM ionomycin in media containing 1.8 mM Ca^{2+} led to an approximate 220% fold increase in fluorescence (Figure 3.1d).

3.4.2 Ciliary cAMP increases with mechanical stimulation

We co-transfected MLO-Y4 cells with ALE and ALR to monitor ciliary cAMP and Ca^{2+} levels, respectively. Use of a Quad-View beam splitter allowed us to collect images through several emission filters, and we simultaneously captured ECFP and YPet fluorescence followed by mApple fluorescence every 0.5 seconds. Application of 1 Hz oscillatory fluid flow resulting in 10 dynes/cm^2 surface shear stress led to ciliary cAMP increases and a Ca^{2+} peak (Figure 3.2a-b). Interestingly, the flow-induced Ca^{2+} peak was rapid, lasting approximately 25 $\pm$ 2 s, while the flow-induced cAMP increase was more gradual and sustained over 5 minutes of flow compared to the Ca^{2+} response (Figure 3.2c). Additionally, our data show that flow-induced ciliary cAMP levels peak after the Ca^{2+} spike ($p<0.05$) (Figure 3.2d).

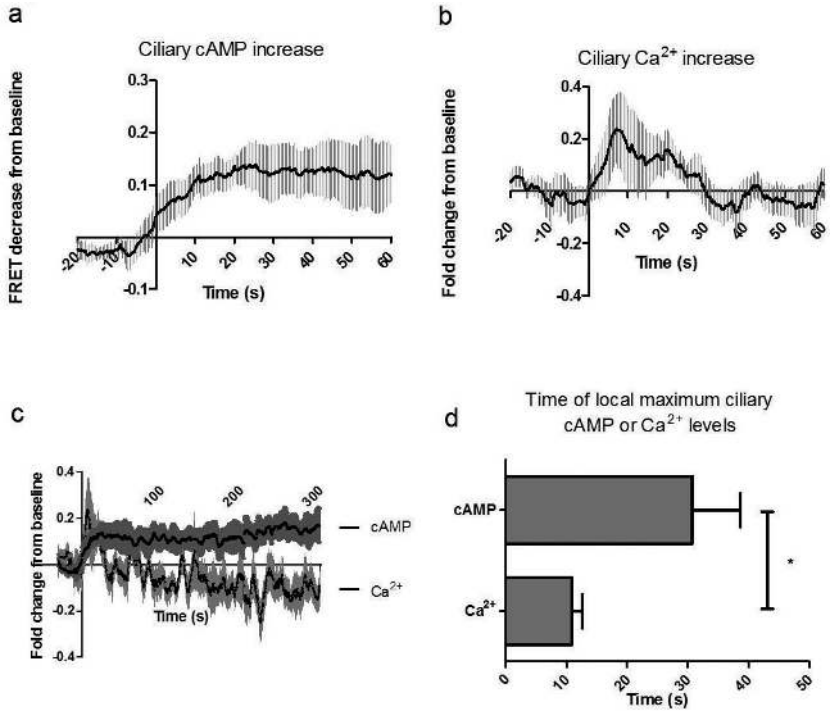

Figure 3.2: Flow-induced ciliary cAMP levels increase after ciliary Ca^{2+}. (a-b) Traces of flow-induced ciliary cAMP and Ca^{2+} increases with flow starting at t = 0 s. (c) The same cAMP and Ca^{2+} traces extended to 5 minutes of flow, demonstrating that the ciliary cAMP increase is sustained over time. (d) Timing of ciliary cAMP and Ca^{2+} peaks after flow onset (n=6 (cAMP) and n=8 (Ca^{2+})). (*, $p<0.05$). Error bars show mean ± SEM (a-d).

3.4.3 Cytosolic cAMP decreases with mechanical stimulation

Flow-induced intracellular cAMP decreases have been reported in kidney epithelial cells and osteocytes, and because our primary cilium-localized cAMP biosensor reported a different flow-induced response, we measured flow-induced cytosolic cAMP levels to verify our experimental approach [Besschetnova et al., 2010, Kwon et al., 2010]. After

transfecting MLO-Y4 cells with untargeted Epac1-camps, we applied oscillatory fluid flow and monitored cytosolic cAMP levels. Fluid flow induced a gradual and sustained decrease in cytosolic cAMP (Figure 3.3a). The peak cytosolic cAMP decrease typically occurred 54 ± 19 s after the start of flow. Although ciliary and cytosolic cAMP measurements were taken in different cells, the average peak ciliary cAMP increase occurred at 31 ± 8 s, and this difference was not significant (p=0.2) (Figure 3.3b).

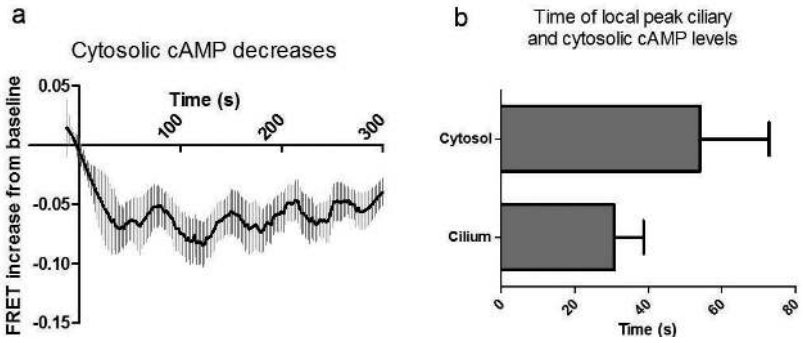

Figure 3.3: Cytosolic cAMP levels decrease during mechanical loading. (a) Traces of flow-induced cytosolic cAMP with flow starting at t = 0 s. (b) Timing of ciliary and cytosolic cAMP peaks after the start of flow (n=9 (ciliary) or n=6 (cytosolic)). Error bars show mean ± SEM.

3.5 Discussion

In this study, we directed a cAMP biosensor and a Ca^{2+} biosensor to the osteocyte primary cilium to characterize the mechanically-loaded ciliary cAMP environment. We monitored ciliary cAMP and Ca^{2+} biosensor signals during flow exposure using an epifluorescence microscopy system and determined that fluid flow mobilized both second messengers. While cAMP levels rose slower than Ca^{2+} changes and remained elevated over 5 minutes of flow, the Ca^{2+} peak returned to baseline within 30 seconds of onset. Additionally, we measured flow-induced cytosolic cAMP changes in real-time using the untargeted cAMP biosensor and found that fluid flow induced a sustained cytosolic cAMP decrease. Here, we demonstrate that the primary cilium forms a distinct cAMP microdomain, and our data suggest that the primary cilium shields ciliary cAMP from cytosolic interactions during mechanical loading.

cAMP microdomains have been detected in several cell types and in multiple subcellular locations such as mitochondria, the nucleus, and near different AC isoforms at the sub-plasma membrane [Zaccolo and Pozzan, 2002, Lefkimmiatis et al., 2013, Zippin et al., 2010, Wachten et al., 2010]. In a recent study, the use of immunoprecipitation and FRET-based biosensors revealed a direct interaction between Ca^{2+}-stimulated AC8, which resides in the lipid raft regions of the plasma membrane, and Orai1, a subunit of store operated Ca^{2+} channels also on the plasma membrane [Willoughby et al., 2012]. In their study, *Willoughby et al* demonstrated that the Orai1 knockdown inhibited local Ca^{2+} increases within the AC8 microdomain and impaired cAMP production by AC8 during store operated calcium entry [Willoughby et al., 2012]. Interestingly, cAMP microdomains at the sub-plasma membrane region lack a physical membrane

barrier and have been shown to contain higher cAMP levels relative to cAMP in the cytosol [Oliveira et al., 2010]. Collectively, these studies show that cAMP microdomains are protected from cytosolic interactions which may be critical for mediating numerous signaling events.

cAMP is only produced by ACs, which indicates that AC activity regulates a wide range of cellular processes including mechanotransduction. AC5 and AC6 are inhibited by physiologic Ca^{2+} levels, which occurs by competitive inhibition for Mg^{2+} binding sites ($K_{d,Ca^{2+}} = 0.2\ \mu M$) [Guillou et al., 1999]. AC1, AC3, and AC8 are activated by Ca^{2+}; however, only AC3, and not AC1 or AC8, is expressed by MLO-Y4 cells [Willoughby and Cooper, 2007, Kwon et al., 2010]. Thus, it is likely that AC3 plays a role in mediating Ca^{2+}-induced cAMP increases within the osteocyte primary cilium. AC3 has been shown to localize to primary cilia in neonatal hippocampal neurons, although it is not clear if this characteristic is shared by osteocytes [Bishop et al., 2007]. Relationships between Ca^{2+} and cAMP have been described by many other groups. For example, synchronous intracellular cAMP oscillations have been associated with Ca^{2+} changes in *Xenopus* embryonic spinal neurons [Gorbunova and Spitzer, 2002]. In their study, *Gorbunova et al* reported that blocking cAMP transients lowered Ca^{2+} spike frequency while raising cAMP levels increased Ca^{2+} oscillation frequency and vice versa. *Gerbino et al* observed sustained cAMP levels coupled with higher frequency Ca^{2+} oscillations in HEK293 cells which is consistent with our measurements in the primary cilium microdomain, and they suggest that cAMP machinery acts as a dampening device for rapid Ca^{2+} transients [Gerbino et al., 2005]. Furthermore, in a study by *Landa et al*, an inverse relationship between Ca^{2+} and cAMP oscillations in β-cells was observed

when Ca^{2+} oscillations were induced, which is consistent with our measurements of flow-induced cytosolic Ca^{2+} and cAMP changes in osteocytes [Landa et al., 2005]. This cAMP-Ca^{2+}cross-talk may provide the opportunity to convey unique signals that regulate a wide range of cellular processes with only a few types of signaling molecules. Additionally, it has been reported that Ca^{2+}oscillation frequency regulates expression of numerous genes, which demonstrates that Ca^{2+}oscillation characteristics create signal specificity [Dolmetsch et al., 1997, Dolmetsch et al., 1998, Li et al., 1998].

In addition to Ca^{2+}inhibition, PKA phosphorylation has been shown to inhibit AC6 [Chen et al., 1997, Sabbatini et al., 2013]. Interestingly, PKA subunits localize to the primary cilium base in mouse embryonic fibroblasts and the primary cilium in cholangiocytes [Tuson et al., 2011, Masyuk et al., 2008]. This localization suggests that the primary cilium could act as a signal release point to the cytosol, in which flow-induced ciliary cAMP increases stimulate PKA activity near the primary cilium base. With elevated activity, PKA could mediate changes in the cytosol such as inhibiting AC6 and decreasing cystosolic cAMP levels. Thus, the genetically-encoded PKA activity biosensor, AKAR, would be useful in future studies [Komatsu et al., 2011]. PKA phosphorylation regulates multiple enzymes and pathways, notably transcription factor cAMP response element-binding protein (CREB) [Delghandi et al., 2005]. CREB binds certain motifs (TGACGTCA and CGTCA) near gene promoters to activate gene targets and increase transcription, and it has been shown to target the bone formation gene marker *Cox-2* [Mayr and Montminy, 2001, Ghosh et al., 2007]. Therefore, examining any flow-induced CREB phosphorylation responses could elucidate how cAMP regulates the primary cilium-dependent mechanism of mechanotransduction.

Our ability to direct a cAMP biosensor to the osteocyte primary cilium has some advantages over the cAMP enzyme-linked immunosorbent assay (ELISA) used previously [Kwon et al., 2010]. First, the Epac1-camps biosensor enabled us to monitor cAMP levels in real-time, in contrast to treating cells with 3-isobutyl-1-methylxanthine (IBMX) to inhibit cAMP breakdown and stopping flow at specific time points before ELISA [Kwon et al., 2010]. While *Kwon et al* detected a transient flow-induced cAMP decrease at the 2 minute time point which recovered at the 5 and 15 minute time points, in this study, we observed a sustained cAMP drop over 5 minutes. A potential reason for the relatively higher cAMP levels after 5 minutes of flow measured by *Kwon et al* is because the cells are exposed to IBMX longer, resulting in cAMP accumulation. A second benefit to using the genetically-encoded cAMP biosensor is the ability to add targeting sequences to biosensor sequence. ELISA does not resolve cAMP levels within the primary cilium from the cytosol since it involves lysing cells to measure intracellular cAMP. In this study, the increased resolution of intracellular cAMP measurements leads to different hypotheses regarding the mechanism of primary cilium-mediated mechanotransduction compared with the study by *Kwon et al.* In particular, while it is likely that Ca^{2+}-inhibited AC6 plays a role in the flow-induced cytosolic cAMP decrease, our results imply that a Ca^{2+}-stimulated AC isoform first mediates the flow-induced ciliary cAMP increase. *Kwon et al* used immunocytochemistry techniques to detect localization of multiple AC isoforms in osteocytes, however, without lateral views of the primary cilium, it is difficult to determine localization of the different AC isoforms. Thus, although *Kwon et* al implicated AC6 on the primary cilium in mediating the flow-induced cAMP decrease, their study lacked subcellular resolution and definitive

immunocytochemistry evidence.

In this study, we show that the primary cilium forms a cAMP microdomain that shields flow-induced ciliary cAMP changes from cytsolic cAMP dynamics. Our data imply that the primary cilium acts as a biochemical and mechanical signaling nexus that potentiates signals contained within the microdomain and suggest that the primary cilium-dependent mechanism of mechanotransduction consists of the following interactions (illustrated in Figure 3.4):

1. Flow-induced ciliary Ca^{2+} increases involving entry through stretch-activated TRPV4 channels and intracellular Ca^{2+}release
2. Ciliary cAMP increases (likely Ca^{2+}-mediated)
3. Cytoslic cAMP decreases (potential PKA and Ca^{2+} inhibition of AC6)
4. Transcriptional activity and osteogenic response (likely mediated by cAMP-dependent pathways)

As described above, AC3 localization to the osteocyte primary cilium has yet to be verified; however, it likely generates the flow-induced Ca^{2+}-mediated cAMP increases in the primary cilium. Furthermore, additional work is required to understand if loading-induced cAMP dynamics regulate PKA activity in the primary cilium leading to downstream osteogenic responses at the transcriptional level. Investigating the role of ACs in primary cilium mechanosensation is attractive due to the multiple modes of AC regulation (Ca^{2+}, PKA, PKC, and G proteins), and we believe this work is a launching point for more studies identifying the molecular mechanisms governing AC activity in osteocyte mechanotransduction.

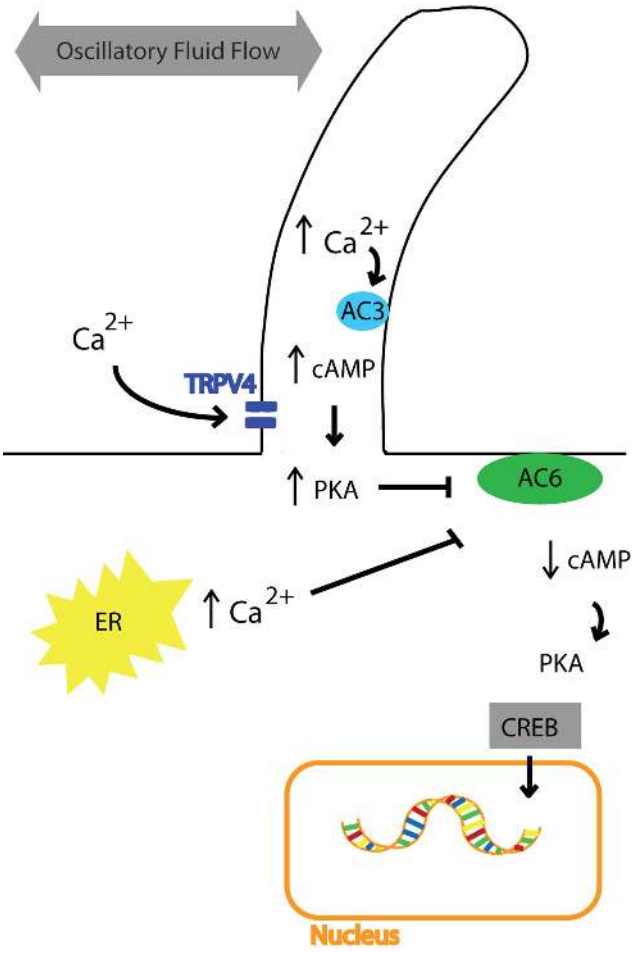

Figure 3.4: Diagram of a potential primary cilium-mediated mechanism of mechanotransduction. Fluid flow induces ciliary Ca^{2+} and cAMP increases We propose that increased Ca^{2+} levels stimulate cAMP production. Then, cAMP-stimulated PKA activity and raised cytosolic Ca^{2+} levels inhibit AC6-mediated cAMP production in the cytosol. Unique loading-induced cAMP dynamics modulate PKA and CREB pathways controlling osteogenic gene transcription.

Chapter 4

Adenylyl Cyclase 6 Mediates Bone Adaptation

Project Collaborators: Kristen L. Lee, David A. Hoey, Milos Spasic, Tong Tang, H. Kirk Hammond, Christopher R. Jacobs

A modified version of this chapter entitled "Adenylyl Cyclase 6 Mediates Loading-Induced Bone Adaptation In Vivo" was published by The Journal of the Federation of American Societies for Experimental Biology in March, 2014.

4.1 Abstract

Primary cilia mediate mechanotransduction in multiple cell types including kidney epithelia, cholangiocytes, and osteocytes. Previously, we demonstrated that adenylyl cyclase 6 (AC6), a membrane-bound enzyme expressed by MLO-Y4 osteocyte-like cells,

may play a role in a primary cilium-dependent mechanism of mechanotransduction *in vitro*. In this study, we examined if AC6 deletion impairs loading-induced bone formation *in vivo*. Skeletally mature mice with a global knockout of AC6 exhibited normal bone morphology and responded to osteogenic chemical stimuli similar to wild-type mice. Following ulnar loading over three consecutive days, bone formation parameters were assessed using dynamic histomorphometry. Mice lacking AC6 formed significantly less bone than control animals (41% lower bone formation rate). Furthermore, primary bone cells isolated from AC6 knockout mice exhibited attenuated flow-induced increases in *Cox-2* mRNA levels compared to controls. Collectively, these data indicate that AC6 plays a role in loading-induced bone adaptation, and these findings are consistent with our previous studies implicating primary cilia and AC6 in a novel mechanism of osteocyte mechanotransduction.

4.2 Introduction

Loading-induced functional adaptation of bone relies on mechanotransduction, the conversion of external physical cues in the local environment into cellular biochemical and transcriptional responses. Osteocytes reside within bone and mediate skeletal adaptation to mechanical loads [Klein-Nulend et al., 1995, Klein-Nulend and Bakker, 2007, Tatsumi et al., 2007]. However, the relevant physical signals, mechanosensors, and mechanisms of mechanotransduction are not well understood [Mullender et al., 2004, Liedert et al., 2006]. Osteocytes, osteoblasts, and most other mammalian cells possess primary cilia, important cellular signaling structures [Jacobs et al., 2010]. Nearly 100 years after the discovery of primary cilia, *Praetorius and Spring* were among the first researchers to demonstrate the mechanosensing ability of primary cilia in kidney epithelial cells [Praetorius and Spring, 2001, Praetorius and Spring, 2003]. Recently, the primary cilium has been implicated in mechanotransduction in skeletal cell types such as chondrocytes and osteocytes [Malone et al., 2007, Kwon et al., 2010, McGlashan et al., 2010, Temiyasathit et al., 2012, Wann et al., 2012].

Adenylyl cyclases are membrane-bound enzymes that convert ATP into cyclic adenosine monophosphate (cAMP), a second messenger [Hanoune and Defer, 2001]. cAMP signal transduction has been implicated in a variety of cellular processes such as the extracellular signal-regulated kinases 1 and 2 and cAMP-response element-binding protein (ERK1/2-CREB) signaling pathway, which mediates osteogenic responses to mechanical stimulation in osteoblasts [Jessop et al., 2001, Ogasawara et al., 2001, Wadhwa et al., 2002]. In a previous study in our lab, *Kwon et al* determined that AC2-7 and AC9 are expressed in osteocytes and reported that AC6 was enriched in the primary cilium

compared with other AC isoforms using immunocytochemistry techniques [Kwon et al., 2010]. Interestingly, the siRNA-mediated knockdown of *Polaris*, a gene necessary for forming functional primary cilia, and the separate knockdown of AC6, both inhibited flow-induced changes in cAMP levels in MLO-Y4 osteoycte-like cells [Kwon et al., 2010]. Furthermore, impairing osteocyte primary cilia formation also attenuated typical flow-induced increases in *Cox-2* mRNA expression [Malone et al., 2007, Kwon et al., 2010]. Strikingly, the knockdown of AC6 also led to a decrease in the levels of flow-induced increases in *Cox-2* mRNA expression, indicating that both AC6 and primary cilia regulate mechanotransduction in osteocytes [Kwon et al., 2010]. Collectively, these data are consistent with a primary cilia-mediated mechanism of mechanotransduction that is dependent on AC6 in osteocytes.

The purpose of this study was to determine if AC6 plays a role in skeletal adaptation *in vivo* using adult AC6 knockout mice. The data in this study suggest that AC6 deletion limits loading-induced bone formation by impairing bone mechanotransduction. These results are consistent with our previous *in vitro* study that implicates primary cilia, AC6, and cAMP second messenger signals in a novel mechanism of bone cell mechanotransduction.

4.3 Materials and Methods

4.3.1 Summary

Mice with a global knockout of AC6 were generated and placed under ulnar compressive loading to induce bone formation. Skeletal morphology and bone microarchitecture characteristics were assessed using microCT. Dissected mouse pup calvariae were digested using collagenase to isolate primary bone cells. Bone formation was induced with BMP-2 treatment *in vitro* and intermittent PTH administration *in vivo*. Primary bone cells isolated from AC6 KO mice and wild-type mice were exposed to fluid flow stimulation, and *Cox-2* mRNA expression levels were quantified. Mechanical loads were placed on mouse ulnae, and loading-induced bone formation parameters were quantified using dynamic histomorphometric analysis.

4.3.2 Animals

Transgenic mice with a C57BL/6 background and a global knockout of AC6 (AC6 KO) were crossed with wild-type (WT) mice to generate heterozygous breeding pairs [Tang et al., 2008]. WT and AC6 KO offspring generated by heterozygous breeding were used for all studies. Tail-biopsy DNA was isolated for genotyping, followed by PCR reactions with primers specific for the AC6 KO allele (5'- GGAGACCTAGAGATGGAGTG-3' and 5'-GCCACTTGTGTAGCGCCAAG-3' and the WT allele 5'-AAGATCTGCTTT GTGGGTGC-3' and 5'-AGCCACTGGCTCGATTCGCGTGGCG-3'. Gel electroporesis of PCR products was used to detect a 2.2 kb-long PCR product for AC6 KO or 550 base-long PCR product for WT. The procedures performed in this study were approved

and in accordance with Columbia University Institutional Animal Care and Use Committee guidelines.

4.3.3 MicroCT analysis

Ulnae and tibiae from 16 week-old mice were dissected and stored at -20°C. Samples were imaged by micro-computed tomography (microCT) (Scanco vivaCT 40; Scanco Medical AG) at 10.5 µm isotropic resolution [Sabsovich et al., 2008]. Bone lengths were determined from scout views. Cortical bone analyses were performed at the ulnar and tibial mid-diaphyses to determine total area, cortical area, cortical thickness (Ct. Th) and minimum and maximum second moments of inertia (I_{min} and I_{max}). Trabecular bone analyses were performed at the tibial proximal metaphysis to determine bone volume/trabecular volume (BV/TV), connectivity density (Conn. D), trabecular number (Tb. N), trabecular thickness (Tb. Th), and trabecular spacing (Tb. Sp).

4.3.4 Primary bone cell isolation

Calvariae from 6-8 day-old neonatal mice were dissected and subject to serial digestions in Dulbecco's Modified Eagle Medium (Life Technologies) containing 2 mg/ml collagenase II (Worthington Biochemical Corp.) at 37°C for 20 minutes in a shaking water bath. Fractions 1-2 were discarded while fractions 3-6 were pooled as primary osteoblasts [Ogasawara et al., 2004]. Following six serial collagenase digestions, fraction 7 was obtained after incubating the calvarial fragments in trypsin/EDTA solution at 37°C for 20 minutes, while fractions 8-9 were subject to collagenase digestions. Fractions 7-9 were pooled as mixed population of primary bone cells consisting of osteoblasts

and osteocytes [Gu et al., 2006]. Bright field microscopy images were acquired on an inverted microscope (CKX41; Olympus) with a 10X air objective on day 4 of culture. In addition to observing stellate morphology in later fractions, we validated osteoblast versus osteocyte cell type by measuring *Dmp1* mRNA expression in cells from fractions 3-6 and fractions 7-9.

4.3.5 Bone morphogenic protein II treatment

An *in vitro* experiment was conducted to investigate if primary osteoblast bone formation was impaired by AC6 deletion. Primary osteoblasts obtained from fractions 3-6 of WT and AC6 KO primary bone cell isolations were seeded at 5,250 cells/cm^2 in 6-well plates and cultured for 5 days in osteoblast media consisting of MEM alpha (Life Technologies) supplemented with 10% FBS, 1% PS, 50 µg/ml ascorbic acid, and 10 mM β-glycerophosphate. On days 6 and 8, fresh osteoblast media containing 250 ng/ml bone morphogenic protein II (BMP-2) (355-BEC; RD Systems) was placed on cells [Lai and Cheng, 2005, Matsubara et al., 2008]. Cell protein was isolated in RIPA buffer and assayed for alkaline phosphatase (ALP) activity (APF; Sigma-Aldrich), and total protein concentrations were determined using the Pierce BCA Protein Assay Kit (Thermo Scientific).

4.3.6 Intermittent PTH administration

To investigate the bone formation of WT and AC6 KO mice, we administered intermittent PTH treatment *in vivo*. WT and AC6 KO female mice at 16 weeks of age were administered parathyroid hormone (PTH) solution, consisting of 20 μl/ml filtered hPTH

(1-34) (80 μg/kg body weight; Bachem) dissolved in PBS with 2% heat-inactivated mouse serum [Ferrari et al., 2005]. Starting on day 1, treatment consisted of daily injections of PTH or vehicle solution for 4 weeks. Calcein (10 mg/kg body weight; Sigma-Aldrich) and alizarin red (70 mg/kg body weight; Sigma-Aldrich) were injected on days 12 and 26, respectively, and mice were sacrificed on day 28 [Elis et al., 2010]. Right ulnae were isolated and processed for dynamic histomorphometric analysis, as described below.

4.3.7 Oscillatory fluid flow

Primary bone cells from fractions 7-9 of the isolation were seeded onto collagen I-coated glass slides at approximately 1,400 cells/cm^2 in MEM alpha (Life Technologies) supplemented with 5% FBS, 5% CS, and 1% PS. After 5 days of culture at 37C and 5% CO_2, cells were approximately 80% confluent. Slides were placed in parallel plate flow chambers (56 $\times$ 24 $\times$ 0.28 mm), incubated for 30 minutes, and then exposed to 1 hour of oscillatory fluid flow at 1 Hz with a peak shear stress of 1 Pa and flow rate of 18.8 ml/min. After flow stimulation, slides were immediately removed from the flow chambers and washed with PBS, and mRNA expression levels were quantified.

4.3.8 mRNA expression levels

RNA was extracted and isolated from cells using TriReagent (Sigma-Aldrich), followed by cDNA synthesis using TaqMan reverse transcriptase (Applied Biosystems). cDNA samples were amplified with *Ac6* (Mm00475772_m1), *Cox-2* (Mm00478374_m1), *Dmp1* (Mm00803833_g1) and *Gapdh* (4352339E) primers and probes (Applied Biosystems)

by quantitative real-time PCR using the ABI PRISM 7900 detection system (Applied Biosystems). Samples and standards were run in triplicate and were normalized to the endogenous *Gapdh* expression. Relative mRNA expression levels between samples were determined using the relative standard curve method.

4.3.9 Strain gauge testing

The forelimbs of 16 week-old WT and AC6 KO mice were isolated and minimally dissected (n=9 WT male and n=8 AC6 KO male, n=9 WT female and n=7 AC6 KO female). A single-element strain gauge (EA-06-015-DJ-120-LE; Vishay Precision Group) was adhered to the medial surface of the ulnar midshaft in the longitudinal direction using MBond adhesive (MB-200; Vishay Precision Group) and connected to a strain gauge signal conditioner (2120B; Vishay Precision Group) and an oscilloscope (MSO6034A; Agilent Technologies). An axial compressive load of 3 N was applied with a 2 Hz sine wave for 30 cycles. The averaged peak-to-peak strain was determined from cycles 10-20.

4.3.10 *In vivo* axial ulnar loading

Mice at 16 weeks of age, consisting of 31 WT mice (16 male and 15 female) and 25 AC6 KO mice (15 male and 10 female), were placed under isofluorane anesthesia. Right forelimbs were placed between two cups attached to an electromagnetic loading system with feedback control (Bose ELF 3220, EnduraTEC, Inc.). After an initial 0.1 N load, a peak compressive load of 3 N was applied with a 2 Hz sine wave for 120 cycles per day on 3 consecutive days. Left forelimbs served as non-loaded internal controls. Body weight

was measured at 16 weeks of age. Mice were subcutaneously injected with calcein (10 mg/kg body weight; Sigma-Aldrich) on day 5 and alizarin red (70 mg/kg body weight; Sigma-Aldrich) on day 9 following initiation of loading. All animals were euthanized on day 15 and prepared for dynamic histomorphometric analysis.

4.3.11 Dynamic histomorphometry

Left and right ulnae were isolated, preserved in ethanol, infiltrated with methyl methacrylate, and embedded in methyl methacrylate and benzoyl peroxide as described previously [Temiyasathit et al., 2012]. Transverse sections of the embedded ulnar midshaft were imaged on a laser scanning confocal microscope (Leica TCS SP5; Leica Microsystems). Measurements of bone perimeter (B. Pm), single label perimeter (sL. Pm), double label perimeter (dL. Pm), and double label area (dL. Ar) were completed with ImageJ and used to calculate mineralizing surface/bone surface (MS/BS=$\frac{\frac{1}{2}sL.Pm+dL.Pm}{B.Pm}\cdot 100$; %), mineral apposition rate (MAR=$\frac{dL.Ar}{dL.Pm}/\#\,days\,between\,labels$; μm per day), and bone formation rate/bone surface (BFR/BS=$\frac{MAR\cdot MS/BS}{3.65}$; μm$^3/\mu$m^2 per year). Relative (r) measurements of rMS/BS, rMAR, and rBFR/BS were determined by subtracting the values of the left ulnae from the right ulnae to show differences due to mechanical loading.

4.3.12 Data analysis

Data are presented as mean ± SEM. The effects of gender and genotype or treatment and genotype were assessed in all measurements using 2-way ANOVA with Bonferroni's multiple comparison post hoc test where appropriate. When gender was a significant

factor, female and male data were analyzed separately. Unpaired t-tests (two-tailed) were used to analyze differences in body weight and bone structure. Dynamic histomorphometric analyses between loaded and non-loaded ulnae were tested for significance using paired t-tests (two-tailed). The corresponding rMS/BS, rMAR, and rBFR/BS values of WT and AC6 KO mice from the loading experiment were analyzed using unpaired t-tests (two-tailed). For all tests, $p < 0.05$ was considered significant.

4.4 Results

4.4.1 Lack of gross morphological and skeletal phenotype in AC6 KO mice

We verified that the body weight and tibial length of AC6 KO mice at 16-weeks of age were not significantly different from WT mice, as originally reported by *Tang et al* with 6-10 month-old mice [Tang et al., 2008]. On average, the body weights of WT and AC6 KO mice were not significantly different for both male and female mice (WT male = 31.1 ± 1.0 g and AC6 KO male = 29.9 ± 1.1 g; WT female = 23.0 ± 0.6 g and AC6 KO female = 23.6 ± 0.6 g). In addition, the ulnar and tibial lengths of control animals and AC6 KO animals were not significantly different (Table B.1). MicroCT analysis was conducted to further examine cortical bone microarchitecture at the ulnar and tibial mid-diaphyses while trabecular bone microarchitecture was examined at the tibial proximal metaphysis. The total area, cortical area, cortical thickness, I_{min}, and I_{max} at the ulnar midshaft of AC6 KO mice were not significantly different from WT mice (Table B.1). The total area, cortical area, I_{min}, and I_{max} of the tibial midsection and the trabecular indices BV/TV, Tb. N, Tb. Th, Tb. Sp, and Conn. D were not significantly different between AC6 KO mice and controls (Table B.1 and Table B.2). Among the static histomorphometric measurements that did not differ between WT and AC6 KO mice, there was one minor difference in skeletal morphology, a 5.9% decrease in cortical thickness at the tibial midshaft in AC6 KO female mice compared to WT female mice that was statistically significant. Collectively, however, these data indicate that there were no substantial differences in the skeletal morphology of young

adult WT and AC6 KO mice. Thus, these results suggest AC6 KO mice do not exhibit a gross morphological or skeletal phenotype.

4.4.2 AC6 deletion does not impair the anabolic response to BMP-2 and PTH treatment

We isolated primary osteoblasts from WT and AC6 KO mice and treated them with BMP-2 to examine osteoblast-mediated bone formation. BMP-2 induced significant increases in intracellular ALP activity relative to total protein concentration in primary osteoblasts of WT mice and AC6 KO mice (Figure 4.1a).

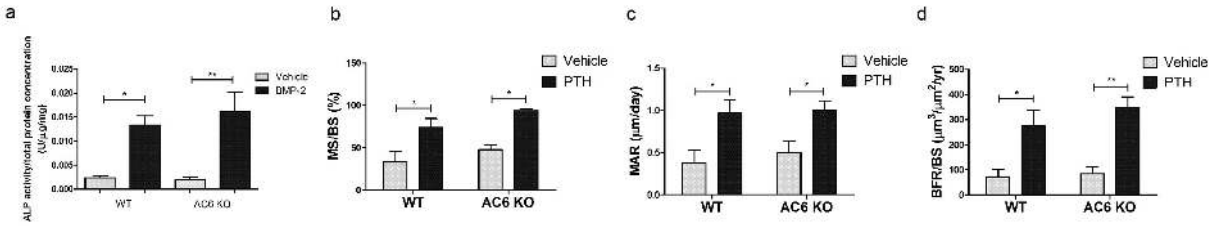

Figure 4.1: Osteogenic chemical agents induce similar bone formation with and without AC6 deletion *in vitro* and *in vivo*. (a) Amount of intracellular ALP activity normalized to total protein concentration in primary osteoblasts isolated from WT mice or AC6 KO mice and cultured with vehicle or BMP-2 (n=6). (b-d) MS/BS, MAR, and BFR/BS measured at the ulnar midshaft of WT and AC6 KO mice injected with PTH or vehicle (n=5). Post hoc analysis using Bonferroni's multiple comparison test indicated significant differences between vehicle and BMP-2 or PTH-treated groups. ($^{*}p < 0.05$, $^{**}p < 0.005$). Error bars show mean ± SEM.

The effect of BMP-2 treatment was significant while there were no significant effects of genotype and treatment-genotype interaction. In the *in vivo* experiment, intermittent

injections of PTH over 28 days (Figure 4.1b-d) led to increases in MS/BS, MAR, and BFR/BS at the ulnar midsection in both WT and AC6 KO mice compared to vehicle treated controls. The effect of treatment on MS/BS, MAR, and BFR/BS was significant while there was no significant effect of genotype or treatment-genotype interaction. Collectively, the results of the bone anabolic treatment experiments indicate that the deletion of AC6 does not disrupt bone formation *per se*.

4.4.3 Attenuated flow-induced increase in *Cox-2* mRNA expression in AC6 KO primary bone cells

Later fractions of cells digested from murine calvariae have been reported to contain a high proportion of primary osteocytes (>60%) [Gu et al., 2006, Stern et al., 2012]. In our hands, primary bone cells isolated in fractions 3-6 generally exhibited cuboidal morphology typical of osteoblasts while primary cells isolated in fractions 7-9 generally exhibited stellate morphology and possessed numerous slender processes typical of osteocytes (Figure 4.2a-b). Furthermore, dentin matrix acidic phosphoprotein 1 (*Dmp1*) is expressed by osteocytes but not by osteoblasts and encodes a noncollagenous protein that is present in the highly mineralized bone matrix [Toyosawa et al., 2001, Gu et al., 2006]. The population of cells isolated in fractions 7-9 expressed more *Dmp1* compared to cells isolated in earlier fractions for both WT and AC6 KO cells, and this difference was significant (Figure 4.2c). Overall, these data suggest that cells pooled from fractions 7-9 of the serial digestion contain a higher proportion of osteocytes compared to earlier fractions; however this method cannot isolate a pure population of osteocytes alone.

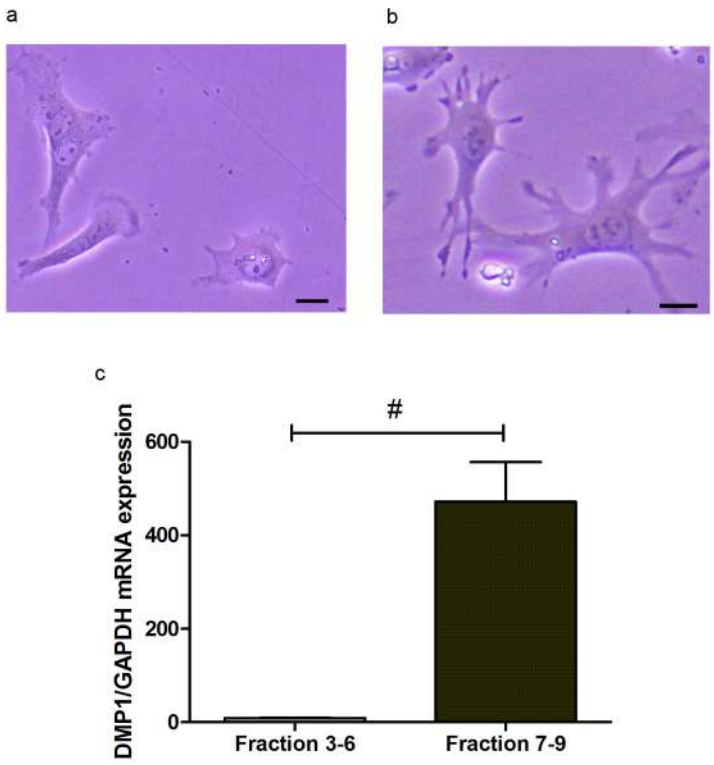

Figure 4.2: Primary bone cells combined from fractions 7–9 exhibit typical osteocyte morphology and express *Dmp1*. (a-b) Bright field images of cells isolated from neonatal calvariae in fractions 3–6 (a) and fractions 7–9 (b) of the serial collagenase digestion. Scale bars = 20 μm. (c) Measurements of *Dmp1* mRNA expression in cells extracted from fractions 3–6 (n=11) were lower than in cells extracted from fractions 7–9 (n=13). ($^{\#}p < 0.0001$). Error bars show mean ± SEM.

Thus, we referred to cells isolated in fractions 7-9 as primary bone cells. As expected, WT primary bone cells expressed *Ac6* mRNA while there was no expression of *Ac6* mRNA in AC6 KO primary bone cells (WT=1.47 ± 0.08 and AC6 KO=0.02 ± 0.01). Following primary bone cell isolation and culture, we exposed the cells to oscillatory fluid flow for 1 hour. There was significant effect of treatment, genotype,

and treatment-genotype interaction of *Cox-2* expression levels, suggesting that loading-induced osteogenic responses depend on AC6. WT primary bone cells exhibited a significant increase in flow-induced *Cox-2* mRNA expression compared to non-flowed cells (2.6 ± 0.2 fold increase). In contrast, there was an attenuated increase in *Cox-2* mRNA expression in AC6 KO primary bone cells in response to flow that was significantly different (1.3 ± 0.1 fold increase) (Figure 4.3). These results imply that primary bone cells lacking AC6 are less mechanosensitive to flow-induced shear stress than WT cells and verify previous work with a siRNA-mediated knockdown of AC6 in MLO-Y4 osteocyte-like cells [Kwon et al., 2010].

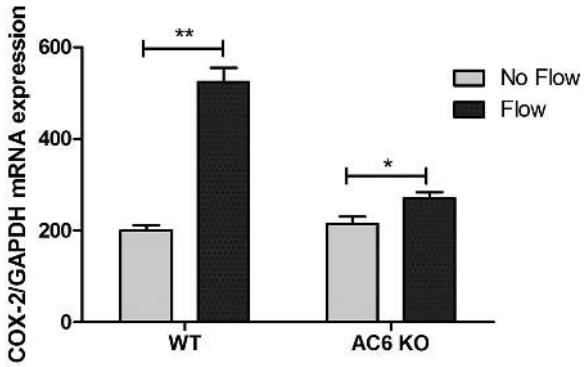

Figure 4.3: 1 hour of oscillatory fluid flow exposure induced *Cox-2* mRNA expression increases in WT (n=5 no flow; n=6 flow) and AC6 KO (n=6 no flow; n=10 flow) primary bone cells. Primary bone cells isolated from AC6 KO mice demonstrate an attenuated flow-induced increase in *Cox-2* mRNA expression compared to control cells. Analysis by 2-way ANOVA identified a significant treatment-genotype interaction, suggesting that the effect of flow depends on AC6. Post hoc analysis using Bonferroni's multiple comparison test indicated significant differences between flow and no flow groups. ($^{*}p < 0.05$, $^{**}p < 0.005$). Error bars show mean ± SEM.

4.4.4 Attenuated loading-induced bone formation in AC6 KO mice

To verify that the strain at the ulnar midshaft experienced by the two mouse groups was not different, we measured strain on the medial surface of the ulnar midshaft of 16-wk-old mice in response to a 3 N peak axial load by strain gauging. At 3 N, average ulnar strain in AC6 KO mice was 8.1% higher in males and 3.7% higher in females compared with WT mice of the same gender (WT male=1782.4 ± 147.0 $\mu\varepsilon$ and AC6 KO male=1927.2 ± 245.1 $\mu\varepsilon$; WT female=2008.6 ± 226.5 $\mu\varepsilon$ and AC6 KO female=2083.5 ± 259.1 $\mu\varepsilon$). The effects of gender, genotype, and gender-genotype interaction on strain were not significant at 3 N by 2-way ANOVA. Thus, we applied the same peak axial compressive force of 3 N to all mice in the ulnar loading experiment. Ulnar loading led to an anabolic response in WT and AC6-KO mice. Right (loaded) ulnae formed significantly more periosteal bone than left (nonloaded) ulnae (Figure 4.4a-d). However, the loading-induced periosteal bone formation response was inhibited in AC6 KO mice. AC6 KO mice exhibited significantly less loading-induced rMS/BS, rMAR, and rBFR relative to WT mice (Figure 4.4e-g and Table 4.1). While genotype had a significant effect on rMS/BS, rMAR, and rBFR, there was no significant effect of gender or gender-genotype interaction on any measure of bone formation by 2-way ANOVA.

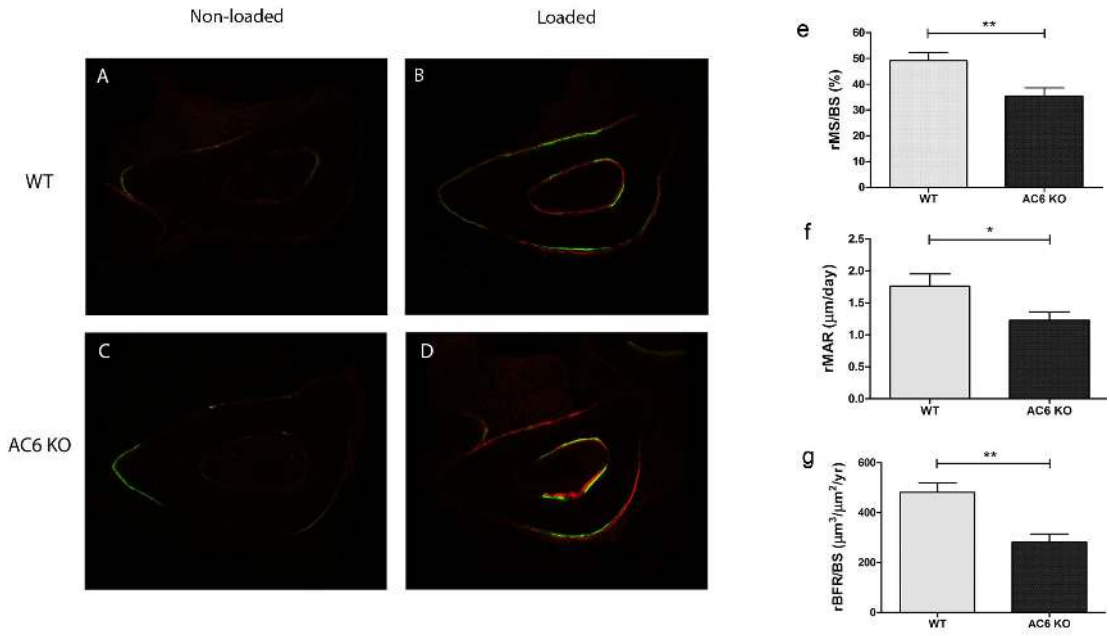

Figure 4.4: Ulnar loading-induced bone formation is attenuated in AC6 KO mice. (a-d) Images of typical nonloaded (left) and loaded (right) ulnae of WT (a,b) and AC6 KO (c,d) mice. (e-g) Relative mineralizing surface over bone surface (rMS/BS, %; (e), mineral apposition rate (rMAR, μm/day; (f), and bone formation rate (rBFR/BS, $\mu m^3/\mu m^2/yr$; (g) at the periosteal surface of mechanically loaded ulnae. AC6 KO mice exhibit 28% less rMS/BS, 30% less rMAR, and 41% less rBFR/BS compared to WT values. ($^{*}p< 0.05$, $^{**}p<0.005$). Error bars show mean $\pm$ SEM.

Genotype and parameter	**Left**	**Right**	**Relative**
WT (n=31)	**nonloaded**	**loaded**	**loaded-nonloaded**
MS/BS (%)	19.2± 2.9	68.4 ± 2.8$^{\#}$	49.1± 3.1
MAR (μm/d)	0.41 ± 0.09	2.18± 0.23$^{\#}$	1.76 ± 0.19
BFR/BS ($\mu m^3/\mu m^2$/yr)	43.5 ± 12.8	524.6 ± 46.1$^{\#}$	481.2 ± 38.8
AC6 KO (n=25)	**nonloaded**	**loaded**	**loaded-nonloaded**
MS/BS (%)	19.2± 4.2	54.6 ± 4.3$^{\#}$	35.4 ± 3.2*
MAR (μm/d)	0.39 ± 0.13	1.62 ± 0.19$^{\#}$	1.23 ± 0.13*
BFR/BS ($\mu m^3/\mu m^2$/yr)	49.2 ± 22.2	331.1 ± 47.7$^{\#}$	281.9± 32.7*

Table 4.1: Parameters of bone formation in loaded and nonloaded ulnae. (*p<0.05 vs. WT control. $^{\#}$p<0.0001 vs. control (nonloaded left ulna)). Data are mean ± SEM.

4.5 Discussion

In this study, we investigated the role of AC6 in bone mechanotransduction *in vivo*. Using high-resolution microCT analysis, we first determined that there is no severe skeletal phenotype in mice with a global deletion of AC6. Additionally, anabolic PTH and BMP-2 treatments stimulated equivalent osteogenic responses with and without AC6 deletion, suggesting that bone formation in AC6 KO mice is not impaired. Next, we determined that the absence of AC6 attenuated flow-induced increases in *Cox-2* mRNA expression in primary bone cells. Using dynamic histomorphometry, we demonstrated that AC6 KO mice form less bone in response to mechanical loads compared to control mice (28% rMS/BS, 30% rMAR, and 41% rBFR/BS less than WT mice). Taken together, these data suggest that a mechanism of mechanotransduction is impaired by AC6 deletion and leads to the loading-induced bone formation defect exhibited by AC6 KO mice. Our study is the first to demonstrate that AC6 is involved in bone functional adaptation *in vivo* and is consistent with our *in vitro* data that link AC6 to the novel primary cilia-mediated mechanism of bone mechanotransduction [Kwon et al., 2010].

We demonstrate here that AC6 deletion impairs loading-induced bone formation *in vivo* and suggest that it is part of a primary cilium-mediated mechanism of mechanotransduction. We previously reported that AC6 knockdown inhibits flow-induced cAMP changes in MLO-Y4 cells [Kwon et al., 2010]. According to *Kwon et al*, this response to flow was characterized by a transient decrease in intracellular cAMP at 2 minutes of mechanical stimulation and is potentialy regulated by flow-induced Ca^{2+} mobilization. Ca^{2+} signaling is dynamic and spatiotemporal, making it a versatile signal that is not characterized by sustained increases or decreases alone [Berridge et al.,

2003]. Thus, specific loading-induced Ca^{2+}-dependent cAMP signaling patterns may mediate bone formation. Through protein kinase A activation, cAMP regulates complex cellular processes such as the ERK1/2-CREB pathway which mediates proliferation and differentiation in osteoblasts [Kaiser and Chandrasekhar, 2003, Yang et al., 2008]. Mechanical stress has been shown to increase ERK1/2 and CREB activation, and these responses could be mediated by loading-induced cAMP signals that are generated by the Ca^{2+}-inhibited AC6 [Schmidt et al., 1998, You et al., 2001a, Husse and Isenberg, 2010]. Thus, AC6 deletion may have impaired this cAMP-dependent mechanism of mechanotransduction within bone, resulting in attenuated loading-induced bone formation. Furthermore, the osteocyte primary cilium microdomain potentially enhances these early signaling kinetics. The findings in this thesis suggest that a distinct primary cilium microdomain exists, and it may foster an environment in which signaling mechanisms are protected from cytosolic interactions.

Recently, a study by *Temiyasathit et al* demonstrated that primary cilia are important for the regulation of loading-induced bone formation *in vivo [Temiyasathit et al., 2012]*. *Kif3a* is an intraflagellar motor protein unit necessary for primary cilia formation and regulates postnatal osteoblast function [Qiu et al., 2012]. *Cola1(I) 2.3-Cre;Kif3a(fl/fl)* mice, which possess an osteoblast and osteocyte-specific deletion of *Kif3a* driven by the *Cola1(I)* promoter, form less bone in response to ulnar loading compared with control mice [Temiyasathit et al., 2012]. Kif3a cKO and AC6 KO mice demonstrate similar defects in loading-induced bone formation which suggests that AC6 and primary cilia are part of the same mechanism of mechanotransduction. Both bone-specific Kif3a cKO mice and AC6 KO mice exhibit approximately 30% less rMAR and

30-40% less rBFR/BS than control mice [Temiyasathit et al., 2012]. Together, the lack of a skeletal phenotype and the attenuated loading-induced bone formation in *Cola1(I) 2.3-Cre;Kif3a(fl/fl)* animals relative to control animals are consistent with AC6 KO mice as described in this study [Temiyasathit et al., 2012].

The absence of a skeletal phenotype in AC6 KO mice might immediately suggest that AC6 does not play a role in skeletal development or mechanotransduction. While the bone architecture measurements in this study were collected at 16 weeks of age, these measurements do not encompass the skeletal development and growth phases of the AC6 KO mice. Thus, phenotypic changes manifest in earlier time points may have gone unobserved. Therefore it is possible that mice lacking AC6 may possess a skeletal phenotype that recovers by young adulthood. However, several other knockout mouse models also do not demonstrate any bone architectural defects but exhibit significantly different responses to mechanical loading. For instance, mice that are deficient in osteopontin, a phosphoprotein secreted by osteoblasts, develop normally but do not exhibit unloading-induced bone loss and form less parietal bone in response to tensile mechanical stress compared to control animals [Salih et al., 1996, Ishijima et al., 2001, Morinobu et al., 2003]. Similarly, *Cola1(I) 2.3-Cre;β1-integrin(fl/fl)* conditional knockout mice do not demonstrate a skeletal phenotype but do exhibit lower rates of loading-induced bone formation compared to control mice [Litzenberger et al., 2009]. The absence of a skeletal phenotype and the normal bone formation exhibited by AC6 KO mice imply that any changes seen in loading-induced bone formation are potentially due to differences in mechanotransduction rather than differences in pre-existing bone structure or osteogenesis ability. One potential explanation for this finding is that mechanotrans-

duction regulating development occurs by different mechanisms and/or there are several compensatory mechanisms utilized during different types of loading. Another potential reason for the lack of skeletal phenotype in AC6 KO mice is that mice do not have osteonal bone or secondary bone structure, suggesting that mouse skeletal morphology is more a result of development and growth rather than remodeling as experienced in humans. Thus, the application of extrinsic loads is needed to demonstrate differences in bone modeling and adaptation. In this study, we applied compressive loads resulting in high physiologic cortical bone strains to stimulate loading-induced bone adaptation, and there was a significant difference in the impaired bone formation response of AC6 KO mice compared with WT mice [Lee et al., 2002].

To determine whether the decrease in loading-induced bone formation in AC6 KO mice occurred because the deletion inhibits a signaling mechanism of mechanotransduction or whether the deletion impairs osteoblast bone formation, we treated AC6 KO mice with osteogenic chemical agents. BMP-2 initiates bone formation by mediating transcription of osteogenic genes such as type I collagen, osteocalcin, osteopontin, and alkaline phosphatase [Cheng et al., 2001]. BMP-2 treatment of primary osteoblasts isolated from WT and AC6 KO animals led to increased intracellular ALP activity, which suggests that osteoblast function remains normal with AC6 deletion. Additionally, intermittent PTH administration induces periosteal bone formation mainly by inhibiting osteoblast apoptosis and stimulating osteoblast activity [Jilka et al., 1999, Masi and Brandi, 2004, Jilka, 2007, Jilka et al., 2009]. We demonstrated that intermittent PTH administration led to increases in cortical bone formation in WT and AC6 KO mice at the ulnar midpoint, the same site which exhibited a loading-induced bone forma-

tion defect in AC6 KO mice. At both cellular and tissue levels, the results of BMP-2 and PTH treatments suggest that osteogenesis is not impaired in AC6 KO mice. Collectively, these results indicate that AC6 plays a role in bone mechanotransduction rather than in general bone formation or development. While this study shows that AC6 is an important enzyme mediating loading-induced bone formation, further work is needed to fully understand how AC6 is involved. Specifically, since there is evidence that osteocytes, osteoblasts, and bone marrow cells all contribute to regulating mechanically induced bone adaptation, use of cre-lox recombination in new mice to isolate the AC6 deletion will be crucial to elucidate which cell types posses an AC6-dependent mechanism of mechanotransduction.

In summary, we demonstrated that AC6 mediates bone formation in response to anabolic mechanical loading *in vivo*. While AC6 KO mice exhibited reduced loading-induced bone formation relative to control mice, at the same time point, the lack of AC6 did not impact adult bone geometry and microarchitecture or impair the response to osteogenic agents. This finding is significant because it suggests that adult bone adaptation is regulated by the primary cilium through an AC6-dependent mechanism. Investigating the role of AC6, other components enriched in the primary cilium microdomain, and other mechanisms of mechanotransduction will collectively elucidate how cells in bone respond to mechanical stimuli.

Chapter 5

Conclusion

5.1 Summary

The primary cilium is an antennae-like nonmotile structure that is required for loading-induced osteogenic responses *in vitro* and loading-induced bone formation *in vivo*. The broad objective of these studies was to elucidate how the osteocyte primary cilium mediates mechanotransduction. Specifically, our goal was to determine if the osteocyte primary cilium forms a microdomain that serves as a biochemical and mechanical signaling nexus. Collectively, the studies comprising this work utilized a range of molecular biology, imaging, and mechanical loading techniques to show that loading induces primary cilium-restricted second messenger changes that mediate osteogenic responses *in vitro* and *in vivo*. Our data suggest that the primary cilium forms a $Ca^{2+}$and cAMP microdomain in response to mechanical loading, which likely creates signal specificity. This primary cilium-mediated mechanism of mechanotransduction may involve loading-

induced Ca^{2+} entry through TRPV4 channels on the primary cilium and AC-mediated cAMP signal transduction, leading to downstream osteogenic transcriptional changes.

5.1.1 Calcium in the Osteocyte Primary Cilium

In our first study, we examined the initial flow-induced ciliary Ca^{2+} increase which was distinct from the cytosolic Ca^{2+} increase in osteocytes. Ca^{2+} regulates numerous signaling pathways and is one of the earliest responses elicited by mechanically-loaded osteocytes. However, whether or not the local Ca^{2+} environment in the primary cilium is distinct from general cytosolic levels during mechanical loading is unknown. Using the primary cilium-specific sequence *Ar1l3b*, we directed a FRET-based Ca^{2+} biosensor to the primary cilium. With this tool, we determined that intracellular Ca^{2+} release is a component of flow-induced ciliary Ca^{2+} mobilization. A second extracellular Ca^{2+}component was identified using siRNA-mediated knockdown of three stretch-activated Ca^{2+}-permeable channels: Polycystin 2 (PC2), Transient Receptor Potential Vanilloid 4 (TRPV4), and PIEZO1. We demonstrated that TRPV4 mediates flow-induced ciliary Ca^{2+} increases and osteogenic responses *in vitro*. Interestingly, TRPV4 played a major role in flow-induced ciliary Ca^{2+} mobilization but not in cytosolic Ca^{2+}. Another study on kidney epithelia primary cilia suggests that fluid flow opens different mechanically-gated ciliary machinery involving PC2, through which Ca^{2+} enters and is critical for triggering intracellular Ca^{2+} release [Jin et al., 2013]. Our study demonstrates that the primary cilium-mediated mechanism of mechanotransduction varies in different tissue contexts. Furthermore, our data demonstrate that the primary cilium forms a Ca^{2+} microdomain that is distinct from cytosolic Ca^{2+}mobilization during

mechanical loading.

5.1.2 Cyclic AMP in the Osteocyte Primary Cilium

Cyclic AMP (cAMP) is another second messenger that also regulates a broad range of intracellular signaling pathways. Flow-induced decreases in intracellular cAMP have been reported by several labs. [Kwon et al., 2010, Besschetnova et al., 2010, Masyuk et al., 2006] The osteocyte primary cilium deflects with mechanical stimulation and forms a Ca^{2+} microdomain; however, the local cAMP signaling environment is unknown. In the second study of this thesis, we targeted a FRET-based cAMP biosensor to the primary cilium and demonstrated that flow stimulation induces ciliary cAMP increases and cytosol cAMP decreases. Additionally, we developed a different primary cilium-localized genetically encoded Ca^{2+} indicator to monitor ciliary Ca^{2+} and cAMP levels simultaneously and found that mechanically-induced ciliary Ca^{2+} peaks preceded ciliary cAMP increases. An interpretation of these data is that Ca^{2+} regulates cAMP levels within the primary cilium microdomain and cytosol, potentially via activation and inhibition of different adenylyl cyclase (AC) enzymes which produce cAMP. Collectively, the use of primary cilium-localized Ca^{2+} and cAMP biosensors have demonstrated that the primary cilium forms a microdomain that is a nexus of biochemical and mechanical signals.

5.1.3 Adenylyl Cyclase 6-Mediated Bone Adaptation

In the third study, we tested a potential mechanism of mechanotransduction involving an adenylyl cyclase in an *in vivo* loading model. Previously, we suggested that adenylyl

cyclase 6 (AC6), a Ca^{2+}-inhibited enzyme, has a role in the primary cilium-dependent mechanism of osteocyte mechanotransduction *in vitro*. Using mice with a global AC6 deletion, we showed that AC6 deficiency impaired loading-induced bone formation. AC6 deficient mice exhibited normal bone architecture and responded to osteogenic chemical stimuli similar to wild-type mice. Interestingly, a similar loading-induced bone adaption defect occurs in mice with with an osteoblast and osteocyte specific knockout of the primary cilia-forming motor unit *Kif3a*. Taken together, our studies provide evidence at the molecular, transcriptional, and tissue level suggesting that a primary cilium-mediated mechanism involving Ca^{2+}-inhibited AC6 plays a role in osteocyte mechanotransduction.

5.2 Future Studies

This thesis demonstrates that the primary cilium forms a microdomain distinct from the cytosol that functions as a nexus of mechanical force and Ca^{2+} and cAMP signals and mediates loading-induced osteogenic responses. With the completion of this work, we have identified other potential components of this signaling mechanism, and here, we describe some additional studies that would further elucidate the intricacies of this primary cilium-mediated osteocyte mechanotransduction pathway.

5.2.1 Role of Ca^{2+} in mediating flow-induced cAMP changes

In our first study, we demonstrated that flow-induced ciliary Ca^{2+} increases were dependent on TRPV4, a stretch-activated Ca^{2+}-permeable channel on the primary cilium. In

our second study, we observed that fluid flow exposure produced ciliary cAMP increases which reached a maximum height after the flow-induced ciliary Ca^{2+} peak returned to baseline. These results suggest that cAMP levels are regulated by the flow-induced Ca^{2+} increase. Thus, the goal of a future study would be to verify that upstream flow-induced Ca^{2+} mobilization mediates downstream cAMP responses. In addition to TRPV4-mediated Ca^{2+} entry, there was an intracellular Ca^{2+}release component to the flow-induced ciliary Ca^{2+} peak, both of which may regulate cAMP levels. To investigate Ca^{2+}-dependent changes in cAMP, it would be important to assess if blocking TRPV4 and impairing intracellular Ca^{2+}release reduce flow-induced ciliary cAMP increases. A second goal would be to identify the Ca^{2+}-regulated enzyme(s) that generates ciliary cAMP. Ca^{2+}-activated AC3 has been observed in kidney epithelia primary cilia, and interestingly, osteocytes only express AC3 and do not express the other Ca^{2+}-stimulated isoforms AC1 and AC8 [Bishop et al., 2007, Ou et al., 2009, Kwon et al., 2010]. Therefore, it is likely that AC3 mediates the observed flow-induced ciliary cAMP increase. Collectively, determing if AC3 localizes to the osteocyte primary cilium and assessing the effect of AC3 deficiency on flow-induced ciliary cAMP responses would demonstrate if AC3 has a role in the primary cilium-regulated mechanism of mechanotransduction.

5.2.2 Role of cAMP-dependent pathways in loading-induced osteogenesis

In this thesis, we suggest that initial flow-induced Ca^{2+} and cAMP signals mediate downstream osteogenic transcriptional changes via cAMP-dependent processes including PKA activation and CREB phosphorylation. Over the past 30 years, several groups

have demonstrated that PKA is enriched in the centrosome of epithelial, fibroblastic, and brain cells, and potentially serves as a regulator of Hedgehog signaling by directing Gli protein distribution in the primary cilium [Barzi et al., 2010, Tuson et al., 2011, Nigg et al., 1985, De Camilli et al., 1986]. PKA accumulation at the primary cilium base implies that PKA activity is sensitive to high concentrations of cAMP in the primary cilium. Our ability to monitor PKA activity in parallel with cAMP dynamics would improve our understanding of cAMP-dependent signal transduction within the osteocyte primary cilium. A FRET-based A kinase Activity Reporter (AKAR), which binds phosphorylated PKA substrate, was previously targeted to lipid raft and non-raft microdomains of the plasma membrane and used to determine that PKA activity is differentially regulated in those compartments [Depry et al., 2011]. Thus, monitoring PKA activity in the primary cilium and cytosol using AKAR would demonstrate if flow-induced PKA activity differs in these regions and if PKA activity is part of the primary cilium-mediated mechanism of mechanotransduction [Bogard et al., 2012, Crossthwaite et al., 2005].

Although PKA regulates multiple enzymes and pathways, CREB phosphorylation is particularly interesting because it has been shown to promote transcription of *Cox-2*, an osteogenic marker [Ghosh et al., 2007, Ogasawara et al., 2001]. The application of fluid flow generates increased *Cox-2* mRNA levels, and the knockdowns of *Trpv4* and *Ac6* impair this response suggesting that TRPV4, AC6, and CREB phosphorylation are involved in a mechanism of mechanotransduction. Fitting with this thesis's fluorescent biosensor motif, a FRET-based CREB phosphorylation biosensor has been created, indicator of CREB activation due to phosphorylation (ICAP), and would be useful

for monitoring CREB phosphorylation levels in real-time [Friedrich et al., 2010]. Together, the spatiotemporal characteristics of PKA activity and CREB phosphorylation in mechanically-loaded osteocytes may be captured using AKAR and ICAP. Finally, determining if the loss of *Trpv4, Ac3,* and *Ac6* impair PKA activity and CREB phosphorylation dynamics would confirm the proposed primary cilium-regulated mechanism of mechanotransduction.

5.2.3 Role of a primary cilium-mediated Ca^{2+}-independent mechanism of mechanotransduction

While the work in this thesis focused on a mechanism involving loading-induced opening of stretch-activated ion channels localized to the primary cilium, it is possible that this process is separate or acts in concert with other primary cilium-mediated Ca^{2+} independent mechanisms of mechanotransduction. In particular, several groups have demonstrated that the cytoskeleton plays a role in mechanotransduction and that cytoskeletal dynamics affect primary cilium length [Kim et al., 2010,Sharma et al., 2011]. Thus, it is likely that as the cytoskeleton distributes mechanical loads in the cell, it directly transmits force to the primary cilium and affects primary cilium mechanics. Pharmacologic cytoskeletal stabilizers and de-stabilizers enable modification of cytoskeletal dynamics: cytochalasin D and latrunculin prevent actin filament formation; phalloidin stabilizes actin; nocodazole and colchicine impair microtubule polymerization; and taxol and epothilone B stabilize microtubules. A combination of modeling primary cilium bending and cytoskeletal mechanical properties and experiments investigating the effects of pharmacologically-modified cytoskeletal dynamics on primary cilia mechanics will

elucidate the cytoskeleton's role in the primary cilium-mediated mechanism of mechanotransduction.

A second Ca^{2+}-independent mechanism of mechanotransduction may involve G protein-mediated regulation of cytoskeletal dynamics and modulation of cAMP signaling. G proteins are components of G protein coupled receptors (GPCRs), and are important for initiating intracellular signalling cascades [Oldham and Hamm, 2008]. The group of GPCR-associated G proteins is classified as a heterotrimeric G protein complex which comprises of α, β, and γ subunits [Downes and Gautam, 1999]. Once the GPCR is activated by a ligand, the GTPase domain of the α subunit (Gα) is exposed and binds GTP, triggering the dissociation of Gα. Gα subunits can be classified into four familys, including stimulatory $G_s\alpha$ and inhibitory $G_i\alpha$ which can regulate AC activity [Hanoune and Defer, 2001]. Thus, it is important to investigate if Gα levels are mechanically regulated and if they mediate a cAMP-dependent mechanism of osteocyte mechanotransduction. Interestingly, *Gudi et al* reported that fluid flow increased G protein activation in endothelial cells within one second of flow onset, demonstrating that G proteins are mechanically-activated [Gudi et al., 1996]. Additionally, the monomeric Rho-family of small GTPases, part of a different class of G proteins, has been shown to regulate cytoskeletal dynamics, such as microtubule stabilization, actin polymerization, and actin contractility, which demonstrates that G proteins mediate cytoskeleton-dependent mechanosensation [Spiering and Hodgson, 2011]. Thus, determining if G proteins have a role in mediating flow-induced AC activity would be critical to fully understanding the mechanotransduction mechanism regulated by primary cilia.

5.3 Significance

We categorize the significance of this work into two areas. First, with our improved understanding of the primary cilium as a microdomain that mediates the conversion of mechanical stimuli into biochemical signals, our research can enhance the development of osteoporosis therapies and tissue engineering methods. Since the primary cilium acts as a mechanosensor, pharmacologic treatments that sensitize the primary cilium to mechanical stimuli such as increasing ciliary length or activating primary cilium-localized mechanosensing machinery (TRPV4 and potentially AC3) would elevate osteogenic responses to insufficient mechanical loads. Additionally, dynamic loading has been shown to improve the functional qualities and architecture of engineered tissue in cartilage and bone bioreactor systems. Therefore, manipulating known mechanotransduction signaling pathways, like the primary cilium-mediated mechanism, may help promote and maintain tissue phenotypes.

Second, this thesis highlights the role of the primary cilium microdomain in mediating cellular processes. The primary cilium constitutes 1/30,000 of the cell volume; however, despite its size, the loss of this tiny cellular structure drastically compromises the cell's ability to sense and transduce chemical and mechanical signals. Here, we show that the primary cilium shields second messenger signals from the rest of the cell during mechanotransduction as a microdomain, similar to lipid rafts, the endoplasmic reticulum, the nucleus, and mitochondria [Alonso et al., 2006, Pani and Singh, 2009, Parry et al., 2005].

Bibliography

[Ajubi et al., 1999] Ajubi, N., Klein-Nulend, J., Alblas, M., Burger, E., and Nijweide, P. (1999). Signal transduction pathways involved in fluid flow-induced pge2 production by cultured osteocytes. *American Journal of Physiology-Endocrinology and Metabolism*, 276(1):E171–E178. 2.2

[Alonso et al., 2006] Alonso, M. T., Villalobos, C., Chamero, P., Alvarez, J., and García-Sancho, J. (2006). Calcium microdomains in mitochondria and nucleus. *Cell calcium*, 40(5):513–525. 5.3

[Baik et al., 2013] Baik, A. D., Qiu, J., Hillman, E., Dong, C., and Guo, X. E. (2013). Simultaneous tracking of 3d actin and microtubule strains in individual mlo-y4 osteocytes under oscillatory flow. *Biochemical and biophysical research communications*, 431(4):718–723. 2.4.2

[Banales et al., 2009] Banales, J. M., Masyuk, T. V., Gradilone, S. A., Masyuk, A. I., Medina, J. F., and LaRusso, N. F. (2009). The camp effectors epac and protein kinase a (pka) are involved in the hepatic cystogenesis of an animal model of autosomal recessive polycystic kidney disease (arpkd). *Hepatology*, 49(1):160–174. 3.2

[Barzi et al., 2010] Barzi, M., Berenguer, J., Menendez, A., Alvarez-Rodriguez, R., and Pons, S. (2010). Sonic-hedgehog-mediated proliferation requires the localization of pka to the cilium base. *Journal of cell science*, 123(1):62–69. 5.2.2

[Berridge et al., 2003] Berridge, M. J., Bootman, M. D., and Roderick, H. L. (2003). Calcium signalling: dynamics, homeostasis and remodelling. *Nature Reviews Molecular Cell Biology*, 4(7):517–529. 1.5, 4.5

[Besschetnova et al., 2010] Besschetnova, T. Y., Kolpakova-Hart, E., Guan, Y., Zhou, J., Olsen, B. R., and Shah, J. V. (2010). Identification of signaling pathways regulating primary cilium length and flow-mediated adaptation. *Current Biology*, 20(2):182–187. 1.4, 3.2, 3.4.3, 5.1.2

[Bishop et al., 2007] Bishop, G. A., Berbari, N. F., Lewis, J., and Mykytyn, K. (2007). Type iii adenylyl cyclase localizes to primary cilia throughout the adult mouse brain. *Journal of Comparative Neurology*, 505(5):562–571. 1.5, 3.5, 5.2.1

[Bogard et al., 2012] Bogard, A. S., Adris, P., and Ostrom, R. S. (2012). Adenylyl cyclase 2 selectively couples to e prostanoid type 2 receptors, whereas adenylyl cyclase 3 is not receptor-regulated in airway smooth muscle. *Journal of Pharmacology and Experimental Therapeutics*, 342(2):586–595. 5.2.2

[Börner et al., 2011] Börner, S., Schwede, F., Schlipp, A., Berisha, F., Calebiro, D., Lohse, M. J., and Nikolaev, V. O. (2011). Fret measurements of intracellular camp concentrations and camp analog permeability in intact cells. *Nature protocols*, 6(4):427–438. 3.2

[Bos, 2003] Bos, J. L. (2003). Epac: a new camp target and new avenues in camp research. *Nature Reviews Molecular Cell Biology*, 4(9):733–738. 3.2

[Bruder and Caplan, 1990] Bruder, S. and Caplan, A. (1990). Terminal differentiation of osteogenic cells in the embryonic chick tibia is revealed by a monoclonal antibody against osteocytes. *Bone*, 11(3):189–198. 1.2

[Cardoso et al., 2009] Cardoso, L., Herman, B. C., Verborgt, O., Laudier, D., Majeska, R. J., and Schaffler, M. B. (2009). Osteocyte apoptosis controls activation of intracortical resorption in response to bone fatigue. *Journal of Bone and Mineral Research*, 24(4):597–605. 1.2

[Castillo et al., 2012] Castillo, A. B., Blundo, J. T., Chen, J. C., Lee, K. L., Yereddi, N. R., Jang, E., Kumar, S., Tang, W. J., Zarrin, S., Kim, J.-B., et al. (2012). Focal adhesion kinase plays a role in osteoblast mechanotransduction in vitro but does not affect load-induced bone formation in vivo. *PloS one*, 7(9):e43291. 1.2, 1.3

[Chen et al., 2003] Chen, C. S., Alonso, J. L., Ostuni, E., Whitesides, G. M., and Ingber, D. E. (2003). Cell shape provides global control of focal adhesion assembly. *Biochemical and biophysical research communications*, 307(2):355–361. 1.3

[Chen et al., 1997] Chen, D., Harris, M., Rossini, G., Dunstan, C., Dallas, S., Feng, J., Mundy, G., and Harris, S. (1997). Bone morphogenetic protein 2 (bmp-2) enhances bmp-3, bmp-4, and bone cell differentiation marker gene expression during the induction of mineralized bone matrix formation in culturesof fetal rat calvarial osteoblasts. *Calcified tissue international*, 60(3):283–290. 3.5

[Cheng et al., 2001] Cheng, S., Lou, J., Wright, N., Lai, C., Avioli, L., and Riew, K. (2001). In vitro andin vivo induction of bone formation using a recombinant adenoviral vector carrying the human bmp-2 gene. *Calcified tissue international*, 68(2):87–94. 4.5

[Chow et al., 1993] Chow, J., Jagger, C., and Chambers, T. (1993). Characterization of osteogenic response to mechanical stimulation in cancellous bone of rat caudal vertebrae. *American Journal of Physiology-Endocrinology And Metabolism*, 265(2):E340–E347. 1.2

[Coste et al., 2010] Coste, B., Mathur, J., Schmidt, M., Earley, T. J., Ranade, S., Petrus, M. J., Dubin, A. E., and Patapoutian, A. (2010). Piezo1 and piezo2 are essential components of distinct mechanically activated cation channels. *Science*, 330(6000):55–60. 2.3.3, 2.4.3

[Crossthwaite et al., 2005] Crossthwaite, A. J., Seebacher, T., Masada, N., Ciruela, A., Dufraux, K., Schultz, J. E., and Cooper, D. M. (2005). The cytosolic domains of ca2+-sensitive adenylyl cyclases dictate their targeting to plasma membrane lipid rafts. *Journal of Biological Chemistry*, 280(8):6380–6391. 5.2.2

[De Camilli et al., 1986] De Camilli, P., Moretti, M., Donini, S. D., Walter, U., and Lohmann, S. (1986). Heterogeneous distribution of the camp receptor protein rii in the nervous system: evidence for its intracellular accumulation on microtubules, microtubule-organizing centers, and in the area of the golgi complex. *The Journal of cell biology*, 103(1):189–203. 5.2.2

[Delaine-Smith et al., 2014] Delaine-Smith, R. M., Sittichokechaiwut, A., and Reilly, G. C. (2014). Primary cilia respond to fluid shear stress and mediate flow-induced calcium deposition in osteoblasts. *The FASEB Journal*, 28(1):430–439. 1.4

[Delghandi et al., 2005] Delghandi, M. P., Johannessen, M., and Moens, U. (2005). The camp signalling pathway activates creb through pka, p38 and msk1 in nih 3t3 cells. *Cellular signalling*, 17(11):1343–1351. 3.5

[Delling et al., 2013] Delling, M., DeCaen, P. G., Doerner, J. F., Febvay, S., and Clapham, D. E. (2013). Primary cilia are specialized calcium signalling organelles. *Nature*, 504(7479):311–314. 2.2

[Dennerll et al., 1988] Dennerll, T., Joshi, H., Steel, V., Buxbaum, R., and Heidemann, S. (1988). Tension and compression in the cytoskeleton of pc-12 neurites. ii: Quantitative measurements. *The Journal of cell biology*, 107(2):665–674. 1.3

[Depry et al., 2011] Depry, C., Allen, M. D., and Zhang, J. (2011). Visualization of pka activity in plasma membrane microdomains. *Molecular BioSystems*, 7(1):52–58. 5.2.2

[Dolmetsch et al., 1997] Dolmetsch, R. E., Lewis, R. S., Goodnow, C. C., and Healy, J. I. (1997). Differential activation of transcription factors induced by ca2+ response amplitude and duration. 3.5

[Dolmetsch et al., 1998] Dolmetsch, R. E., Xu, K., and Lewis, R. S. (1998). Calcium oscillations increase the efficiency and specificity of gene expression. *Nature*, 392(6679):933–936. 3.5

[Downes and Gautam, 1999] Downes, G. and Gautam, N. (1999). The g protein subunit gene families. *Genomics*, 62(3):544–552. 5.2.3

[Duncan and Hruska, 1994] Duncan, R. L. and Hruska, K. A. (1994). Chronic, intermittent loading alters mechanosensitive channel characteristics in osteoblast-like cells. *American Journal of Physiology-Renal Physiology*, 267(6):F909–F916. 1.2

[Dunn et al., 2013] Dunn, K. M., Hill-Eubanks, D. C., Liedtke, W. B., and Nelson, M. T. (2013). Trpv4 channels stimulate ca2+-induced ca2+ release in astrocytic endfeet and amplify neurovascular coupling responses. *Proceedings of the National Academy of Sciences*, 110(15):6157–6162. 2.5

[Elis et al., 2010] Elis, S., Courtland, H.-W., Wu, Y., Rosen, C. J., Sun, H., Jepsen, K. J., Majeska, R. J., and Yakar, S. (2010). Elevated serum levels of igf-1 are sufficient to establish normal body size and skeletal properties even in the absence of tissue igf-1. *Journal of Bone and Mineral Research*, 25(6):1257–1266. 4.3.6

[Ferrari et al., 2005] Ferrari, S., Pierroz, D., Glatt, V., Goddard, D., Bianchi, E., Lin, F., Manen, D., and Bouxsein, M. (2005). Bone response to intermittent parathyroid hormone is altered in mice null for β-arrestin2. *Endocrinology*, 146(4):1854–1862. 4.3.6

[Fill and Copello, 2002] Fill, M. and Copello, J. A. (2002). Ryanodine receptor calcium release channels. *Physiological reviews*, 82(4):893–922. 2.2

[Franz-Odendaal et al., 2006] Franz-Odendaal, T. A., Hall, B. K., and Witten, P. E. (2006). Buried alive: how osteoblasts become osteocytes. *Developmental Dynamics*, 235(1):176–190. 1.2

[Friedrich et al., 2010] Friedrich, M. W., Aramuni, G., Mank, M., Mackinnon, J. A., and Griesbeck, O. (2010). Imaging creb activation in living cells. *Journal of biological chemistry*, 285(30):23285–23295. 5.2.2

[Geiger et al., 2009] Geiger, B., Spatz, J. P., and Bershadsky, A. D. (2009). Environmental sensing through focal adhesions. *Nature Reviews Molecular Cell Biology*, 10(1):21–33. 1.3

[Gerbino et al., 2005] Gerbino, A., Ruder, W. C., Curci, S., Pozzan, T., Zaccolo, M., and Hofer, A. M. (2005). Termination of camp signals by ca2+ and gαi via extracellular ca2+ sensors a link to intracellular ca2+ oscillations. *The Journal of cell biology*, 171(2):303–312. 3.5

[Ghosh et al., 2007] Ghosh, R., Garcia, G. E., Crosby, K., Inoue, H., Thompson, I. M., Troyer, D. A., and Kumar, A. P. (2007). Regulation of cox-2 by cyclic amp response element binding protein in prostate cancer: potential role for nexrutine. *Neoplasia (New York, NY)*, 9(11):893. 3.5, 5.2.2

[Gillespie and Walker, 2001] Gillespie, P. G. and Walker, R. G. (2001). Molecular basis of mechanosensory transduction. *Nature*, 413(6852):194–202. 1.4

[Gorbunova and Spitzer, 2002] Gorbunova, Y. V. and Spitzer, N. C. (2002). Dynamic interactions of cyclic amp transients and spontaneous ca2+ spikes. *Nature*, 418(6893):93–96. 3.5

[Gu et al., 2006] Gu, G., Nars, M., Hentunen, T. A., Metsikkö, K., and Väänänen, H. K. (2006). Isolated primary osteocytes express functional gap junctions in vitro. *Cell and tissue research*, 323(2):263–271. 4.3.4, 4.4.3

[Gudi et al., 1996] Gudi, S. R., Clark, C. B., and Frangos, J. A. (1996). Fluid flow rapidly activates g proteins in human endothelial cells involvement of g proteins in mechanochemical signal transduction. *Circulation Research*, 79(4):834–839. 5.2.3

[Guillou et al., 1999] Guillou, J.-L., Nakata, H., and Cooper, D. M. (1999). Inhibition by calcium of mammalian adenylyl cyclases. *Journal of Biological Chemistry*, 274(50):35539–35545. 3.5

[Hamasaki et al., 1995] Hamasaki, K., Mimura, T., Furuya, H., Morino, N., Yamazaki, T., Komuro, I., Yazaki, Y., and Nojima, Y. (1995). Stretching mesangial cells stimulates tyrosine phosphorylation of focal adhesion kinase pp125¡ sup¿ fak¡/sup¿. *Biochemical and biophysical research communications*, 212(2):544–549. 1.3

[Hamill and Martinac, 2001] Hamill, O. P. and Martinac, B. (2001). Molecular basis of mechanotransduction in living cells. *Physiological reviews*, 81(2):685–740. 1.3

[Han et al., 2012] Han, S. J., Bielawski, K. S., Ting, L. H., Rodriguez, M. L., and Sniadecki, N. J. (2012). Decoupling substrate stiffness, spread area, and micropost density: a close spatial relationship between traction forces and focal adhesions. *Biophysical journal*, 103(4):640–648. 1.3

[Han et al., 2014] Han, S. J., Kim, J. I., and Park, K. M. (2014). P26 hydrogen sulfide elongates primary cilia in the kidney tubular epithelial cells. *Nitric Oxide*, 39:S24. 2.5

[Han et al., 2004] Han, Y., Cowin, S. C., Schaffler, M. B., and Weinbaum, S. (2004). Mechanotransduction and strain amplification in osteocyte cell processes. *Proceedings of the National Academy of Sciences of the United States of America*, 101(47):16689–16694. 1.2

[Hanoune and Defer, 2001] Hanoune, J. and Defer, N. (2001). Regulation and role of adenylyl cyclase isoforms. *Annual review of pharmacology and toxicology*, 41(1):145–174. 4.2, 5.2.3

[Hayakawa et al., 2011] Hayakawa, K., Tatsumi, H., and Sokabe, M. (2011). Actin filaments function as a tension sensor by tension-dependent binding of cofilin to the filament. *The Journal of cell biology*, 195(5):721–727. 1.3

[Haycraft et al., 2007] Haycraft, C. J., Zhang, Q., Song, B., Jackson, W. S., Detloff, P. J., Serra, R., and Yoder, B. K. (2007). Intraflagellar transport is essential for endochondral bone formation. *Development*, 134(2):307–316. 1.1

[Heino et al., 2004] Heino, T. J., Hentunen, T. A., and Väänänen, H. K. (2004). Conditioned medium from osteocytes stimulates the proliferation of bone marrow mesenchymal stem cells and their differentiation into osteoblasts. *Experimental cell research*, 294(2):458–468. 1.2

[Hoey et al., 2011] Hoey, D. A., Kelly, D. J., and Jacobs, C. R. (2011). A role for the primary cilium in paracrine signaling between mechanically stimulated osteocytes and mesenchymal stem cells. *Biochemical and biophysical research communications*, 412(1):182–187. 1.2

[Huang et al., 2006] Huang, B. Q., Masyuk, T. V., Muff, M. A., Tietz, P. S., Masyuk, A. I., and LaRusso, N. F. (2006). Isolation and characterization of cholangiocyte

primary cilia. *American Journal of Physiology-Gastrointestinal and Liver Physiology*, 291(3):G500–G509. 1.4

[Huber and Cormier-Daire, 2012] Huber, C. and Cormier-Daire, V. (2012). Ciliary disorder of the skeleton. In *American Journal of Medical Genetics Part C: Seminars in Medical Genetics*, volume 160, pages 165–174. Wiley Online Library. 1.1

[Hung et al., 1996] Hung, C., Allen, F., Pollack, S., and Brighton, C. (1996). Intracellular ca2+ stores and extracellular ca2+ are required in the real-time ca2+ response of bone cells experiencing fluid flow. *Journal of biomechanics*, 29(11):1411–1417. 1.5, 2.2

[Hung et al., 1995] Hung, C. T., Pollack, S. R., Reilly, T. M., and Brighton, C. T. (1995). Real-time calcium response of cultured bone cells to fluid flow. *Clinical orthopaedics and related research*, 313:256–269. 1.2

[Huo et al., 2008] Huo, B., Lu, X. L., Hung, C. T., Costa, K. D., Xu, Q., Whitesides, G. M., and Guo, X. E. (2008). Fluid flow induced calcium response in bone cell network. *Cellular and molecular bioengineering*, 1(1):58–66. 1.2, 1.5

[Husse and Isenberg, 2010] Husse, B. and Isenberg, G. (2010). Cyclic mechanical strain causes camp-response element binding protein activation by different pathways in cardiac fibroblasts. *Heart international*, 5(1):e3–e3. 4.5

[Ikura et al., 1992] Ikura, M., Clore, G. M., Gronenborn, A. M., Zhu, G., Klee, C. B., and Bax, A. (1992). Solution structure of a calmodulin-target peptide complex by multidimensional nmr. *Science*, 256(5057):632–638. 2.3.2

[Ingber, 2006] Ingber, D. E. (2006). Cellular mechanotransduction: putting all the pieces together again. *The FASEB journal*, 20(7):811–827. 1.3

[Ishijima et al., 2001] Ishijima, M., Rittling, S. R., Yamashita, T., Tsuji, K., Kurosawa, H., Nifuji, A., Denhardt, D. T., and Noda, M. (2001). Enhancement of osteoclastic bone resorption and suppression of osteoblastic bone formation in response to reduced mechanical stress do not occur in the absence of osteopontin. *The Journal of experimental medicine*, 193(3):399–404. 4.5

[Jacobs et al., 1998] Jacobs, C., Yellowley, C., Davis, B., Zhou, Z., Cimbala, J., and Donahue, H. (1998). Differential effect of steady versus oscillating flow on bone cells. *Journal of biomechanics*, 31(11):969–976. 2.2

[Jacobs et al., 2010] Jacobs, C. R., Temiyasathit, S., and Castillo, A. B. (2010). Osteocyte mechanobiology and pericellular mechanics. *Annual review of biomedical engineering*, 12:369–400. 4.2

[Jensen et al., 2004] Jensen, C., Poole, C., McGlashan, S., Marko, M., Issa, Z., Vujcich, K., and Bowser, S. (2004). Ultrastructural, tomographic and confocal imaging of the chondrocyte primary cilium in situ. *Cell biology international*, 28(2):101–110. 1.4

[Jessop et al., 2001] Jessop, H., Sjöberg, M., Cheng, M. Z., Zaman, G., Wheeler-Jones, C., and Lanyon, L. E. (2001). Mechanical strain and estrogen activate estrogen receptor α in bone cells. *Journal of Bone and Mineral Research*, 16(6):1045–1055. 4.2

[Jilka, 2007] Jilka, R. L. (2007). Molecular and cellular mechanisms of the anabolic effect of intermittent pth. *Bone*, 40(6):1434–1446. 4.5

[Jilka et al., 2009] Jilka, R. L., O'Brien, C. A., Ali, A. A., Roberson, P. K., Weinstein, R. S., and Manolagas, S. C. (2009). Intermittent pth stimulates periosteal bone formation by actions on post-mitotic preosteoblasts. *Bone*, 44(2):275–286. 4.5

[Jilka et al., 1999] Jilka, R. L., Weinstein, R. S., Bellido, T., Roberson, P., Parfitt, A. M., Manolagas, S. C., et al. (1999). Increased bone formation by prevention of osteoblast apoptosis with parathyroid hormone. *Journal of Clinical Investigation*, 104(4):439–446. 4.5

[Jin et al., 2013] Jin, X., Mohieldin, A. M., Muntean, B. S., Green, J. A., Shah, J. V., Mykytyn, K., and Nauli, S. M. (2013). Cilioplasm is a cellular compartment for calcium signaling in response to mechanical and chemical stimuli. *Cellular and Molecular Life Sciences*, pages 1–14. 2.2, 2.4.5, 2.5, 5.1.1

[Jing et al., 2013] Jing, D., Baik, A. D., Lu, X. L., Zhou, B., Lai, X., Wang, L., Luo, E., and Guo, X. E. (2013). In situ intracellular calcium oscillations in osteocytes in intact mouse long bones under dynamic mechanical loading. *The FASEB Journal*, pages fj–13. 1.2, 2.2

[Kaiser and Chandrasekhar, 2003] Kaiser, E. and Chandrasekhar, S. (2003). Distinct pathways of extracellular signal-regulated kinase activation by growth factors, fibronectin and parathyroid hormone 1–34. *Biochemical and biophysical research communications*, 305(3):573–578. 4.5

[Katsumi et al., 2004] Katsumi, A., Orr, A. W., Tzima, E., and Schwartz, M. A. (2004). Integrins in mechanotransduction. *Journal of Biological Chemistry*, 279(13):12001–12004. 1.3

[Kim et al., 2010] Kim, J., Lee, J. E., Heynen-Genel, S., Suyama, E., Ono, K., Lee, K., Ideker, T., Aza-Blanc, P., and Gleeson, J. G. (2010). Functional genomic screen for modulators of ciliogenesis and cilium length. *Nature*, 464(7291):1048–1051. 1.4, 5.2.3

[Kiprilov et al., 2008] Kiprilov, E. N., Awan, A., Desprat, R., Velho, M., Clement, C. A., Byskov, A. G., Andersen, C. Y., Satir, P., Bouhassira, E. E., Christensen, S. T., et al. (2008). Human embryonic stem cells in culture possess primary cilia with hedgehog signaling machinery. *The Journal of cell biology*, 180(5):897–904. 1.4

[Klein-Nulend and Bakker, 2007] Klein-Nulend, J. and Bakker, A. D. (2007). Osteocytes: mechanosensors of bone and orchestrators of mechanical adaptation. *Clinical Reviews in Bone and Mineral Metabolism*, 5(4):195–209. 4.2

[Klein-Nulend et al., 1995] Klein-Nulend, J., Van der Plas, A., Semeins, C., Ajubi, N., Frangos, J., Nijweide, P., and Burger, E. (1995). Sensitivity of osteocytes to biomechanical stress in vitro. *The FASEB Journal*, 9(5):441–445. 4.2

[Komatsu et al., 2011] Komatsu, N., Aoki, K., Yamada, M., Yukinaga, H., Fujita, Y., Kamioka, Y., and Matsuda, M. (2011). Development of an optimized backbone of fret biosensors for kinases and gtpases. *Molecular biology of the cell*, 22(23):4647–4656. 3.5

[Köttgen et al., 2008] Köttgen, M., Buchholz, B., Garcia-Gonzalez, M. A., Kotsis, F., Fu, X., Doerken, M., Boehlke, C., Steffl, D., Tauber, R., Wegierski, T., et al. (2008). Trpp2 and trpv4 form a polymodal sensory channel complex. *The Journal of cell biology*, 182(3):437–447. 1.3, 2.4.3, 2.5

[Kwon et al., 2010] Kwon, R. Y., Temiyasathit, S., Tummala, P., Quah, C. C., and Jacobs, C. R. (2010). Primary cilium-dependent mechanosensing is mediated by adenylyl cyclase 6 and cyclic amp in bone cells. *The FASEB Journal*, 24(8):2859–2868. 1.5, 1.5, 3.2, 3.4.3, 3.5, 4.2, 4.4.3, 4.5, 5.1.2, 5.2.1

[Lai and Cheng, 2005] Lai, C.-F. and Cheng, S.-L. (2005). $\alpha v\beta$ integrins play an essential role in bmp-2 induction of osteoblast differentiation. *Journal of bone and mineral research*, 20(2):330–340. 4.3.5

[Lancaster et al., 2011] Lancaster, M. A., Schroth, J., and Gleeson, J. G. (2011). Subcellular spatial regulation of canonical wnt signalling at the primary cilium. *Nature cell biology*, 13(6):700–707. 1.4

[Landa et al., 2005] Landa, L. R., Harbeck, M., Kaihara, K., Chepurny, O., Kitiphongspattana, K., Graf, O., Nikolaev, V. O., Lohse, M. J., Holz, G. G., and Roe, M. W. (2005). Interplay of ca2+ and camp signaling in the insulin-secreting min6 β-cell line. *Journal of Biological Chemistry*, 280(35):31294–31302. 3.5

[Lang et al., 2004] Lang, T., LeBlanc, A., Evans, H., Lu, Y., Genant, H., and Yu, A. (2004). Cortical and trabecular bone mineral loss from the spine and hip in long-duration spaceflight. *Journal of Bone and Mineral Research*, 19(6):1006–1012. 1.2

[Lee et al., 2002] Lee, K., Maxwell, A., and Lanyon, L. (2002). Validation of a technique for studying functional adaptation of the mouse ulna in response to mechanical loading. *Bone*, 31(3):407–412. 4.5

[Lee et al., 2010] Lee, K. L., Hoey, D. A., and Jacobs, C. R. (2010). Primary cilia-mediated mechanotransduction in bone. *Clinical Reviews in Bone and Mineral Metabolism*, 8(4):201–212. 1.4

[Lefkimmiatis et al., 2013] Lefkimmiatis, K., Leronni, D., and Hofer, A. M. (2013). The inner and outer compartments of mitochondria are sites of distinct camp/pka signaling dynamics. *The Journal of cell biology*, 202(3):453–462. 3.5

[Leucht et al., 2013] Leucht, P., Monica, S., Temiyasathit, S., Lenton, K., Manu, A., Longaker, M., Jacobs, C., Spilker, R., Guo, H., Brunski, J., et al. (2013). Primary cilia act as mechanosensors during bone healing around an implant. *Medical engineering & physics*, 35(3):392–402. 1.1

[Li et al., 1998] Li, W.-h., Llopis, J., Whitney, M., Zlokarnik, G., and Tsien, R. Y. (1998). Cell-permeant caged insp3 ester shows that ca2+ spike frequency can optimize gene expression. *Nature*, 392(6679):936–941. 3.5

[Liedert et al., 2006] Liedert, A., Kaspar, D., Blakytny, R., Claes, L., and Ignatius, A. (2006). Signal transduction pathways involved in mechanotransduction in bone cells. *Biochemical and biophysical research communications*, 349(1):1–5. 4.2

[Litzenberger et al., 2010] Litzenberger, J. B., Kim, J.-B., Tummala, P., and Jacobs, C. R. (2010). β1 integrins mediate mechanosensitive signaling pathways in osteocytes. *Calcified tissue international*, 86(4):325–332. 2.5

[Litzenberger et al., 2009] Litzenberger, J. B., Tang, W. J., Castillo, A. B., and Jacobs, C. R. (2009). Deletion of β1 integrins from cortical osteocytes reduces load-induced bone formation. *Cellular and Molecular Bioengineering*, 2(3):416–424. 1.2, 2.5, 4.5

[Lo et al., 2000] Lo, C.-M., Wang, H.-B., Dembo, M., and Wang, Y.-l. (2000). Cell movement is guided by the rigidity of the substrate. *Biophysical journal*, 79(1):144–152. 1.3

[Lu et al., 2012] Lu, X. L., Huo, B., Park, M., and Guo, X. E. (2012). Calcium response in osteocytic networks under steady and oscillatory fluid flow. *Bone*, 51(3):466–473. 1.2, 1.5, 2.2

[Malone et al., 2007] Malone, A. M., Anderson, C. T., Tummala, P., Kwon, R. Y., Johnston, T. R., Stearns, T., and Jacobs, C. R. (2007). Primary cilia mediate mechanosensing in bone cells by a calcium-independent mechanism. *Proceedings of the National Academy of Sciences*, 104(33):13325–13330. 1.2, 1.4, 1.5, 2.2, 2.4.6, 2.5, 4.2

[Martinac, 2004] Martinac, B. (2004). Mechanosensitive ion channels: molecules of mechanotransduction. *Journal of cell science*, 117(12):2449–2460. 1.3

[Masi and Brandi, 2004] Masi, L. and Brandi, M. (2004). Molecular, biochemical and cellular biology of pth anabolic action. *Journal of endocrinological investigation*, 28(8 Suppl):37–40. 4.5

[Masuyama et al., 2012] Masuyama, R., Mizuno, A., Komori, H., Kajiya, H., Uekawa, A., Kitaura, H., Okabe, K., Ohyama, K., and Komori, T. (2012). Calcium/calmodulin-signaling supports trpv4 activation in osteoclasts and regulates bone mass. *Journal of Bone and Mineral Research*, 27(8):1708–1721. 2.5

[Masyuk et al., 2008] Masyuk, A. I., Gradilone, S. A., Banales, J. M., Huang, B. Q., Masyuk, T. V., Lee, S.-O., Splinter, P. L., Stroope, A. J., and LaRusso, N. F. (2008). Cholangiocyte primary cilia are chemosensory organelles that detect biliary nucleotides via p2y12 purinergic receptors. *American Journal of Physiology-Gastrointestinal and Liver Physiology*, 295(4):G725. 3.2, 3.5

[Masyuk et al., 2006] Masyuk, A. I., Masyuk, T. V., Splinter, P. L., Huang, B. Q., Stroope, A. J., and LaRusso, N. F. (2006). Cholangiocyte cilia detect changes in luminal fluid flow and transmit them into intracellular ca¡ sup¿ 2+¡/sup¿ and camp signaling. *Gastroenterology*, 131(3):911–920. 1.4, 1.5, 5.1.2

[Matsubara et al., 2008] Matsubara, T., Kida, K., Yamaguchi, A., Hata, K., Ichida, F., Meguro, H., Aburatani, H., Nishimura, R., and Yoneda, T. (2008). Bmp2 regulates osterix through msx2 and runx2 during osteoblast differentiation. *Journal of biological chemistry*, 283(43):29119–29125. 4.3.5

[Mayr and Montminy, 2001] Mayr, B. and Montminy, M. (2001). Transcriptional regulation by the phosphorylation-dependent factor creb. *Nature Reviews Molecular Cell Biology*, 2(8):599–609. 3.5

[McGlashan et al., 2010] McGlashan, S. R., Knight, M. M., Chowdhury, T. T., Joshi, P., Jensen, C. G., Kennedy, S., and Poole, C. A. (2010). Mechanical loading modulates chondrocyte primary cilia incidence and length. *Cell biology international*, 34(5):441–446. 1.3, 1.4, 4.2

[Miyoshi et al., 2011] Miyoshi, K., Kasahara, K., Miyazaki, I., and Asanuma, M. (2011). Factors that influence primary cilium length. *Acta Med Okayama*, 65:279–285. 1.4, 2.5

[Mizoguchi et al., 2008] Mizoguchi, F., Mizuno, A., Hayata, T., Nakashima, K., Heller, S., Ushida, T., Sokabe, M., Miyasaka, N., Suzuki, M., Ezura, Y., et al. (2008). Transient receptor potential vanilloid 4 deficiency suppresses unloading-induced bone loss. *Journal of cellular physiology*, 216(1):47–53. 2.5

[Morinobu et al., 2003] Morinobu, M., Ishijima, M., Rittling, S. R., Tsuji, K., Yamamoto, H., Nifuji, A., Denhardt, D. T., and Noda, M. (2003). Osteopontin expression in osteoblasts and osteocytes during bone formation under mechanical stress in the calvarial suture in vivo. *Journal of Bone and Mineral Research*, 18(9):1706–1715. 4.5

[Mullender et al., 2004] Mullender, M., El Haj, A., Yang, Y., Van Duin, M., Burger, E., and Klein-Nulend, J. (2004). Mechanotransduction of bone cellsin vitro: mechanobiology of bone tissue. *Medical and Biological Engineering and Computing*, 42(1):14–21. 4.2

[Myers et al., 2007] Myers, K. A., Rattner, J. B., Shrive, N. G., and Hart, D. A. (2007). Osteoblast-like cells and fluid flow: cytoskeleton-dependent shear sensitivity. *Biochemical and biophysical research communications*, 364(2):214–219. 1.2

[Nauli et al., 2003] Nauli, S. M., Alenghat, F. J., Luo, Y., Williams, E., Vassilev, P., Li, X., Elia, A. E., Lu, W., Brown, E. M., Quinn, S. J., et al. (2003). Polycystins 1 and

2 mediate mechanosensation in the primary cilium of kidney cells. *Nature genetics*, 33(2):129–137. 1.3, 1.4, 2.2, 2.4.3, 2.5

[Nelson and Bissell, 2006] Nelson, C. M. and Bissell, M. J. (2006). Of extracellular matrix, scaffolds, and signaling: tissue architecture regulates development, homeostasis, and cancer. *Annual review of cell and developmental biology*, 22:287. 1.3

[Nelson et al., 1995] Nelson, M., Cheng, H., Rubart, M., Santana, L., Bonev, A., Knot, H., and Lederer, W. (1995). Relaxation of arterial smooth muscle by calcium sparks. *Science*, 270(5236):633–637. 2.2

[Nguyen and Jacobs, 2013] Nguyen, A. M. and Jacobs, C. R. (2013). Emerging role of primary cilia as mechanosensors in osteocytes. *Bone*, 54(2):196–204. 1.1

[Nigg et al., 1985] Nigg, E., Schäfer, G., Hilz, H., and Eppenberger, H. (1985). Cyclic-amp-dependent protein kinase type ii is associated with the golgi complex and with centrosomes. *Cell*, 41(3):1039–1051. 5.2.2

[OConor et al., 2014] OConor, C. J., Leddy, H. A., Benefield, H. C., Liedtke, W. B., and Guilak, F. (2014). Trpv4-mediated mechanotransduction regulates the metabolic response of chondrocytes to dynamic loading. *Proceedings of the National Academy of Sciences*, 111(4):1316–1321. 2.5

[Ogasawara et al., 2001] Ogasawara, A., Arakawa, T., Kaneda, T., Takuma, T., Sato, T., Kaneko, H., Kumegawa, M., and Hakeda, Y. (2001). Fluid shear stress-induced cyclooxygenase-2 expression is mediated by c/ebp β, camp-response element-binding protein, and ap-1 in osteoblastic mc3t3-e1 cells. *Journal of Biological Chemistry*, 276(10):7048–7054. 4.2, 5.2.2

[Ogasawara et al., 2004] Ogasawara, T., Kawaguchi, H., Jinno, S., Hoshi, K., Itaka, K., Takato, T., Nakamura, K., and Okayama, H. (2004). Bone morphogenetic protein 2-induced osteoblast differentiation requires smad-mediated down-regulation of cdk6. *Molecular and cellular biology*, 24(15):6560–6568. 4.3.4

[Oldham and Hamm, 2008] Oldham, W. M. and Hamm, H. E. (2008). Heterotrimeric g protein activation by g-protein-coupled receptors. *Nature Reviews Molecular Cell Biology*, 9(1):60–71. 5.2.3

[Oliveira et al., 2010] Oliveira, R. F., Terrin, A., Di Benedetto, G., Cannon, R. C., Koh, W., Kim, M., Zaccolo, M., and Blackwell, K. T. (2010). The role of type 4 phosphodiesterases in generating microdomains of camp: large scale stochastic simulations. *PloS one*, 5(7):e11725. 3.5

[Ou et al., 2009] Ou, Y., Ruan, Y., Cheng, M., Moser, J. J., Rattner, J. B., and van der Hoorn, F. A. (2009). Adenylate cyclase regulates elongation of mammalian primary cilia. *Experimental cell research*, 315(16):2802–2817. 1.5, 5.2.1

[Ouyang et al., 2008] Ouyang, M., Sun, J., Chien, S., and Wang, Y. (2008). Determination of hierarchical relationship of src and rac at subcellular locations with fret biosensors. *Proceedings of the National Academy of Sciences*, 105(38):14353–14358. 2.2, 2.4.1

[Owan et al., 1997] Owan, I., Burr, D. B., Turner, C. H., Qiu, J., Tu, Y., Onyia, J. E., and Duncan, R. L. (1997). Mechanotransduction in bone: osteoblasts are more responsive to fluid forces than mechanical strain. *American Journal of Physiology-Cell Physiology*, 273(3):C810–C815. 2.2

[Palmer et al., 2011] Palmer, A. E., Qin, Y., Park, J. G., and McCombs, J. E. (2011). Design and application of genetically encoded biosensors. *Trends in biotechnology*, 29(3):144–152. 1.1

[Pani and Singh, 2009] Pani, B. and Singh, B. B. (2009). Lipid rafts/caveolae as microdomains of calcium signaling. *Cell calcium*, 45(6):625–633. 5.3

[Parry et al., 2005] Parry, H., McDougall, A., and Whitaker, M. (2005). Microdomains bounded by endoplasmic reticulum segregate cell cycle calcium transients in syncytial drosophila embryos. *The Journal of cell biology*, 171(1):47–59. 5.3

[PaszeK et al., 2005] PaszeK, M. J., Zahir, N., Johnson, K. R., Lakins, J. N., Rozenberg, G. I., Gefen, A., Reinhart-King, C. A., Margulies, S. S., Dembo, M., Boettiger, D., et al. (2005). Tensional homeostasis and the malignant phenotype. *Cancer cell*, 8(3):241–254. 1.3

[Perez et al., 2005] Perez, V., Bouschet, T., Fernandez, C., Bockaert, J., and Journot, L. (2005). Dynamic reorganization of the astrocyte actin cytoskeleton elicited by camp and pacap: a role for phosphatidylinositol 3-kinase inhibition. *European Journal of Neuroscience*, 21(1):26–32. 3.2

[Ponsioen et al., 2004] Ponsioen, B., Zhao, J., Riedl, J., Zwartkruis, F., van der Krogt, G., Zaccolo, M., Moolenaar, W. H., Bos, J. L., and Jalink, K. (2004). Detecting camp-induced epac activation by fluorescence resonance energy transfer: Epac as a novel camp indicator. *EMBO reports*, 5(12):1176–1180. 3.2

[Praetorius et al., 2004] Praetorius, H., Prætorius, J., Nielsen, S., Frokiaer, J., and Spring, K. R. (2004). β1-integrins in the primary cilium of mdck cells potentiate fibronectin-induced ca2+ signaling. *American Journal of Physiology-Renal Physiology*, 287(5):F969–F978. 2.5

[Praetorius and Spring, 2001] Praetorius, H. and Spring, K. R. (2001). Bending the mdck cell primary cilium increases intracellular calcium. *The Journal of membrane biology*, 184(1):71–79. 1.4, 2.2, 3.2, 4.2

[Praetorius and Spring, 2003] Praetorius, H. and Spring, K. R. (2003). Removal of the mdck cell primary cilium abolishes flow sensing. *The Journal of membrane biology*, 191(1):69–76. 1.1, 1.4, 2.2, 3.2, 4.2

[Prasad et al., 2014] Prasad, R. M., Jin, X., and Nauli, S. M. (2014). Sensing a sensor: Identifying the mechanosensory function of primary cilia. *Biosensors*, 4(1):47–62. 2.2

[Provenzano et al., 2008] Provenzano, P. P., Inman, D. R., Eliceiri, K. W., Knittel, J. G., Yan, L., Rueden, C. T., White, J. G., and Keely, P. J. (2008). Collagen density promotes mammary tumor initiation and progression. *BMC medicine*, 6(1):11. 1.3

[Putnam et al., 2001] Putnam, A., Schultz, K., and Mooney, D. (2001). Control of microtubule assembly by extracellular matrix and externally applied strain. *American Journal of Physiology-Cell Physiology*, 280(3):C556–C564. 1.3

[Putnam et al., 2003] Putnam, A. J., Cunningham, J. J., Pillemer, B. B., and Mooney, D. J. (2003). External mechanical strain regulates membrane targeting of rho gtpases by controlling microtubule assembly. *American Journal of Physiology-Cell Physiology*, 284(3):C627–C639. 1.3

[Qiu et al., 2012] Qiu, N., Xiao, Z., Cao, L., Buechel, M. M., David, V., Roan, E., and Quarles, L. D. (2012). Disruption of kif3a in osteoblasts results in defective bone formation and osteopenia. *Journal of cell science*, 125(8):1945–1957. 1.4, 4.5

[Ridge et al., 2005] Ridge, K. M., Linz, L., Flitney, F. W., Kuczmarski, E. R., Chou, Y.-H., Omary, M. B., Sznajder, J. I., and Goldman, R. D. (2005). Keratin 8 phosphorylation by protein kinase c δ regulates shear stress-mediated disassembly of keratin intermediate filaments in alveolar epithelial cells. *Journal of Biological Chemistry*, 280(34):30400–30405. 1.3

[Risca et al., 2012] Risca, V. I., Wang, E. B., Chaudhuri, O., Chia, J. J., Geissler, P. L., and Fletcher, D. A. (2012). Actin filament curvature biases branching direction. *Proceedings of the National Academy of Sciences*, 109(8):2913–2918. 1.3

[Romet-Lemonne and Jégou, 2013] Romet-Lemonne, G. and Jégou, A. (2013). Mechanotransduction down to individual actin filaments. *European journal of cell biology*, 92(10):333–338. 1.3

[Rudolf et al., 2003] Rudolf, R., Mongillo, M., Rizzuto, R., and Pozzan, T. (2003). Looking forward to seeing calcium. *Nature Reviews Molecular Cell Biology*, 4(7):579–586. 1.1

[Sabbatini et al., 2013] Sabbatini, M. E., DAlecy, L., Lentz, S. I., Tang, T., and Williams, J. A. (2013). Adenylyl cyclase 6 mediates the action of cyclic amp-dependent secretagogues in mouse pancreatic exocrine cells via protein kinase a pathway activation. *The Journal of physiology*, 591(15):3693–3707. 3.5

[Sabsovich et al., 2008] Sabsovich, I., Clark, J. D., Liao, G., Peltz, G., Lindsey, D. P., Jacobs, C. R., Yao, W., Guo, T.-Z., and Kingery, W. S. (2008). Bone microstructure and its associated genetic variability in 12 inbred mouse strains: μct study and¡ i¿ in silico¡/i¿ genome scan. *Bone*, 42(2):439–451. 4.3.3

[Sai et al., 1999] Sai, X., Naruse, K., and Sokabe, M. (1999). Activation of pp60 (src) is critical for stretch-induced orienting response in fibroblasts. *Journal of cell science*, 112(9):1365–1373. 1.3

[Salih et al., 1996] Salih, E., Ashkar, S., Gerstenfeld, L. C., and Glimcher, M. J. (1996). Protein kinases of cultured osteoblasts: selectivity for the extracellular matrix proteins of bone and their catalytic competence for osteopontin. *Journal of Bone and Mineral Research*, 11(10):1461–1473. 4.5

[Schmidt et al., 1998] Schmidt, C., Pommerenke, H., Dürr, F., Nebe, B., and Rychly, J. (1998). Mechanical stressing of integrin receptors induces enhanced tyrosine phosphorylation of cytoskeletally anchored proteins. *Journal of Biological Chemistry*, 273(9):5081–5085. 4.5

[Seino and Shibasaki, 2005] Seino, S. and Shibasaki, T. (2005). Pka-dependent and pka-independent pathways for camp-regulated exocytosis. *Physiological reviews*, 85(4):1303–1342. 1.5, 3.2

[Shah et al., 2004] Shah, S. B., Davis, J., Weisleder, N., Kostavassili, I., McCulloch, A. D., Ralston, E., Capetanaki, Y., and Lieber, R. L. (2004). Structural and functional roles of desmin in mouse skeletal muscle during passive deformation. *Biophysical journal*, 86(5):2993–3008. 1.3

[Sharma et al., 2011] Sharma, N., Kosan, Z. A., Stallworth, J. E., Berbari, N. F., and Yoder, B. K. (2011). Soluble levels of cytosolic tubulin regulate ciliary length control. *Molecular biology of the cell*, 22(6):806–816. 1.4, 2.4.1, 5.2.3

[Siddappa et al., 2009] Siddappa, R., Mulder, W., Steeghs, I., van de Klundert, C., Fernandes, H., Liu, J., Arends, R., van Blitterswijk, C., and de Boer, J. (2009). camp/pka signaling inhibits osteogenic differentiation and bone formation in rodent models. *Tissue Engineering Part A*, 15(8):2135–2143. 3.2

[Solon et al., 2007] Solon, J., Levental, I., Sengupta, K., Georges, P. C., and Janmey, P. A. (2007). Fibroblast adaptation and stiffness matching to soft elastic substrates. *Biophysical journal*, 93(12):4453–4461. 1.3

[Spiering and Hodgson, 2011] Spiering, D. and Hodgson, L. (2011). Dynamics of the rho-family small gtpases in actin regulation and motility. *Cell adhesion & migration*, 5(2):170. 5.2.3

[Stern et al., 2012] Stern, A. R., Stern, M. M., Van Dyke, M. E., Jähn, K., Prideaux, M., and Bonewald, L. F. (2012). Isolation and culture of primary osteocytes from the long bones of skeletally mature and aged mice. *Biotechniques*, 52(6):361. 4.4.3

[Su et al., 2013] Su, S., Phua, S. C., DeRose, R., Chiba, S., Narita, K., Kalugin, P. N., Katada, T., Kontani, K., Takeda, S., and Inoue, T. (2013). Genetically encoded calcium indicator illuminates calcium dynamics in primary cilia. *Nature methods*. 2.2

[Sutherland et al., 1972] Sutherland, E. W., for the Advancement of Science, A. A., et al. (1972). Studies on the mechanism of hormone action. American Association for the Advancement of Science. 3.2

[Tang et al., 2008] Tang, T., Gao, M. H., Lai, N. C., Firth, A. L., Takahashi, T., Guo, T., Yuan, J. X.-J., Roth, D. M., and Hammond, H. K. (2008). Adenylyl cyclase type 6 deletion decreases left ventricular function via impaired calcium handling. *Circulation*, 117(1):61–69. 4.3.2, 4.4.1

[Tatsumi et al., 2007] Tatsumi, S., Ishii, K., Amizuka, N., Kobayashi, T., Kohno, K., Takeshita, S., and Ikeda, K. (2007). Targeted ablation of osteocytes induces osteoporosis with defective mechanotransduction. *Cell Metabolism*, 5(6):464–475. 1.2, 1.3, 4.2

[Taylor et al., 2007] Taylor, A. F., Saunders, M. M., Shingle, D. L., Cimbala, J. M., Zhou, Z., and Donahue, H. J. (2007). Mechanically stimulated osteocytes regulate osteoblastic activity via gap junctions. *American Journal of Physiology-Cell Physiology*, 292(1):C545–C552. 1.2

[Tee et al., 2011] Tee, S.-Y., Fu, J., Chen, C. S., and Janmey, P. A. (2011). Cell shape and substrate rigidity both regulate cell stiffness. *Biophysical journal*, 100(5):L25–L27. 1.3

[Temiyasathit et al., 2012] Temiyasathit, S., Tang, W. J., Leucht, P., Anderson, C. T., Monica, S. D., Castillo, A. B., Helms, J. A., Stearns, T., and Jacobs, C. R. (2012). Mechanosensing by the primary cilium: deletion of kif3a reduces bone formation due to loading. *PLoS One*, 7(3):e33368. 1.1, 1.4, 4.2, 4.3.11, 4.5

[Thorneloe et al., 2008] Thorneloe, K. S., Sulpizio, A. C., Lin, Z., Figueroa, D. J., Clouse, A. K., McCafferty, G. P., Chendrimada, T. P., Lashinger, E. S., Gordon, E., Evans, L., et al. (2008). N-((1s)-1-{[4-((2S)-2-{[(2, 4-dichlorophenyl) sulfonyl] amino}-3-hydroxypropanoyl)-1-piperazinyl] carbonyl}-3-methylbutyl)-1-benzothiophene-2-carboxamide (gsk1016790a), a novel and potent transient receptor potential vanilloid 4 channel agonist induces urinary bladder contraction and hyperactivity: Part i. *Journal of Pharmacology and Experimental Therapeutics*, 326(2):432–442. 2.5

[Toyosawa et al., 2001] Toyosawa, S., Shintani, S., Fujiwara, T., Ooshima, T., Sato, A., Ijuhin, N., and Komori, T. (2001). Dentin matrix protein 1 is predominantly expressed in chicken and rat osteocytes but not in osteoblasts. *Journal of Bone and Mineral Research*, 16(11):2017–2026. 4.4.3

[Tsuzuku et al., 1999] Tsuzuku, S., Ikegami, Y., and Yabe, K. (1999). Bone mineral density differences between paraplegic and quadriplegic patients: a cross-sectional study. *Spinal Cord*, 37(5). 1.2

[Turner et al., 1994] Turner, C., Forwood, M., and Otter, M. (1994). Mechanotransduction in bone: do bone cells act as sensors of fluid flow? *The FASEB journal*, 8(11):875–878. 1.2

[Tuson et al., 2011] Tuson, M., He, M., and Anderson, K. V. (2011). Protein kinase a acts at the basal body of the primary cilium to prevent gli2 activation and ventralization of the mouse neural tube. *Development*, 138(22):4921–4930. 3.5, 5.2.2

[van der Eerden et al., 2013] van der Eerden, B., Oei, L., Roschger, P., Fratzl-Zelman, N., Hoenderop, J., van Schoor, N., Pettersson-Kymmer, U., Schreuders-Koedam, M., Uitterlinden, A., Hofman, A., et al. (2013). Trpv4 deficiency causes sexual dimorphism in bone metabolism and osteoporotic fracture risk. *Bone*, 57(2):443–454. 2.5

[Vincent et al., 2009] Vincent, F., Acevedo, A., Nguyen, M. T., Dourado, M., DeFalco, J., Gustafson, A., Spiro, P., Emerling, D. E., Kelly, M. G., and Duncton, M. A. (2009). Identification and characterization of novel trpv4 modulators. *Biochemical and biophysical research communications*, 389(3):490–494. 2.5

[Violin et al., 2008] Violin, J. D., DiPilato, L. M., Yildirim, N., Elston, T. C., Zhang, J., and Lefkowitz, R. J. (2008). β2-adrenergic receptor signaling and desensitization elucidated by quantitative modeling of real time camp dynamics. *Journal of biological chemistry*, 283(5):2949–2961. 3.2

[Wachten et al., 2010] Wachten, S., Masada, N., Ayling, L.-J., Ciruela, A., Nikolaev, V. O., Lohse, M. J., and Cooper, D. M. (2010). Distinct pools of camp centre on different isoforms of adenylyl cyclase in pituitary-derived gh3b6 cells. *Journal of cell science*, 123(1):95–106. 3.5

[Wadhwa et al., 2002] Wadhwa, S., Choudhary, S., Voznesensky, M., Epstein, M., Raisz, L., and Pilbeam, C. (2002). Fluid flow induces cox-2 expression in mc3t3-e1 osteoblasts via a pka signaling pathway. *Biochemical and biophysical research communications*, 297(1):46–51. 1.5, 4.2

[Wang et al., 2004] Wang, S.-Q., Wei, C., Zhao, G., Brochet, D. X., Shen, J., Song, L.-S., Wang, W., Yang, D., and Cheng, H. (2004). Imaging microdomain ca2+ in muscle cells. *Circulation research*, 94(8):1011–1022. 2.2

[Wang et al., 2005] Wang, Y., Botvinick, E. L., Zhao, Y., Berns, M. W., Usami, S., Tsien, R. Y., and Chien, S. (2005). Visualizing the mechanical activation of src. *Nature*, 434(7036):1040–1045. 2.3.2, 2.4.1, 3.3.2, 3.4.1

[Wann et al., 2012] Wann, A. K., Zuo, N., Haycraft, C. J., Jensen, C. G., Poole, C. A., McGlashan, S. R., and Knight, M. M. (2012). Primary cilia mediate mechanotransduction through control of atp-induced ca2+ signaling in compressed chondrocytes. *The FASEB Journal*, 26(4):1663–1671. 2.5, 4.2

[Watanabe et al., 2003] Watanabe, H., Vriens, J., Prenen, J., Droogmans, G., Voets, T., and Nilius, B. (2003). Anandamide and arachidonic acid use epoxyeicosatrienoic acids to activate trpv4 channels. *Nature*, 424(6947):434–438. 2.5

[Wehrle-Haller, 2012] Wehrle-Haller, B. (2012). Assembly and disassembly of cell matrix adhesions. *Current opinion in cell biology*, 24(5):569–581. 1.3

[Weinbaum et al., 1994] Weinbaum, S., Cowin, S., and Zeng, Y. (1994). A model for the excitation of osteocytes by mechanical loading-induced bone fluid shear stresses. *Journal of biomechanics*, 27(3):339–360. 1.2

[Wheatley et al., 1996] Wheatley, D. N., Wang, A. M., and Strugnell, G. E. (1996). Expression of primary cilia in mammalian cells. *Cell biology international*, 20(1):73–81. 1.4

[Whitaker, 2010] Whitaker, M. (2010). Genetically-encoded probes for measurement of intracellular calcium. *Methods in cell biology*, 99:153. 2.2

[Whitfield, 2008] Whitfield, J. (2008). The solitary (primary) cilium–a mechanosensory toggle switch in bone and cartilage cells. *Cellular signalling*, 20(6):1019–1024. 1.4

[Willoughby and Cooper, 2007] Willoughby, D. and Cooper, D. M. (2007). Organization and ca2+ regulation of adenylyl cyclases in camp microdomains. *Physiological Reviews*, 87(3):965–1010. 1.5, 3.5

[Willoughby et al., 2012] Willoughby, D., Everett, K. L., Halls, M. L., Pacheco, J., Skroblin, P., Vaca, L., Klussmann, E., and Cooper, D. M. (2012). Direct binding between orai1 and ac8 mediates dynamic interplay between ca2+ and camp signaling. *Science Signaling*, 5(219):ra29. 3.5

[Wilsman and Fletcher, 1978] Wilsman, N. J. and Fletcher, T. F. (1978). Cilia of neonatal articular chondrocytes incidence and morphology. *The Anatomical Record*, 190(4):871–889. 1.4

[Wong and Reiter, 2008] Wong, S. Y. and Reiter, J. F. (2008). The primary cilium: at the crossroads of mammalian hedgehog signaling. *Current topics in developmental biology*, 85:225–260. 1.4

[Yang et al., 2008] Yang, D.-C., Tsay, H.-J., Lin, S.-Y., Chiou, S.-H., Li, M.-J., Chang, T.-J., and Hung, S.-C. (2008). camp/pka regulates osteogenesis, adipogenesis and ratio of rankl/opg mrna expression in mesenchymal stem cells by suppressing leptin. *PLoS One*, 3(2):e1540. 4.5

[Yellowley et al., 1997] Yellowley, C. E., Jacobs, C. R., Li, Z., Zhou, Z., and Donahue, H. J. (1997). Effects of fluid flow on intracellular calcium in bovine articular chondrocytes. *American Journal of Physiology-Cell Physiology*, 273(1):C30–C36. 1.2

[Yeung et al., 2005] Yeung, T., Georges, P. C., Flanagan, L. A., Marg, B., Ortiz, M., Funaki, M., Zahir, N., Ming, W., Weaver, V., and Janmey, P. A. (2005). Effects of substrate stiffness on cell morphology, cytoskeletal structure, and adhesion. *Cell motility and the cytoskeleton*, 60(1):24–34. 1.3

[You et al., 2001a] You, J., Reilly, G. C., Zhen, X., Yellowley, C. E., Chen, Q., Donahue, H. J., and Jacobs, C. R. (2001). Osteopontin gene regulation by oscillatory fluid flow via intracellular calcium mobilization and activation of mitogen-activated protein kinase in mc3t3–e1 osteoblasts. *Journal of Biological Chemistry*, 276(16):13365–13371. 1.5, 2.2, 4.5

[You et al., 2001b] You, L., Cowin, S. C., Schaffler, M. B., and Weinbaum, S. (2001). A model for strain amplification in the actin cytoskeleton of osteocytes due to fluid drag on pericellular matrix. *Journal of biomechanics*, 34(11):1375–1386. 1.2, 2.2

[Young et al., 2012] Young, Y.-N., Downs, M., and Jacobs, C. (2012). Dynamics of the primary cilium in shear flow. *Biophysical journal*, 103(4):629–639. 1.4, 2.5

[Zaccolo and Pozzan, 2002] Zaccolo, M. and Pozzan, T. (2002). Discrete microdomains with high concentration of camp in stimulated rat neonatal cardiac myocytes. *Science*, 295(5560):1711–1715. 3.5

[Zippin et al., 2010] Zippin, J. H., Chadwick, P. A., Levin, L. R., Buck, J., and Magro, C. M. (2010). Soluble adenylyl cyclase defines a nuclear camp microdomain in keratinocyte hyperproliferative skin diseases. *Journal of Investigative Dermatology*, 130(5):1279–1287. 3.5

Appendix A

Calcium

A.1 Supplemental Figures

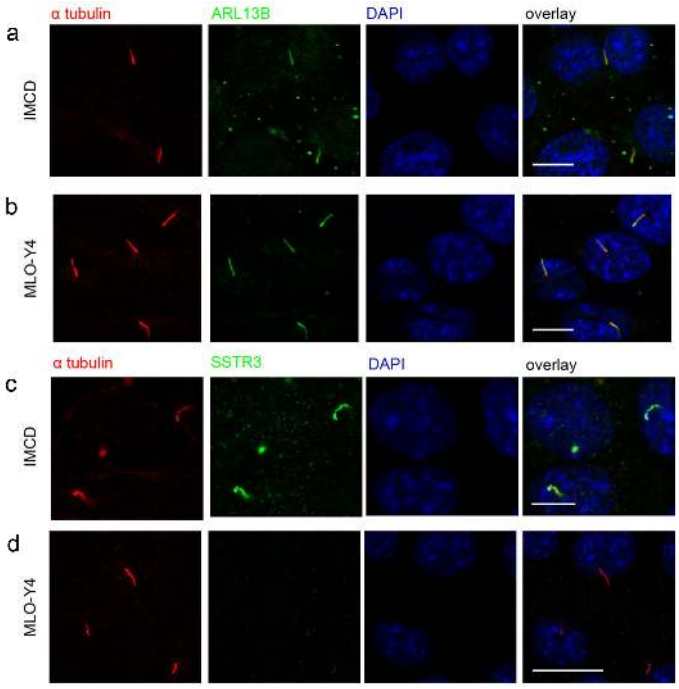

Figure A.1: ARL13B localizes to primary cilia in MLO-Y4 and IMCD cells. (a-b) IMCD and MLO-Y4 cells stained for acetylated α-tubulin and ARL13B. (c-d) IMCD and MLO-Y4 cells stained for acetylated α-tubulin and SSTR3. Scale bars, 5 μm.

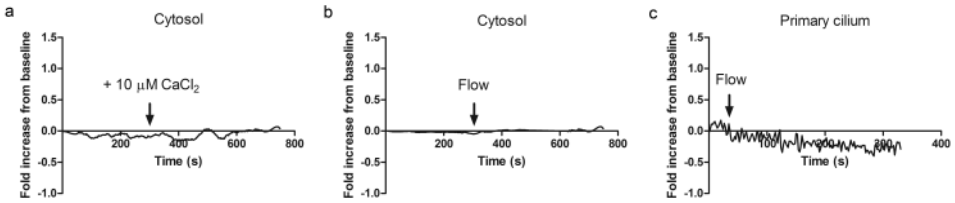

Figure A.2: Mutant CaB and ALC do not exhibit flow-induced FRET signal changes. (a-b) MutCaB failed to detect flow-induced Ca^{2+} increase with the addition of 10 μM $CaCl_2$ (n=3) and steady flow (5 dynes/cm^2) (n=2). (c) MutALC failed to detect flow-induced Ca^{2+} increases (10 dynes/cm^2) (n=4).

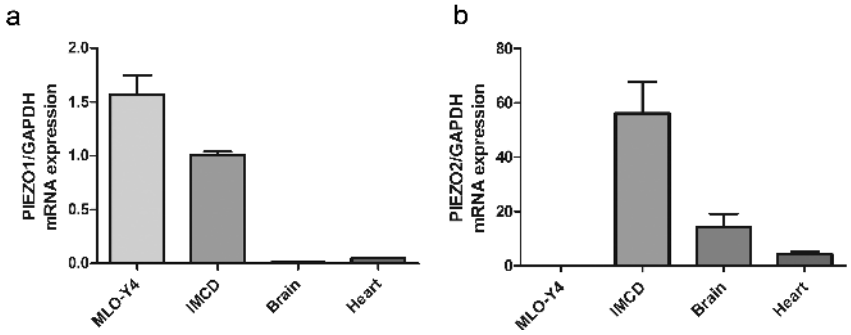

Figure A.3: MLO-Y4 cells express *Piezo1* but not *Piezo2*. *Piezo1* and *Piezo2* mRNA levels in MLO-Y4 cells, IMCD cells, and adult murine (C57BL/6) brain and heart tissue (n=4-5). Error bars show mean ± SEM.

Appendix B

Adenylyl Cyclase 6

B.1 Supplemental Data

Ulnar Midshaft	**Female**		**Male**	
	WT	**AC6 KO**	**WT**	**AC6 KO**
n	11	8	12	10
Length (mm)	12.9±0.3	12.9±0.2	13.9±0.1	13.3±0.3
Total area(mm^2)	0.234±0.011	0.255±0.006	0.247±0.003	0.236±0.01
Cortical area (mm^2)	0.211±0.010	0.241±0.006	0.247±0.003	0.236±0.010
Cortical thickness (mm)	0.171±0.002	0.175±0.005	0.172±0.002	0.169±0.002
$I_{max}\,(mm^{4)}$	0.012±0.002	0.013±0.002	0.021±0.002	0.019±0.003
$I_{min}\,(mm^4)$	0.006±0.001	0.005±0.002	0.010±0.002	0.008±0.002
Tibial Midshaft	**Female**		**Male**	
	WT	**AC6 KO**	**WT**	**AC6 KO**
n	10	7	14	10
Length (mm)	17.0±0.1	17.0±0.2	17.5±0.2	17.4±0.1
Total area(mm^2)	0.595±0.008	0.587±0.017	0.752±0.025	0.670±0.03
Cortical area (mm^2)	0.568±0.008	0.559±0.17	0.721±0.025	0.670±0.03
Cortical thickness (mm)	0.222±0.002	0.209±0.003**	0.223±0.010	0.224±0.007
$I_{max}\,(mm^{4)}$	0.068±0.004	0.063±0.004	0.133±0.008	0.118±0.009
$I_{min}\,(mm^4)$	0.055±0.006	0.045±0.003	0.102±0.007	0.091±0.009

Table B.1: Cortical bone geometry. Data are mean ± SEM. $^{**}p < 0.005$ vs. gender-matched WT control.

Proximal Tibia	**Female**		**Male**	
	WT	**AC6 KO**	**WT**	**AC6 KO**
n	10	7	14	12
BV/TV (%)	10.2±0.6	9.2±0.7	15.9±1.4	15.0±1.4
Tb. N. (mm^{-1})	3.66±0.15	3.51±0.24	5.15±0.24	5.06±0.15
Tb. Th (mm)	0.049±0.001	0.048±0.002	0.049±0.002	0.047±0.002
Tb. Sp. (mm)	0.280±0.012	0.297±0.021	0.195±0.010	0.194±0.007
Conn. D. (mm^{-3})	75.5±9.6	72.4±17.5	150.7±19.1	141.9±10.5

Table B.2: Trabecular bone microarchitecture. Data are mean ± SEM.